AD NUMBER
AD381517
CLASSIFICATION CHANGES
TO: **UNCLASSIFIED**
FROM: **CONFIDENTIAL**
LIMITATION CHANGES
TO: **Approved for public release; distribution is unlimited.**
FROM: **Distribution authorized to U.S. Gov't. agencies and their contractors; Administrative/Operational Use; JUN 1967. Other requests shall be referred to Arnold Engineering Development Center, Arnold AFB, TN 37389.**
AUTHORITY
27 Jun 1973, per document markings; USAEDC ltr, 27 Jun 1973

AEDC-TR-67-87

SIMULATED SPACE START INVESTIGATION OF THE INTEGRATED LUNAR MODULE DESCENT STAGE THROTTLABLE ENGINE AND ENGINE COMPARTMENT (U)

K. L. Farrow, J. A. German,

T. M. Gernstein, and E. H. Matkins

ARO, Inc.

June 1967

ROCKET TEST FACILITY
ARNOLD ENGINEERING DEVELOPMENT CENTER
AIR FORCE SYSTEMS COMMAND
ARNOLD AIR FORCE STATION, TENNESSEE

NOTICES

When U. S. Government drawings specifications, or other data are used for any purpose other than a definitely related Government procurement operation, the Government thereby incurs no responsibility nor any obligation whatsoever, and the fact that the Government may have formulated, furnished, or in any way supplied the said drawings, specifications, or other data, is not to be regarded by implication or otherwise, or in any manner licensing the holder or any other person or corporation, or conveying any rights or permission to manufacture, use, or sell any patented invention that may in any way be related thereto.

Qualified users may obtain copies of this report from the Defense Documentation Center.

References to named commercial products in this report are not to be considered in any sense as an endorsement of the product by the United States Air Force or the Government.

Do not return this copy. When not needed, destroy in accordance with pertinent security regulations.

SIMULATED SPACE START INVESTIGATION OF THE INTEGRATED LUNAR MODULE DESCENT STAGE THROTTLABLE ENGINE AND ENGINE COMPARTMENT (U)

K. L. Farrow, J. A. German,
T. M. Gernstein, and E. H. Matkins
ARO, Inc.

FOREWORD

(U) The tests reported herein were sponsored by the Manned Spacecraft Center (MSC), National Aeronautics and Space Administration (NASA), under System 921E/9158. Two Lunar Module Descent Engines (LMDE) manufactured by TRW Systems, Inc., were tested using a Grumman Aircraft Engineering Company (GAEC) manufactured, heavy-duty, LMDE cavity (HD-4 rig) in Propulsion Engine Test Cell (J-2A) of the Rocket Test Facility (RTF).

(U) The results of the tests presented were obtained by ARO, Inc. (a subsidiary of Sverdrup & Parcel and Associates, Inc.), contract operator of the Arnold Engineering Development Center (AEDC), Air Force Systems Command (AFSC), Arnold Air Force Station, Tennessee, under Contract AF 40(600)-1200. The tests were conducted between July 19 and December 10, 1966, under ARO Project Number RL1618. Preparation commenced on this interim report covering the first three test periods of the project on December 27, 1966, and the manuscript was submitted for publication on April 7, 1967.

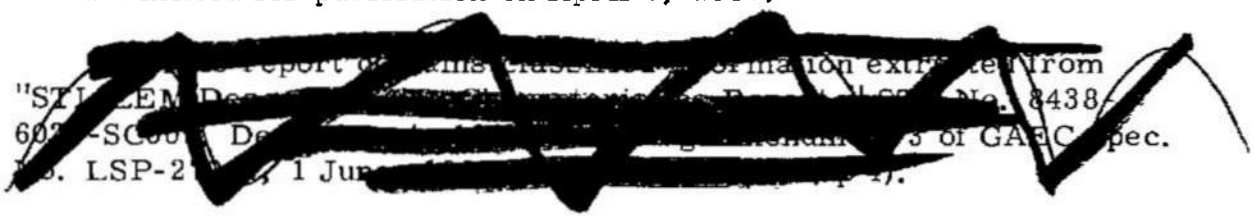

(U) This technical report has been reviewed and is approved.

Joseph R. Henry
Lt Col, USAF
AF Representative, RTF
Directorate of Test

Leonard T. Glaser
Colonel, USAF
Director of Test

UNCLASSIFIED ABSTRACT

(U) Two Lunar Module Descent Engines (LMDE) were tested under simulated altitude conditions in Propulsion Engine Test Cell (J-2A) to (1) evaluate the thermal characteristics of the engine and engine compartment, and (2) evaluate starting characteristics of the engine after temperature conditioning in the simulated space environment. The first engine was subjected to an initial simulated space coast of 73.6 hr followed by three short firings alternated with two shorter coast periods. Combustion instability occurred during the first firing conducted at the 30-percent thrust level. Testing was discontinued because of an oxidizer leak and apparent loss of the primary instrumentation. After repairs, testing was resumed, and coast periods ranging from 3.3 to 74.8 hr followed by firings ranging from 3 to 50 sec were made at thrust levels ranging from 10 to 94 percent of rated thrust. Combustion instability occurred during seven of these 18 firings at thrust levels of 20, 30, and 35 percent, and acceleration levels above 1000 g's were experienced during 11 firings. Post-test inspection revealed a damaged injector pintle. The injector and engine were rebuilt and returned as the second test engine which was subjected to a 51.5-hr coast. The subsequent four short firings resulted in off-mixture-ratio operation of the engine because of propellant system contamination. Analysis of the test article thermal data and engine starting and operating characteristics are presented over the pre-fire pressure altitude range from 299,000 to 346,000 ft. (AFR 310-2, Statement 2)

CONTENTS

APPENDIXES

I. ILLUSTRATIONS

Figure

SECTION I
INTRODUCTION

(U) After the Lunar Module (LM) separates from the Saturn SIVB stage, it will be exposed to the space environment for approximately 66 hr prior to powered descent or first ignition of the Lunar Module Descent Engine (LMDE) for transfer orbit insertion. During this time, the Descent engine nozzle will be exposed to the space thermal and vacuum environment, and the thrust chamber and headend assembly will be exposed to the space vacuum and to the thermal environment of the LMDE cavity. In order to closely approximate these conditions during this test series, the engine was installed in a heavy-duty structure which simulated the LMDE cavity on the LM vehicle. This structure was designated the HD-4 rig and was furnished by Grumman Aircraft Engineering Corporation (GAEC) specifically for this test program. The engine was equipped with the GAEC, lightweight heat shield (Fig. 1 - Appendix I).

(U) Two test projects using the throttlable LMDE and simulated engine cavity have been conducted to date in the Propulsion Engine Test Cell (J-2A). The first test project was conducted under ARO Project Number RL1433 between September 30 and December 2, 1965, during which two engines were tested. Thermal studies and mission simulation firings were included. The results of these tests are reported in Ref. 1.

(U) The general objectives of the second test program, reported herein, were to provide performance and thermal data and to evaluate the start transient characteristics of the LMDE when exposed to a simulated space thermal-vacuum environment. The specific objectives were to:

1. Determine the terminal temperatures of the engine when exposed to a simulated space thermal-vacuum environment while installed in a heavy-duty LM vehicle Descent Engine cavity.
2. Establish engine start characteristics with propellants supplied at 40, 70, and 120°F at various thrust levels.
3. Obtain vacuum-corrected engine performance data at various thrust levels and propellant temperatures.

(U) To simulate the space vacuum and space thermal environment, the engine and HD-4 rig were installed in the J-2A cell, a liquid-nitrogen (LN_2)-cooled test cell equipped with vacuum pumping systems and a variable output thermal radiation system. Three test periods were conducted with simulated space coast periods ranging in duration from 3.3 to 74.8 hr at altitudes in excess of 300,000 ft preceding all firings.

1. The first test period (AA) was discontinued after three of the scheduled 10 firings because of an oxidizer leak inside the test cell and apparent loss of the primary instrumentation.
2. The second test period (AB) consisted of 18 firings and was completed as scheduled; however, injector damage was incurred.
3. The third test period (AC) was discontinued after four of the scheduled 16 firings because of erratic mixture ratio operation. Propellant system contamination and engine flow control valve damage were discovered during post-test investigations.

SECTION II
APPARATUS

2.1 TEST ARTICLE

(U) The test article consisted of the LMDE and the HD-4 Propulsion Test Rig. The LMDE (Fig. 2) is manufactured by TRW Systems, a subsidiary of Thompson-Ramo-Woolridge, Inc. It is designed for throttled operation from 10 to 60 percent of rated thrust in addition to rated thrust operation. The overall length of the LMDE is approximately 85 in., and it weighs approximately 350 lb including the engine gimbal assembly, which allows 6 deg of gimbal from the neutral position. The engine produces a rated thrust of 10,500 lb at a total propellant flow rate of 34.0 lb_m/sec at a design mixture ratio of 1.6. The hypergolic propellants are inhibited nitrogen tetroxide (N_2O_4) as the oxidizer (NASA Spec. MSC-PPD-2A) and equal gravimetric parts of hydrazine (N_2H_4), and unsymmetrical dimethylhydrazine $\left[N_2H_2(CH_3)_2\right]$ as the fuel (MIL-P-27402). Rated chamber pressure is 107.3 psia. Engine accessories consist of propellant flow control valves, propellant shutoff valves, and throttle actuator. Engine design and performance characteristics are shown in Table I (Appendix II).

(U) The HD-4 rig (Fig. 3) is a heavyweight support structure for the LMDE. It was manufactured by GAEC for use as a test fixture for the environmental tests at AEDC. The rig resembles the engine cavity of the LM Descent Stage center compartment.

(U) Test hardware identification by part drawing numbers and serial numbers is shown in Tables II and III. The individual components of the test article are described below.

2.1.1 Ablative Chamber

(U) The thrust chamber is ablatively cooled to an expansion ratio of 16:1 and weighs approximately 130 lb in the unfired condition. The ablative chamber consists of four sections:

1. Face plate
2. Turbulence ring
3. Throat
4. Divergent section

All are enclosed in a continuous titanium shell and are jacketed by a stainless steel foil/glass wool composite thermal blanket (Fig. 4). Sections 1, 2, and 4 are made of Fiberite MX2525®, a randomly oriented material composed of 0.50-in. squares of chopped silica impregnated with phenolic resin. The throat is made of Fiberite MX2600®, a silica-phenolic tape, oriented at 60 deg to the centerline to minimize erosion. All four sections are wrapped externally with Fiberite MX2600 tape. All ablative components of the chamber are bonded to the titanium shell with Sylgard 182®.

2.1.2 Nozzle Extension

(U) A crushable, radiation-cooled, columbium nozzle extension is normally bolted to the thrust chamber at the 16:1 expansion ratio position and provides controlled expansion of the combustion products to a ratio of 47.4:1. However, during this test series, the engine was equipped with a heavy-duty 0.030-in. wall thickness columbium nozzle extension. The extension exit flange was installed especially for this test program and was used for attachment of a flexible rubber diffuser inlet seal for compatibility with the operation of the J-2A test cell. An Inconel X750® seal with a "K" cross section was used to prevent leakage between the thrust chamber and nozzle extension flange. The bolt holes in both the chamber and extension upstream flange were slotted, and the bolt torque values were limited to allow for differential thermal expansion.

2.1.3 Gimbal Ring Assembly

(U) The gimbal ring assembly consists of a rectangular aluminum beam frame and four aluminum trunnion subassemblies. Two of the trunnions are bolted to the engine through two Z-rings on the titanium chamber case, and the other two are bolted to the vehicle thrust mount struts. The thrust load is taken in shear across the bolts that fasten the trunnions directly to the chamber; the Z-rings do not transmit any thrust load. The trunnion bearings are single steel balls in a two-layer Teflon®-lined steel race.

2.1.4 Thrust Control Assembly

(U) The thrust control assembly (Figs. 5 and 6) includes the propellant shutoff valves, throttle actuator, flow-control valves, and injector.

2.1.4.1 Shutoff Valves

(U) The propellant shutoff valves are two-position, fuel-actuated, mechanically linked, series-parallel ball valves. The fuel and oxidizer valves each consist of four independent ball valves in series-parallel arrangement. The parallel arrangement provides redundancy for valve opening, and the series arrangement provides valve closing redundancy. Each fuel valve ball is mechanically linked to a corresponding ball in the oxidizer valve. In the normally closed position, the actuation fuel is shut off by the action of the spring-loaded plunger on the caged ball within the solenoid-operated pilot valve, and the actuator piston pressures are vented overboard. In the open position, the spring-loaded plungers are retracted by the solenoids, simultaneously sealing the overboard vents and permitting fuel to flow to the actuator pistons.

(U) The prevalve is a two-way, solenoid-operated valve located in the shutoff valve actuation line (Fig. 6). It is activated to the open position when the engine electrical circuits are armed. The prevalve is normally closed, functioning as a safety device to prevent propellant from being discharged overboard should the solenoid-operated pilot valve for the shutoff valve fail to seat properly in the closed position.

2.1.4.2 Throttle Actuator

(U) The throttle control is an electromechanical, linear servo-actuator which positions the fuel and oxidizer pintles of the flow control valve in response to an electrical command input signal. The unit is powered by three d-c motors connected to a common output shaft. The three motors drive the rotating member of an output jackscrew which

simultaneously adjusts the mechanical linkage connecting the flow control valve pintles and the injector metering sleeve for the desired throttle position.

2.1.4.3 Flow Control Valve

(U) The functions of the flow control valve are to provide mixture ratio control over the full range of operation and to maintain a linear throttle position versus thrust relationship for the engine. The flow control valve consists of a pair of mechanically linked, variable area venturi valves. The valve pintles are contoured to vary the fuel and oxidizer flow rates linearly with pintle displacement over the engine thrust range.

(U) At maximum thrust, the major portion of the controlling pressure drop (GAEC/TRW interface pressure minus chamber pressure) occurs in the injector manifold and orifices, and the engine operates as a calibrated fixed-thrust pressure-fed engine. As thrust decreases, the pressure drop across the flow control valves increases by an amount equal to the decrease in chamber pressure and the decrease in injector manifold pressure losses. At approximately 65 percent of rated thrust, cavitation occurs in the venturi throats, and propellant flow rates are controlled entirely by the flow control valve.

2.1.4.4 Injector

(U) The injector (Fig. 7) is a variable-area, single-coaxial-element, impingement-type injector with a regeneratively cooled face plate and a fuel manifold assembly. The primary fuel is injected through an annular gap between the face plate and the metering sleeve. Oxidizer is injected radially into the chamber through radial slots located in the oxidizer feed tube and the metering sleeve (the only moving part in the injector). The areas of the fuel and oxidizer metering orifices are controlled by movement of the metering sleeve. The sleeve moves axially approximately 0.15 in. over the engine operating range. Fuel for film cooling is injected through 36 equally spaced fuel orifices on the face plate and is directed onto the chamber walls.

(U) All metal parts in the injector are made from high temperature alloys of 17-4 PH® and Inconel 718®. The dynamic seals attached to the metering sleeve are two-ply nested bellows. The bearing between the element housing and the metering sleeve is a multiple-leaf-flexural bushing consisting of two concentric cylindrical tubes joined at each end by a series of thin circumferentially slotted disks. Relative axial movement between the tubes is permitted by flexing of the slotted disks.

2.1.5 HD-4 Propulsion Test Rig

(U) The main frame assembly of the HD-4 rig (Fig. 3) was fabricated of welded steel beams and angles with a bolted-on heat shield support assembly at the aft end. Both fixed and removable double-walled side panels were installed around the inside of the main frame assembly. An eight-piece LM base heat shield was mounted around the aft end of the rig, forming an eight-sided collar that surrounds the engine nozzle extension. The engine was equipped with a GAEC, one-piece, lightweight heat shield (Fig. 2) that fits around the radiation-cooled nozzle extension attachment flange and inside the periphery of the HD-4 rig heat shield. Provisions in the rig for mounting the engine include the engine truss mount, propellant supply lines, and gimbal actuators. For these tests, the gimbal actuators were removed, and rod assemblies were installed to hold the engine stationary.

2.1.6 Special Insulation

(U) Two types of special super insulation[1] were supplied and installed by GAEC during these tests to reduce the heat loss of the engine and compartment during the simulated altitude coasts. Similar insulation installations will be used on the flight vehicle. Twenty-five layers of 0.00025-in.-thick aluminized Mylar® (polyester resin) were draped and taped to the engine side of both the HD-4 rig base heat shield and the engine heat shield (Fig. 8). A nozzle thermal plug fabricated from five layers of 0.0005-in.-thick H-film (Kapton, polyimide resin) stretched over a Styrofoam® ring was glued to the divergent section of the ablative chamber nozzle at the 16:1 area ratio station (Fig. 9). This plug was installed to minimize the radiation heat transfer from the internal surfaces of the thrust chamber to the low temperature test cell environment. For the second test period (AB), in addition to the above insulation, 50 layers of aluminized Mylar were taped to the outside surface of the HD-4 rig blast deflectors, and the number of layers of H-film used on the nozzle thermal plug was increased from five to ten. For the third test period (AC), the insulation on the heat shields and nozzle thermal plug was identical to that used during the second test period; however, the upper half of the HD-4 rig blast deflector was removed, and a hole was cut in the +Z axis removable side panel to allow TV and motion-picture camera access to the engine headend. Fifty layers

---

[1]Multiple layers of lightweight, reflective film used for reducing the transfer of radiant heat in a near vacuum.

of aluminized Mylar were draped from the cameras to the HD-4 rig, tent fashion, to reduce radiation losses from the engine headend (Fig. 8).

2.2 INSTALLATION

2.2.1 Test Cell

(U) The Propulsion Engine Test Cell (J-2A) (Fig. 10 and Refs. 2 and 3) is a near-space simulation, rocket engine test chamber, capable of attaining pressure altitudes in excess of 300,000 ft. The test cell consists of a LN_2-cooled, 18-ft-diam, 30-ft-long, stainless-steel, thermopanel liner installed within the 20-ft-diam basic test cell ducting. The liner interior and all major test cell components were painted flat black to increase the absorptivity for thermal radiation. Independent pumping systems provide the high vacuum.

(U) The independent pumping systems consist of four mechanical vacuum pumps, two two-stage oil diffusion pumps, associated valves and ducting, and a cryogenic pumping system.

(U) The cryogenic pumping system consists of the LN_2-cooled liner and diffuser (-320°F) and 12 helium (He)-cooled 4- by 4-ft thermopanels (cryoplates) located symmetrically at the downstream end of the test cell liner (Fig. 10).

2.2.2 Radiation Systems

(U) The outside surface of the HD-4 rig was maintained at the desired temperature, while radiating to the test cell liner walls, by 12 rows of infrared heat lamps equally spaced around the liner. Each row normally contains 26 heat lamps on 6-in. centers. The five lamps in the downstream end of each row were removed for these tests so that the nozzle extension and downstream side of the LM base heat shield would receive no direct radiation. Four specially mounted variable output lamps located inside the HD-4 rig were directed at the engine headend to provide variable control of engine temperatures when required. Four additional lamps, mounted outside the HD-4 rig, were directed at the rig blast shield (upstream vertical panel) (Fig. 10) to control the blast shield temperature.

2.2.3 Thrust Measuring System

(U) The HD-4 rig containing the engine was mounted on a thrust cradle. The thrust cradle was suspended from an LN_2-cooled support structure by four vertical and two horizontal double universal flexure assemblies. Axial movement of the thrust cradle was restrained by the LN_2-cooled thrust butt through a temperature-controlled load cell (Fig. 10).

2.2.4 Diffuser System

(U) The exit plane of the exhaust nozzle extension was located at the LN_2-cooled diffuser inlet bulkhead. The outer diameter of a heated flexible silicon rubber seal was attached to the cooled bulkhead. The seal inner diameter was attached to the nozzle extension exit flange. The seal was used to minimize exhaust gas flow into the liner during and after an engine firing.

(U) The exhaust diffuser consists of a 72-in.-diam by 20.5-ft-long, LN_2-cooled section; a 72-in.-diam by 18-ft-long water-cooled section; a hydraulically operated 72-in.-diam multiple Mylar disk changer or restart valve; and a hydraulically actuated exhaust diffuser valve. The multiple disk changer provides the test cell with a 24 rocket-firing capability during a single test period and consists of twenty-four 20-mil Mylar disks, 24 disk mounting rings, a traversing disk holder, a hydraulic actuation system, and a pyrotechnic system for rupturing the disks. One disk is positioned in the exhaust diffuser duct to seal the liner from the facility exhauster pressure during high vacuum operation (when the exhaust diffuser valve is open), and the remaining disks are located under the exhaust diffuser duct in the disk holder inside the test cell exhaust ducting (20-ft-diam). The Mylar disk in the diffuser duct is cut away at engine ignition by pyrotechnics ignited by an electrical signal from a rocket thrust chamber pressure transducer. After an engine firing, the diffuser valve is closed, the 72-in.-diam exhaust diffuser duct is opened, the expended disk mounting ring is removed, and a new disk inserted. The duct is then closed, and procedures for the next firing are initiated. The disk changer is operated remotely from the J-2A control room.

(U) The exhaust diffuser valve is installed to prevent atmospheric pressure from rupturing the inplace disk during periods when the facility exhaust system (Ref. 4) is not required. Also, the valve is closed immediately after a firing to prevent an excessive pressure rise in the liner. During engine firings, the rocket exhaust gases serve as the driving fluid by which the supersonic diffuser, in series with the

facility exhaust system, maintains the pressure altitude at the nozzle exit plane of the engine (approximately 130,000 ft for throttle settings above approximately 27-percent thrust).

2.2.5 Propellant System

(U) The propellant system (Fig. 11a) consisted of a GN_2 pressurizing system; 1500-gal supply tanks; wire mesh supply line filters (one 40-μ absolute filter in each propellant supply line for test periods AA and AB, one 40- and one 25-μ absolute filter in each supply line for test period AC); flow measuring sections, each with two turbine-type flowmeters; temperature conditioning systems; recirculation circuits; and associated valves, pumps, and piping.

(U) Three recirculation circuits were used in each propellant system. The primary circuit allowed propellant recirculation from the supply tanks to the ARO/GAEC interface (test periods AA and AB) or to the 25-μ absolute filters (test period AC); the return line was 1 in. in diameter. The two secondary circuits allowed recirculation from the supply tanks to either the engine flow control valves or the engine shutoff valves, returning through 0.5-in.-diam lines.

(U) The oxidizer and fuel propellant supply systems were designed such that the dynamic pressure losses through each would be approximately equal.

2.3 INSTRUMENTATION

(U) Instrumentation systems were provided to obtain measurements of axial thrust; engine and test cell pressures and temperatures; propellant flow rates, pressures, and temperatures; and various engine accelerations, control voltages, currents, and actuator positions. All primary engine parameters were recorded redundantly on different recording systems.

(U) A statistical analysis was made to determine the estimated accuracy of the parameters affecting performance calculations. The statistical sum of these errors was determined using the methods described in Ref. 5. The estimated accuracies of axial thrust, oxidizer flow, and fuel flow are presented in Table IV.

2.3.1 Axial Thrust

(U) Engine thrust was measured with one 10,000-lb, dual-column, strain-gage-type load cell. To permit operation in a cryogenic environment, the load cell contained thermostatically controlled heaters and an external heater remotely controlled from the control room. The outputs from the load cell were recorded in analog form on light-beam oscillograph and null-balance potentiometer and in frequency form on magnetic tape. A deadweight calibrator was provided for calibration of the thrust measuring system at altitude before and after each firing. The calibrator consisted of a flexure-mounted balanced beam to which calibrated weights were suspended in steps of 100 and 150 lb up to a total of 1150 lb. The calibrator beam provided a known mechanical advantage, and incremental axial loads up to approximately 11,500 lb were applied to the thrust cradle. The applied loads were measured with a secondary standard at sea level and were corrected for buoyancy loss of the weights at altitude and thrust butt deflection under thrust load.

2.3.2 Pressure

(U) Propellant system and engine pressures (Figs. 11a and b) were measured with strain-gage-type transducers. The transducers used to measure propellant system line pressures, shutoff valve inlet pressures, and injector manifold pressures were mounted near the pressure source inside the test cell.

(U) Thrust chamber pressure was measured by five transducers, four of which were strain-gage type connected to a manifold from a single tap located on the injector. Two of the four transducers were used for data, and two were used to provide a chamber pressure signal to activate the pyrotechnic system for rupturing the diffuser Mylar disk. The fifth was a TRW-supplied Model 615A Kistler® piezoelectric pressure transducer close coupled to the injector with the Model 504 Kistler charge amplifier for recording high frequency fluctuations during the engine starting transient. The output was transmitted to an additional d-c amplifier to obtain dual-range (0 to 200 and 0 to 1000 psia) signals for recording in analog form on light-beam oscillograph and in frequency form on magnetic tape. The thrust chamber pressure data acquisition system was inplace certified by a direct comparison with a secondary standard. The Kistler transducer used a GHe purge, which was initiated at ignition fire switch -0.5 sec, for cooling and to improve the frequency response of the data.

(U) Test cell pressure was measured with three variable-capacitance pressure transducers and five ionization gages. The ionization gage data were recorded in analog form on null-balance potentiometers, and the three transducer channels were recorded in frequency form on magnetic tape.

(U) All transducers were laboratory calibrated with a secondary standard before installation in the test cell and after completion of testing. Before, during, and at the end of each test period, the pressure transducers were calibrated by an electrical, four-step, resistance substitution calibration using precision resistances in the transducer circuits to simulate selected pressure levels. The ionization gages and capacitance-type transducers were laboratory calibrated using a secondary standard.

2.3.3 Engine, HD-4 Rig, and Propellant Temperatures

(U) Temperatures were measured on the test article with Chromel®-Alumel® and copper-constantan thermocouples at the locations shown in Fig. 11. Immersion thermocouples were used in each propellant system at selected locations to measure propellant temperature. The electrical outputs from the thermocouples were recorded on magnetic tape by an analog-to-digital commutating data system and were converted to engineering units and tabulated by a digital computer. Propellant temperatures downstream of the flowmeters were measured by resistance temperature transducer probes, recorded in frequency form on magnetic tape, converted to engineering units, and tabulated by a digital computer. Selected temperature measurements from thermocouples used to monitor the engine, test cell components, and propellant system temperatures were recorded on null-balance potentiometers located in the test cell control room.

2.3.4 Propellant Flow Rates

(U) Two turbine-type flowmeters were installed in each propellant feed line to measure propellant flow rates (Fig. 11a). The outputs of the flowmeters were recorded in frequency form on both a light-beam-type oscillograph and magnetic tape and in analog form on null-balance potentiometers. The flowmeter outputs were also converted to instantaneous digital and analog displays of mixture ratio in the control room. The flow measuring sections, consisting of the flowmeters, flow straighteners, and tubing, were bench calibrated before and after the test series, utilizing both water and propellants as the flowing media. The bench calibration data obtained using the propellants were used to

reduce the flowmeter data for the engine performance calculations presented in this report. The flow measuring recording systems were calibrated before, during, and after each test period by applying a known frequency at the flowmeter electrical connector to simulate a selected flowmeter output.

(U) Two null-balance, two-axis plotters were located in the control room to give a direct indication of fuel and oxidizer flow, mixture ratio, throttle-actuator-command voltage, and throttle position during the firing.

2.3.5 Vibration

(U) Nine piezoelectric-type accelerometers (Figs. 11b and e) provided acceleration measurements along the three principal axes (X-X, Y-Y, Z-Z) of the test article. These accelerometers were mounted on the injector, gimbal ring, and truss assemblies. All accelerometers were spanned to 1000 g's except for those on the injector for test period AC, which were spanned to 2000 g's. The data were recorded on both magnetic tape and lightbeam oscillograph. The frequency response range was 0 to 5000 cps on the magnetic tape and 0 to 2000 cps on the lightbeam oscillograph.

2.3.6 Visual Coverage

(U) Three motion-picture cameras and two closed-circuit television cameras were used to provide permanent documentation of test article operation and continuous visual monitoring, respectively. The pre- and post-fire conditions of the test articles were documented by still photographs.

SECTION III
PROCEDURE

3.1 TESTING

(U) Pre-test procedures included electrical and mechanical checks, pressure checks, and a final inspection of the test article. The propellant tanks were loaded, and samples were taken from each tank and analyzed to determine the specific gravity and that the applicable propellant specification requirements were met. The diffuser restart valve Mylar disk pyrotechnic circuits were installed, instrumentation calibrations were performed, and the test cell pumpdown was initiated followed by test cell chilldown as described in Refs. 2 and 3.

(U) Prior to chilldown, the propellant lines were vented to the reduced test cell pressure. The propellant bleed-in was then accomplished by permitting pressurized propellants to flow to the engine through the evacuated propellant lines. The high points in the propellant system and the liquid pressure transducers outside the test cell were manually rebled to allow any entrained gas to escape. During the cell pumpdown and chilldown, the propellant system and bulk temperatures of the propellants in the tanks were maintained at approximately 40°F by use of the propellant temperature conditioning system and the recirculation systems. The engine and HD-4 rig were maintained at approximately 70°F by using the test cell thermal radiation systems and specially installed heaters both inside and outside the HD-4 rig. When stable test cell temperatures and pressures were reached, all heat sources within the HD-4 rig were secured, and the test cell radiation system was adjusted to maintain the rig surfaces at 40 to 50°F. The outside surfaces of the double-walled rig panels were used as the temperature control surfaces for test period AA and AB and the inside surfaces for test period AC. Propellant recirculation through the engine was discontinued prior to starting coast periods. For coast periods AA and AB, propellants were recirculated at 40 ± 5°F to the ARO/GAEC interface. Recirculation to the 25-μ absolute filters was accomplished during coast period AC (see Fig. 11a).

(U) During the altitude coast periods, stagnant propellants were in the engine and HD-4 rig propellant lines simulating the conditions which will exist in flight. The heat input to the HD-4 rig by the test cell thermal radiation system simulated the heat source of the flight vehicle propellant tanks which surround the engine compartment. The downstream side of the HD-4 rig base heat shield and engine nozzle extension, which in the flight vehicle would view the heat sink of space, were allowed to radiate directly to the -320°F LN_2-cooled surfaces of the test cell aft heat shield and diffuser. Installation precautions were taken to ensure that no surfaces downstream of the base heat shield viewed direct radiation from the test cell thermal radiation system. Prior to each engine firing, instrumentation altitude calibrations were performed, the facility exhausters (Ref. 4) were valved to evacuate the J-2A exhaust ducting, and propellant recirculation was stopped. In addition, the propellant systems were pressurized, the exhaust diffuser valve was opened, and the LN_2 flow to the diffuser was increased. After these test procedures were performed, the engine firing was initiated. The diffuser Mylar disk pyrotechnic detonation system cut the disk from the diffuser to allow the rocket exhaust gases to be pumped away by the facility rotating exhausters.

(U) After engine shutdown, the exhaust diffuser valve was closed, the next exhaust diffuser restart valve Mylar disk was positioned in the diffuser, the LN_2 flow to the diffuser was reduced, and post-fire instrumentation calibrations were performed. The propellant tanks were vented to 40 psia, and the propellant temperature conditioning systems were reactivated.

(U) At the completion of each test period, the thermal radiation system and propellant recirculation systems were utilized to maintain engine and propellant system temperatures near 70°F during the test cell warmup, and ambient conditions were restored in the test cell as outlined in Ref. 2. The test cell was opened, and post-test procedures were performed on the test article and test cell.

(U) A test summary is included in Table V.

3.2 DATA REDUCTION

(U) The three major divisions of the data reduction effort which support the testing reported herein proceeded chronologically from quick-look, to primary, to performance data.

3.2.1 Quick-Look Data

(U) During the space simulation coast periods preceding the first firings of each test period and during the periods between the firings, temperatures on the HD-4 rig and engine were monitored at 30-min intervals and on demand. The data were presented in tabulated engineering units. The same commutating digital system used for recording the above was used during the firings to record selected temperatures, pressures, and thrust which were used as inputs for a basic quick-look engine performance program. Data from strip charts and oscillograms were reduced manually between firings as backup information to the quick-look performance program.

(U) The accelerometers and Kistler chamber pressure transducer signals recorded on magnetic tape were converted to oscillograms for wave analysis and determination of peak accelerations and pressures immediately after each firing. The magnitude of these data aided in determining thrust set conditions and propellant and hardware set temperatures for the next firing.

3.2.2 Primary Data

(U) Data recorded on magnetic tape using the commutating digital and analog-to-frequency conversion systems provided the highest accuracy and greatest utility data and are considered the primary data. Generally, the commutating digital system was used to record temperatures and other low-response parameters. The analog-to-frequency systems provided better response rates and were used to record pressures, thrust, flows, and selected temperatures, voltages, and currents. These data were presented in tabulated engineering units at the conclusion of each test period.

3.2.3 Performance Data

(U) Primary data from the analog-to-frequency systems and manual inputs were used to calculate the classic rocket engine performance parameters of vacuum corrected thrust (F_V), mixture ratio (MR), total flow (W_t), vacuum specific impulse (I_{sp_V}), characteristic velocity (c*), vacuum thrust coefficient (C_F), and other parameters of interest. These data were tabulated in engineering units printed at 0.5- and 0.1-sec intervals.

3.2.3.1 Vibration

(U) In addition to the quick-look data reduction, a machine wave analysis was made to determine the frequency content and the root-mean-square acceleration values for the firings of particular interest after the test period.

3.2.3.2 Thrust

(U) Thrust was redundantly recorded, and each of the data channels was converted to lb_f using scale factors obtained from the deadweight calibrations. The calibrator was certified before and after each test series using a secondary standard traceable to the National Bureau of Standards. Vacuum thrust (F_V) was calculated from

$$F_v = F_M + P_a A_e - A_{se}(P_{exp} - P_a) \qquad (1)$$

where:

F_M = Measured thrust, lb_f

P_a = Test cell pressure, psia

P_{exp} = Diffuser pressure, psia

and the nozzle seal effective area (A_{se}) was determined by applying a known differential pressure across the nozzle exit area (A_e) and seal area and measuring the force (F_d) on the thrust measuring system with a 500-lbf load cell. Then,

$$A_{se} = \frac{F_d}{P_{exp} - P_a} - A_e \tag{2}$$

Percent of nominal rated vacuum thrust ($\%F_V$) was calculated from:

$$\%F_V = \frac{F_V}{10{,}500} \times 100 \tag{3}$$

3.2.3.3 Thrust Chamber Pressure

(U) Thrust chamber pressure measured at the injector face was redundantly recorded on magnetic tape, and four of the five channels (the Kistler chamber pressure data were presented in wave form only) were converted to engineering units using scale factors obtained from laboratory calibrations of the transducers. The average of the chamber pressure data (P_{ch}) was adjusted to a total pressure at the nozzle throat (P_{ch_t}) by the relationship

$$P_{ch_t} = 0.975\, P_{ch} \tag{4}$$

where the factor 0.975 was supplied by the engine manufacturer. The flight-type chamber pressure transducer data were not used in any of the engine performance calculations because of erroneous data.

(U) Percent of nominal rated chamber pressure was calculated from:

$$\%P_{ch_t} = \frac{P_{ch_t}}{107.3} \times 100 \tag{5}$$

3.2.3.4 Engine Performance Parameters

(U) Vacuum specific impulse (I_{sp_V}), characteristics velocity (c*), and thrust coefficient (C_{F_V}) were calculated from the following equations:

$$I_{sp_v} = F_V/\dot{W}_t \tag{6}$$

$$c^* = \frac{P_{ch_t} A_t g}{\dot{W}_t} \tag{7}$$

$$C_{F_v} = F_V/A_t P_{ch_t} \tag{8}$$

where:

$\dot{W}_t$ = Total propellant flow, lb_m/sec

g = Dimensional constant, 32.174 lb_m-ft/lb_f-sec^2

A_t = Pre-fire throat area, $in.^2$

3.2.3.5 Operating Times

(U) Shutoff valves actuation time (t_S) was determined from data recorded on oscillograms as follows:

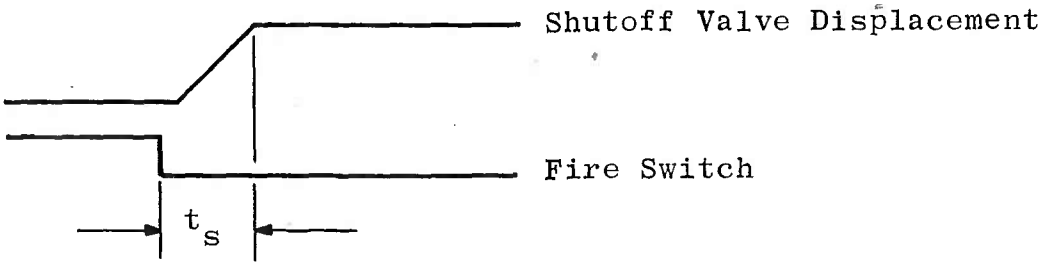

(U) Chamber pressure rise time (t_{ch}) was determined from oscillograms as follows:

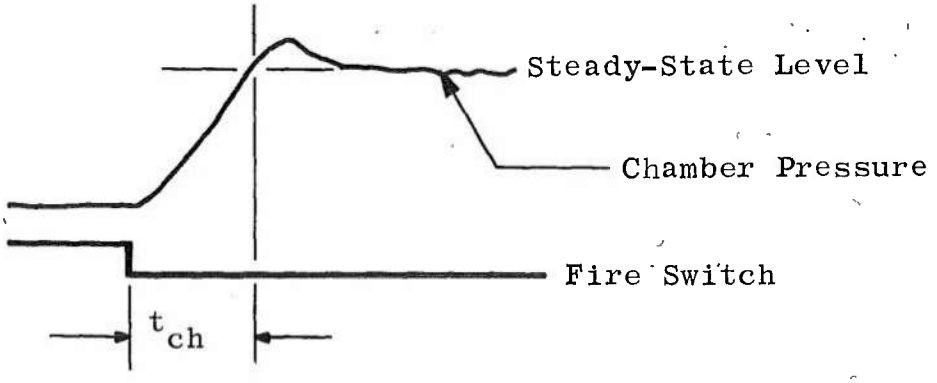

3.2.3.6 Mixture Ratio Adjustment

(U) Engine operating mixture ratio is a function of the propellant supply pressures. Since the LMDE was designed to operate with interface pressures matched to within 2 psi, it is helpful, for observing the adequacy of the engine flow control capabilities, to perform a mixture ratio adjustment to account for mismatched propellant interface pressures.

(U) Engine propellant flow conductance from the engine interface to the chamber for oxidizer (C_{ox}) and fuel (C_f) was calculated for each firing during steady-state operation using the following equations:

$$C_{ox} = \frac{\dot{W}_{ox}}{\sqrt{(P_{I_{ox}} - P_{ch})\, SG_{ox}}} \qquad (9)$$

and

$$C_f = \frac{\dot{W}_f}{\sqrt{(P_{I_f} = P_{ch})\, SG_f}} \tag{10}$$

where:

$\dot{W}$ = Flow rate, lb_m/sec

P_I = Interface pressure, psia

SG = Specific gravity

$( )_{ox}$ = Oxidizer

$( )_f$ = Fuel

For small changes in interface pressure at a fixed throttle setting, Eqs. (9) and (10) describe with negligible error the steady-state hydraulic characteristics of the LMDE. By imposing the restraints of equal interface pressures, dividing Eq. (9) by Eq. (10), and rearranging, an equation for adjusted mixture ratio (MR_A) to account for mismatched interface pressures was obtained:

$$MR_A = \frac{C_{ox}}{C_f} \sqrt{\frac{SG_{ox}}{SG_f}} \tag{11}$$

SECTION IV
RESULTS AND DISCUSSION

(U) The results of testing two LMDE during three separate test periods under the simulated pressures and thermal radiation environment of outer space while housed in a heavy-duty mockup of the LM engine cavity are discussed.

(U) Each of the three test series began with a simulated space coast to determine the various engine component temperatures at the end of the earth-moon transit and to determine the thermal insulating qualities of the engine compartment or HD-4 rig. The thermal data obtained were used by GAEC to determine the accuracy of the heat-transfer mathematical models used for design of the LM and establishment of the LMDE thermal design specifications.

(U) After each of the space simulation coast periods, a series of firings ranging from constant-thrust-level 3-sec firings to throttling tests of 50-sec duration were conducted. The coast periods between firings ranged from 3.3 to 38.2 hr depending on the desired hardware and propellant temperature for the succeeding firing.

(U) The firing numbers from the three test series are identified by test period (AA, AB, and AC) and by consecutive numbers (AA-01 through AC-25) (see Table V).

(U) The coast thermal data are discussed followed by an analysis of the engine steady-state operating characteristics, engine ignition and combustion stability, and mechanical difficulties.

4.1 SIMULATED SPACE COASTS

(U) Thermal coast data were obtained during the 73.6-hr period prior to test AA-01, the 74.8-hr period preceding test AB-04, and the 51.5 hr prior to test AC-22. The temperature data have been averaged to show engine component temperature histories for each of the three coast periods. For comparison, some data taken during Project No. RL1433 (Ref. 1) are also shown.

(U) The AB coast period was considered the best simulation of the space environment of the three coast periods. During coast AA, a recirculation valve was incorrectly left open which allowed 40°F propellants to recirculate through the oxidizer flow control and shut-off valves until approximately 47 hr into the coast, thereby affecting engine temperatures. In addition, oxidizer leakage and subsequent evaporation inside the HD-4 rig affected temperatures on the engine headend. During soak AC, modifications were made to the HD-4 rig (see Section 2.1.6) in support of other test objectives which violated, to some extent, the authenticity of the HD-4 rig as a true simulation of the LMDE flight cavity.

(U) An average of the HD-4 rig panel temperatures during coast AB and the data spread band are shown in Fig. 12. These data are representative of the panel temperatures for all three coasts and show the heat-sink temperature to which the engine headend radiated. The data band encloses the HD-4 rig panel temperatures and is less than 10°F wide.

(U) The average temperature of the inside surface of the ablative chamber at the throat is shown in Fig. 13 for all test periods. Five layers of H-film were used on the nozzle radiation plug (see Section 2.1.6) for coasts AA and AB and 10 layers for coast AC. There is no significant difference in throat temperature as a result of the difference in the radiation plugs.

(U) Flow control and shutoff valve temperature histories are shown in Fig. 14. Flow control valve temperature data from Ref. 1 are presented for comparison. Shutoff valve temperature data were not available from Ref. 1. Engine valve temperatures appeared to stabilize at approximately 40°F in approximately 24 hr for all test periods. The decrease in the temperature of the valves to 35°F during coast AA is believed to be the combined result of an intentional lowering of the bulk propellant temperature to 30°F, oxidizer leakage within the HD-4 rig, and closing of the oxidizer recirculation valve at the engine (Event 4, Fig. 14a). The bulk propellant temperature was lowered from the nominal 40 to 30°F to investigate heat transmission to the engine from the propellants which were being recirculated to the ARO/GAEC interface (Fig. 11a). During coast period AB, the bulk propellants were maintained at a temperature below the temperature of the engine valves to remove the possibility of heat transmission to the engine from the conditioned propellants. During coast period AC, propellants were recirculated to the 25-μ filters in the propellant supply lines only (see Section 3.1). The sudden increase and subsequent decrease in valve temperatures occurring between 14 and 19 hr into the AB soak is the result of 3.8 hr of propellant recirculation through the engine, which occurred during engine leak checks.

(U) Injector pintle temperature histories are shown in Fig. 15. The pintle tip temperature from cold soak AA was invalid and has been omitted. The effect of the nozzle radiation plug can be seen in these data. No plug was installed for the RL1433-AD soak, five layers of H-film were used for soak AB, and 10 layers for soak AC (see Section 2.1.6). The pintle tip temperature using the 10-layer plug was about 11°F higher than that obtained without the plug after a coast of 28 hr.

(U) The geometry of the chamber, throat, and radiation plug is such that less than one percent of the energy radiated by the engine headend would be directly incident upon the radiation plug; therefore, any significant heat losses by the headend through the throat would be preceded by decreasing temperatures in the ablative chamber. Therefore, the histories of the pintle tip temperature for the two radiation plug configurations tested exhibit similar slopes and relatively little difference in terminal temperatures. An analysis of these data and other external engine headend temperatures suggests that the radiation losses of the injector through the throat to space are quite small as compared with the radiation heat gain potential from the HD-4 rig panels to the external surfaces of the engine headend.

(U) It can be concluded generally from these simulated coast periods that the engine headend and flow control components stabilized within 5°F of the temperature at which the HD-4 rig panels are maintained.

4.2 ENGINE STEADY-STATE PERFORMANCE

(U) Although the primary purposes for conducting these tests were to determine thermal characteristics in a space environment and engine start characteristics over a matrix of propellant temperatures and throttle levels, it is of interest to examine the steady-state performance. A summary of steady-state performance is presented in Table VI for test periods AA and AB.

(U) All data presented in this section are a 1-sec average taken during the last second of engine operation, or in the case of firing AB-14, which was a throttling firing, during the last second at each throttle level. No performance data are presented for test period AC because of contaminants in the engine propellant flow passages which resulted in improper engine operation.

(U) The relationship between throttle actuator command voltage and total propellant flow is shown in Fig. 16. The design specifications for the LMDE require a linear relationship between these parameters, and, as may be seen, such is the case. The spread in these data are attributed largely to the effects of (1) the slight deviation of propellant interface pressures from design, (2) propellant viscosity differences as a result of varying the propellant temperatures over the range from 40 to 120°F, and (3) injector pintle damage subsequent to firing AB-18. By neglecting firings AB-19, -20, and -21 during which anomalies were known to exist, all propellant flow data fall within approximately a 1.5-percent band of linearity.

(U) The relationship between vacuum thrust and command thrust is shown in Fig. 17. Ideal performance is represented by the 45-deg sloped line. All firings below 30-percent command thrust resulted in deceptively high thrust because the low chamber pressure was insufficient to produce exhaust gas jet attachment to the diffuser; therefore, the optimum ejector action of the diffuser was not attained. The resulting back pressure caused the exhaust flow to separate from the nozzle extension; consequently, data from these firings have been omitted. The thrust data recorded during firing AB-14 at thrust levels above 30 percent are unexplainably high and are not shown. It is hypothesized

that these force data were influenced by thermal gradients in the base heat shield which caused the shield to deform and interact with the stationary propellant lines which, in the HD-4 rig, are routed close to the shield. The effect of injector pintle damage, which will be discussed in Section 4.4.2, while readily apparent in firing AB-21, is less obvious in firing AB-20.

(U) Mixture ratio during steady-state operation as a function of percent of rated propellant flow is shown in Fig. 18. These data are presented as measured in relation to the mixture ratio specification envelope (Ref. 7). The general trend of the data is toward decreasing mixture ratio with decreasing total propellant flow. Data scatter also increased with decreasing flow rate as would be expected since the accuracy of the propellant flow measurement decreases with decreasing flow. The effects of any mismatch in interface propellant supply pressures and varying propellant temperatures also contribute to the scatter of the data at all flow rates.

(U) To fully understand all the effects of mixture ratio, it is necessary to examine engine flow conductance and the relationships that exist between mixture ratio, propellant temperature, and throttle level.

(U) Engine flow conductances from the engine propellant interfaces to the chamber were calculated by the methods presented in Section 3.2.3.6 and are shown as a function of percent of total flow in Fig. 19. Firing AB-07 is of particular interest in this figure. The unusually low mixture ratio already seen in Fig. 18 is depicted here as 91 percent of rated fuel flow and 98 percent of rated oxidizer flow. As explained in Section 2.1.4.3, propellant flow rate into the chamber is controlled primarily by the cavitating flow control valves at flows below approximately 65 percent and by the injector oxidizer and fuel metering orifices above 65 percent. A mechanical stop is used in the throttle actuator to limit the maximum throttle position to 94 percent of rated thrust at approximately 95.5 percent of rated propellant flow. When the engine is being operated at 94-percent thrust, the throttle actuator is normally driven hard against the stop by using a slight excess of command voltage. The command voltage used for firing AB-07 was 13.64 v, which corresponded to approximately 92.5 percent of rated thrust, and consequently the throttle position was determined by the feedback and servosystems of the throttle actuator, as is normal for all throttle positions below 94 percent, rather than the mechanical stop. Thus, it appears that mixture ratio control by the engine in the noncavitating mode of operation, except where hard against the maximum thrust stop, should be investigated further if operation in this region is anticipated.

(U) It can be concluded from Fig. 19 that no malfunctions occurred in the engine, which significantly affected the engine flow conductance, and that the relationships between interface pressure, propellant temperatures, chamber pressures, and flow rates may be legitimately examined and compared for all firings in determining engine operation.

(U) Mixture ratio adjusted for mismatched propellant interface pressures by the procedure presented in Section 3.2.3.6 is shown in Fig. 20 as a function of propellant temperature. Lines of constant thrust level are also shown. The trend toward decreasing mixture ratio with decreasing total propellant flow, which was first seen in Fig. 18, is quite obvious in this figure. A trend toward decreasing mixture ratio at the higher propellant temperatures is also readily apparent. Data from firings AB-07, at approximately 92.5-percent thrust, and the 60-percent thrust level of firing AB-14 are the only data that do not conform to the trend of decreasing mixture ratio with decreasing total flow. A cross plot of the nominal 70°F mixture ratio data shown in Fig. 20 with the data averaged at the target thrust levels is shown in Fig. 21 as a function of total flow. Based on the data available, the profile shown depicts the mixture ratio control capabilities of engine P1009 when operated at near the design propellant temperature of 70°F and equal oxidizer and fuel interface pressures. The mixture ratio data at both rated and 10-percent thrust fall outside the specification envelope.

(U) Characteristic velocity as a function of propellant temperature is shown in Fig. 22 with lines of constant thrust level. It can be seen that high propellant temperature had a pronounced effect on combustion efficiency particularly at 10-percent thrust. As propellant temperature was increased, the rate of propellant vaporization at a given pressure also increased. Since the vapor pressure of the oxidizer is higher than that of the fuel, the vaporization rate of the oxidizer is greater.[1] At 10-percent thrust, a larger percentage of the total propellants flashed to vapor than at the higher thrust levels. Design chamber pressure for the LMDE at 10-percent thrust is approximately 11 psia. Chamber pressure for firings AB-12 and AB-16, which were the only two firings conducted with propellants at a nominal 120°F and at 10-percent thrust, never exceeded 6.5 psia. It is surmized that the impingement and

---

[1]At 120°F the vapor pressures of N_2O_4 and AZ-50 are approximately 50 and 6 psia, respectively (Ref. 8).

mixing of vaporized oxidizer and two-phase fuel in the thrust chamber at the very low thrust levels and high propellant temperatures resulted in low combustion efficiency.

(U) The low c* values for firings AB-19, -20, and -21 are the result of injector damage which is discussed in Section 4.4.2 of this report.

(U) Characteristic velocity as a function of chamber pressure for the nominal 70°F propellant temperature firings is shown in Fig. 23 with shifting equilibrium and frozen flow theoretical performance. This comparison indicates that the efficiency of the injector is very good over a wide range of chamber pressure. The low performance for firings AB-07 and -21 has been discussed previously. At 10-percent thrust, the resolution error in the flow rate data is approximately 3 percent, which could easily account for the low value of characteristic velocity for firing AB-15.

(U) Vacuum thrust coefficient is shown as a function of mixture ratio with theoretical shifting equilibrium and frozen flow curves in Fig. 24. A definitive relationship between propellant temperature and C_{F_V} is evident in this figure. The data also indicate a maximum C_{F_V} at a mixture ratio of about 1.64.

(U) Vacuum specific impulse as a function of mixture ratio is shown in Fig. 25 with lines of constant throttle level. All data exceed the specification minimums of Ref. 7. A maximum value of 311.4 lb_f-sec/lb_m was recorded during firing AB-11. Over the range investigated, a trend toward decreasing specific impulse with decreasing mixture ratio and throttle level is evident. No 10- and 20-percent thrust level data are shown because the nozzle extension was not flowing full, and no data from firings AB-20 and -21 are shown because injector damage resulted in low thrust.

4.3 COMBUSTION INSTABILITY

(U) During the AA and AB test periods of the LMDE, eight of the 21 firings were unstable during ignition. The instability occurred during six of the eight 30-percent thrust ignitions and for firings AB-19 and -20 which were 20- and 35-percent throttle levels, respectively.

(U) Combustion instability or "rough burning" may be attributed to a number of variables including ignition pressure altitude, thrust chamber and injector design, hardware/propellant temperatures,

physical and chemical properties of the propellants, and design of the propellant feed system. All of these have some effect on ignition delay. Combustion instability may be classified broadly into three categories: low, intermediate, and high frequency modes (Ref. 10). The low frequency, or "chugging" mode, ranges up to approximately 50 cps and is usually associated with interaction of the combustion chamber and propellant feed system impedance. The intermediate frequency mode usually ranges from 100 to 1000 cps and is usually related to the resonance of various structural components and vortex formation in the fluid flow through an irregular system, usually of minor concern. The high frequency or "screaming" mode varies from 500 cps up and is associated with the chamber acoustical frequency modes. These are given in Ref. 7 for the LMDE as follows: First tangential mode - 1750 cps; first spinning mode - 1750 cps; and first radial mode - 3500 cps.

(U) Ignition experience with nitrogen-based storable propellants has shown that ultrahigh altitude and low propellant/hardware temperatures are conducive to ignition overpressures in the combustion chamber commonly referred to as hardstarts (Ref. 11). This was shown to be related to ignition delay, the longer ignition delays being more conducive to hardstarts. Ignition delays are also conducive to initiating combustion instability.

(U) For the LMDE tests, the data were analyzed in specific thrust level groups, of which the 30-percent level was of primary interest because instability occurred most frequently at this level. The following parameters were considered in this analysis of ignition transients and were based on data taken from the fire switch signal to the beginning of steady-state operation:

1. Ignition delay
2. Mixture ratio
3. Chamber pressure
4. Acceleration data

(U) It was also desirable to consider the propellant temperature representative of the first slug of reactants to enter the combustion chamber. Because no propellant temperature probes existed downstream of the flow control valves, the skin thermocouples installed on the propellant ducting between the flow control valves and the shutoff valves were used for obtaining the stagnant-propellant temperatures. The AA series oxidizer duct reference temperature was adjusted to the trend of the simulated altitude coast data to compensate for the oxidizer leak which affected the skin temperatures by evaporation.

4.3.1 Ignition Delay

(U) Ignition delay is defined herein as the time interval between initial movement of the propellant shutoff valves and the initial combustion chamber pressure rise. This time interval includes the time required to fill the volume from the shutoff valve to the injector/chamber interface.

(U) Figure 26 illustrates that ignition delay is a function of propellant temperature and affects the lower thrust levels to a larger degree. By considering the 30-percent thrust data, up to 230-msec difference in ignition delay was obtained from approximately 22 to 77°F. Figure 27, which is shutoff valve actuation time as a function of propellant temperature, exhibits some data scatter but shows that actuation time is apparently independent of temperature and, therefore, does not contribute to the ignition delay trends seen in Fig. 26. Shutoff valve actuation time for all AA and AB test series firings are shown in Table VII.

4.3.2 Mixture Ratio

(U) Mixture ratio during ignition was determined from the flowmeter data during the time interval between initial flow (first flowmeter movement) and initial combustion chamber pressure rise. A decreasing mixture ratio trend with increasing propellant temperatures, already seen during steady-state operation and shown in Fig. 20, is evident in Fig. 28.

4.3.3 Chamber Pressure

(U) Other than the accelerometers, the only high response instrumentation installed on the engine was the Kistler Model 615A piezoelectric-type transducer. However, post-test investigation of the Kistler transducer revealed that the data were biased by the high acceleration levels and chamber combustion gas temperatures. Therefore, a quantitative analysis of these data is meaningless. For comparative purposes, however, it is believed that the first positive ignition shock is representative of the severity of the instability and was utilized in Fig. 29 to show the relationship between chamber pressure and ignition delay. The firings exhibiting combustion instability had larger chamber pressure peaks at the longer ignition delays.

4.3.4 Acceleration Data

(U) The zero-to-peak g values recorded during the two test periods are contained in Table VIII. Both the first ignition spike and the maximum peak g during the ignition period are given for the thrust axis accelerometer.

4.3.4.1 Test Period AA

(U) Data recorded during this period varied from zero g's to greater than the calibrated upper limit of 1000 g's zero-to-peak. Firing AA-01 (30-percent thrust) was unstable from ignition to approximately 450 msec. Accelerations in the longitudinal or thrust axis were most severe, and values greater than 1000 g's zero-to-peak were recorded on the injector.

(U) Firings AA-02 (94-percent thrust) and AA-03 (10-percent thrust) appeared to function normally with no evidence of instability. A maximum acceleration of 180 g's peak was recorded on the injector along the thrust axis for firing AA-02 with negligible levels being recorded from all accelerometers for firing AA-03.

4.3.4.2 Test Period AB

(U) This test period consisted of 18 firings; five at 10 percent, seven at 30 percent, four at 94 percent, and one each at 20 and 35 percent. The temperatures of the propellants were varied and were approximately 40, 70, and 120°F.

(U) All of the 30-percent thrust level firings again showed the same unstable ignition characteristics as AA-01 with the exceptions of AB-10 and -13. These were the only two at the 30-percent level with 120°F propellants (72 to 78°F duct temperatures). The warmer propellants are associated with shorter ignition delays contributing to smoother ignition transients.

(U) Anomalies existed in firings AB-07 and -11 (94 percent) and in firing AB-18 (10 percent); these consisted of high g loadings during a randomly occurring instability period of approximately 10- to 100-msec duration during engine steady-state operation. A time correlation of accelerometer, combustion chamber, and propellant system data proved that the instability occurred in the chamber proper and was not induced by the propellant feed system.

(U) Firings AB-19 through AB-21 exhibited a more severe instability than previous ignitions under comparable conditions. AB-19

was unstable for the entire firing duration, whereas AB-20 and -21 consisted of a number of randomly occurring instability periods. These firings occurred after the injector pintle damage discussed in Section 4.4.2.

4.3.4.3 Analyses

(U) The acceleration data levels during the unstable ignitions were consistently higher than the accelerometer linear calibration range of 1000 g's. Initial ignition shock levels as a function of average propellant temperature and ignition delay are shown in Figs. 30 and 31, respectively. These accelerations are not necessarily the largest values obtained during the ignition, and only 30-percent thrust level data are shown. Trends can be seen that follow the accepted theory; that is, longer ignition delays and lower propellant temperatures are conducive to harder starts or combustion instability.

(U) A typical accelerometer and combustion chamber pressure waveform of an unstable ignition is shown in Fig. 32. A power spectral density (PSD) graph of the same time interval (approximately 450 msec) is shown in Fig. 33 for firing AA-01. The frequency is representative within ±30 cps, and the g^2/cps values are of comparative value. (The PSD graphs presented herein are representative of a single statistical data sample.) The PSD graph of the longitudinal or thrust axis accelerometer revealed that most of the energy occurred at 2800 and 3340 cps with minor peaks at 60 and 180 cps. The waveform agreed with the raw data (Fig. 32) in that the large amplitude shock pulses start with a 40-cps frequency and build up to 140 cps at the end of the instability. The damping frequency of the combustion shock approximates the 2800- to 3300-cps response. This is believed to correspond to the three previously mentioned combustion chamber acoustical frequency modes or harmonics thereof. The majority of the instability energy occurs as a high-frequency function rather than the low-frequency combustion shocks. A time correlation of propellant system interface, engine injector, and chamber pressures showed that the initial shock originated in the combustion chamber.

(U) Power spectral density graphs of firings AB-05 and -14 (Figs. 34 and 35) reveal a slightly different spectrum. It is not known whether the response change is a statistical data variation or an engine characteristic change. However, firing AB-19 (Fig. 36) shows a significant response spectrum change. These data are representative of a 1270-msec combustion instability period which occurred after the ignition shock. It is surmized that this change in instability spectrum is the result of the injector pintle damage discussed in Section 4.4.2.

4.3.5 Recapitulation

(U) During the LMDE tests, the combustion instability encountered was characterized by short-duration, random, low-frequency pressure spikes with a high-frequency damping component. The magnitude of the pressure spikes was approximately 2 to 3 times nominal chamber pressure; corresponding accelerations measured on the thrust chamber were in excess of 1000 g's peak.

(U) Six of the eight 30-percent thrust firings had combustion instability periods of from 180- to 1270-msec duration. The two 30-percent thrust firings that did not exhibit combustion instability were at the 72 to 78°F duct temperatures and had approximately 8 msec shorter ignition delays. Both the longer ignition delays and higher acceleration levels were found to be associated with the lower propellant temperatures. The engine propellant shutoff valve actuation time was unaffected by propellant temperature.

(U) The cause of the combustion instability is unknown. However, the instability at ignition is thought to be triggered by pressure pulses which are functions of ignition delay and the resulting reaction characteristics of the propellants. Classification of the instability into one of the basic theoretical combustion chamber modes was not possible. It was evident from a time correlation that the initial shock originated in the combustion chamber and was transmitted through the injector assembly into the injector manifolds. This is characterized by the injector manifold pressure exhibiting a similar unstable waveform corresponding to the combustion instability period, but occurring later in time.

4.4 MECHANICAL DIFFICULTIES

(U) The following incidents occurred relative to the reliability of the test article during the conduct of the tests reported herein.

4.4.1 Sticking Propellant Shutoff Valves

(U) Approximately 27 days elapsed between test period AA, during which the engine shutoff valves operated normally, and test period AB when difficulties were encountered. Flushing of the valves with the engine installed in the test cell after test period AA was not allowed by TRW because of possible damage to the ablative chamber by the flushing agent. Therefore, the engine flow passages downstream of and including the shutoff valves were subjected to 5 min of GN_2 purge and 10 min of 0.5-psia aspiration followed by 2 hr of purge with 140°F GN_2 for cleaning.

(U) Considerable difficulty was experienced by TRW personnel in opening the shutoff valves during the engine functional checks which immediately preceded test period AB (Ref. 12). During the subsequent test firings AB-05, -06, -07, and -08, the "A" set of propellant shutoff valves failed to open (Fig. 5). Valve sets "A" and "B" of the four sets were the only two equipped with linear potentiometers for recording the actual movement of the valves. Operation with one set of shutoff valves allowed normal engine operation with a negligible increase in propellant dynamic pressure losses because of the reduced flow passage area. During disassembly of the engine at TRW, Redondo Beach, California, contaminants were reported found in the shutoff valve balls, but no analysis was conducted to determine the nature of the foreign particles.

(U) Propellant gumming and/or salting which accumulated between test periods AA and AB and contaminants in the fuel were the probable cause of the sticking shutoff valves.

4.4.2 Injector Pintle Damage

(U) The injector pintle metering sleeve and tube were damaged apparently during the ignition of firing AB-19 (Ref. 12). Figure 37 shows the extent of the damage, and Fig. 38 is an oscillogram showing the AB-19 ignition and the indication of a pressure rise within the oxidizer passages as sensed by the oxidizer injector pressure transducer 1.05 sec after the ignition signal. The peak pressure was approximately 173 psia as compared with the normal 20-percent thrust level valve of 75 psia. It should be recognized that the peak pressure within the cavity between the pintle tube and the sleeve may have been several times the peak pressure measured by the oxidizer injector pressure transducer since the oxidizer flow passages and the cavity in which the explosion undoubtedly occurred are separated by the pintle tube (Fig. 7). Examination of the engine performance data, particularly characteristic velocity (Fig. 22), shows a marked performance degradation commencing with firing AB-19 with indications of degenerating performance during firing AB-18.

(U) Oxidizer injector conductance as a function of oxidizer flow is shown in Fig. 39. A noticeable increase in oxidizer conductance from the injector to the chamber occurred commencing with firing AB-20; however, conductance during firing AB-19 appeared normal. Thus, it would appear that the pintle damage occurred progressively, commencing as early as firing AB-18 with more conclusive evidence of damage occurring during firings AB-19 and -20. The change in conductance from the

injector to the chamber is not seen in the conductance from the interface to the chamber (Fig. 19) because the pressure drop across the injector is a relatively small portion of the drop from the interface to the chamber with flow cavitation (approximately 30 percent at 30-percent thrust). Therefore, a small change in injector conductance is not evident in the overall engine conductance. The reversal in the conductance curve at approximately 50 percent of rated flow was also evident in the data taken by TRW at the Capistrano test site for engine P1009 prior to shipment to AEDC.

(U) Various injector purging techniques have been used during the two LMDE test programs conducted at AEDC in Propulsion Engine Test Cell (J-2A). In all cases, gaseous nitrogen was admitted to the fuel duct and the oxidizer duct of the engine downstream of the shutoff valves.

(U) During the first test project (Project RL1433), an ignition purge was sequenced on two seconds prior to fire switch and off at one second after fire switch. A shutdown purge was initiated at shutdown and secured at shutdown plus 10 sec. No difficulties were experienced using this technique for 12 firings.

(U) During test periods AA and AB of the second test project (Project RL1618) only, a shutdown purge commencing at shutdown plus 5 sec and ending at shutdown plus 15 sec was used. The injector damage is believed to have occurred near the end of test period AB after 18 firings had been accomplished.

(U) To possibly circumvent this problem during the next test period (AC), a drain valve and associated plumbing was attached to the low point of the injector fuel manifold and was terminated in the facility exhaust diffuser. The shutdown purge sequence was as follows:

Shutdown + 5 sec	Start oxidizer purge
Shutdown + 10 sec	Start fuel purge and open fuel manifold drain valve
Shutdown + 130 sec	Stop fuel purge and close fuel manifold drain valve
Shutdown + 135 sec	Stop oxidizer purge

(U) No difficulties were encountered; however, only four firings were conducted using this procedure (AC series).

(U) Current planning for the LM flight vehicle does not include an injector purge for the LMDE at either start or shutdown. According to TRW, GAEC, and NASA, the post-fire purges used during all of the J-2A tests were necessary to clear the injector of propellants which remained in the injector low points because of the horizontal attitude of the engine during J-2A testing. Residual propellants in the injector were advanced by TRW as a possible cause of the explosion which damaged the injector pintle (Ref. 12). It is probable that propellants will remain in the injector passages after engine shutdown in the weightless environment of space when no shutdown purge is used. Since no internal injector leakage could be found by TRW during post-test engine inspections which would permit propellants to enter the cavity through the bellows, it was concluded that fuel and oxidizer entered the cavity between the metering sleeve and the pintle tube (Fig. 7) near the oxidizer discharge ports, a condition which is as likely to occur in a weightless environment as in a horizontal attitude. The implications as to the possibility of a recurrence of this failure mode should be of immediate concern for the flight vehicle.

4.4.3 Flow Control Valve Damage

(U) During the four firings of the last test period (AC), mixture ratio control was extremely erratic. Post-test investigations revealed that the seats in six facility valves had disintegrated and contaminated the engine flow control mechanisms. Further investigations by the engine manufacturer disclosed a crack in the oxidizer flow control valve cruciform which supports the upstream end of the flow control valve pintle and a pin hole leak in the fuel ducting between the flow control valve and the shutoff valve. No performance data were analyzed from these four firings.

SECTION V
SUMMARY OF RESULTS

(U) Two Lunar Module Descent engines were tested in the J-2A test cell during three test periods. The results of these tests are included below:

1. Combustion instability was encountered during six of the eight 30-percent throttle level firings.
2. The combustion instability was found to be primarily a function of propellant temperature and ignition delay.

3. The only stable 30-percent throttle level firings were those with 120°F bulk propellant temperature.
4. The 10- and 94-percent throttle starts were generally more stable at all propellant temperatures than the 30-percent firings.
5. A time correlation revealed that the accelerometer and chamber pressure initial shocks occurred prior to the injector manifold and propellant interface pressure responses, indicating that the instability originated in the combustion chamber.
6. An explosion which apparently occurred during the ignition transient of firing AB-19 damaged the injector pintle. Mixing of propellants in the cavity between the pintle tube and the metering sleeve imploded the pintle tube and ejected five teeth of the metering sleeve.
7. Valve set "A" of the redundant two-position propellant shutoff valves stuck in the closed position during firings AB-05 through -08.
8. The engine headend and flow control mechanism stabilized within 5°F of the HD-4 rig panel temperatures, or between 35 and 40°F.
9. The injector pintle temperature for the coast with the 10-layer radiation plug stabilized at 39°F, or 3°F higher than for the 5-layer plug.
10. Insignificant chamber throat temperature differences as a result of the 5- and 10-layer radiation plugs were recorded. The temperature stabilized at approximately 14°F after 56 hr.
11. Vacuum specific impulse, which maximized at 311 $lb\text{-}sec/lb_m$ at 94-percent throttle and mixture ratios above 1.60, showed a decreasing trend with both decreasing mixture ratio and throttle level.
12. All vacuum specific impulse data exceeded the minimum specifications.
13. Characteristic velocity data fell between theoretical shifting equilibrium and frozen flow for throttle levels between 30 and 94 percent.

14. Characteristic velocity was a strong function of propellant temperature exhibiting a general decrease with increasing propellant temperature and a pronounced decrease at the 120°F temperatures and 10-percent throttle.

15. Mixture ratio was found to be a strong function of throttle level, varying from approximately 1.46 to 1.63 over the thrust range from 10 to 94 percent of rated with 70°F propellants.

16. An apparent discontinuity in mixture ratio control capabilities existed for engine P1009 at near 94-percent throttle.

17. Vacuum thrust coefficient showed definitive relationships with both mixture ratio and propellant temperature, exhibiting a maximum value at a mixture ratio of approximately 1.63 and at the higher propellant temperatures.

REFERENCES

1. Farrow, K. L., Matkins, E. H., and Gernstein, T. M. "A Performance Evaluation of the Integrated LEM descent Stage Throttlable Engine and Engine Compartment at Altitudes from 100,000 to 300,000 ft." AEDC-TR-66-122 (AD374883), August 1966.

2. Ansley, S. P., Jr. "Cryogenics as Applied to the Design and Fabrication of a Space Simulation Test Cell." AEDC-TR-62-201 (AD293898), January 1963.

3. Reeves, J. R., Jr. "General Description and Performance of the Propulsion Engine Test Cell (J-2A)." AEDC-TDR-64-138 (AD444326), August 1964.

4. Test Facilities Handbook (6th Edition). "Rocket Test Facility, Vol. 2." Arnold Engineering Development Center, November 1966.

5. Harper, C. W. "Analysis of the Accuracy of Liquid-Propellant Rocket Engine Performance Measurements in the Propulsion Engine Test Cell (J-2A)." AEDC-TR-65-51 (AD460563), April 1965.

6. Minzer, R. A., Champion, K. S. W., and Pond, H. L. "The ARDC Model Atmosphere, 1959." AFCRC-TR-59-267, August 1959.

7. STL LEM Engine Characteristics Report. (U) GAEC Para. No. 5.1, STL No. 8438-6020-SC001, 4 December 1964, including Amendment 3 page 38-a, GAEC Spec. No. LSP-270-6, 1 June 1965. (Confidential)

8. "Performance and Properties of Liquid Propellants." Revision A, Aerojet-General Corporation, June 1961.

9. Goldford, A. and Haupt, C. "Theoretical Performance of Nitrogen Tetroxide-Aerozine-50 Propellant System." Grumman Aircraft Engineering Corporation, Report No. LED-271-2, August 20, 1963.

10. Sutton, G. P. Rocket Propulsion Elements. Third Edition, John Wiley and Sons, Inc., New York, 1963.

11. Barebo, R. L., Ansley, R. C., and Runyan, R. B. "Start Investigation of the Modified XLR 81-BA-13 Rocket Engine in a Simulated Space Environment." AEDC-TR-66-134 (AD488518), August 1966.

12. TRW LEM Descent Engine Preliminary Analysis, AEDC Test Series Engine 1009, TRW No. 01827-6036-T000, November 7, 1966.

APPENDIXES

I. ILLUSTRATIONS

II. TABLES

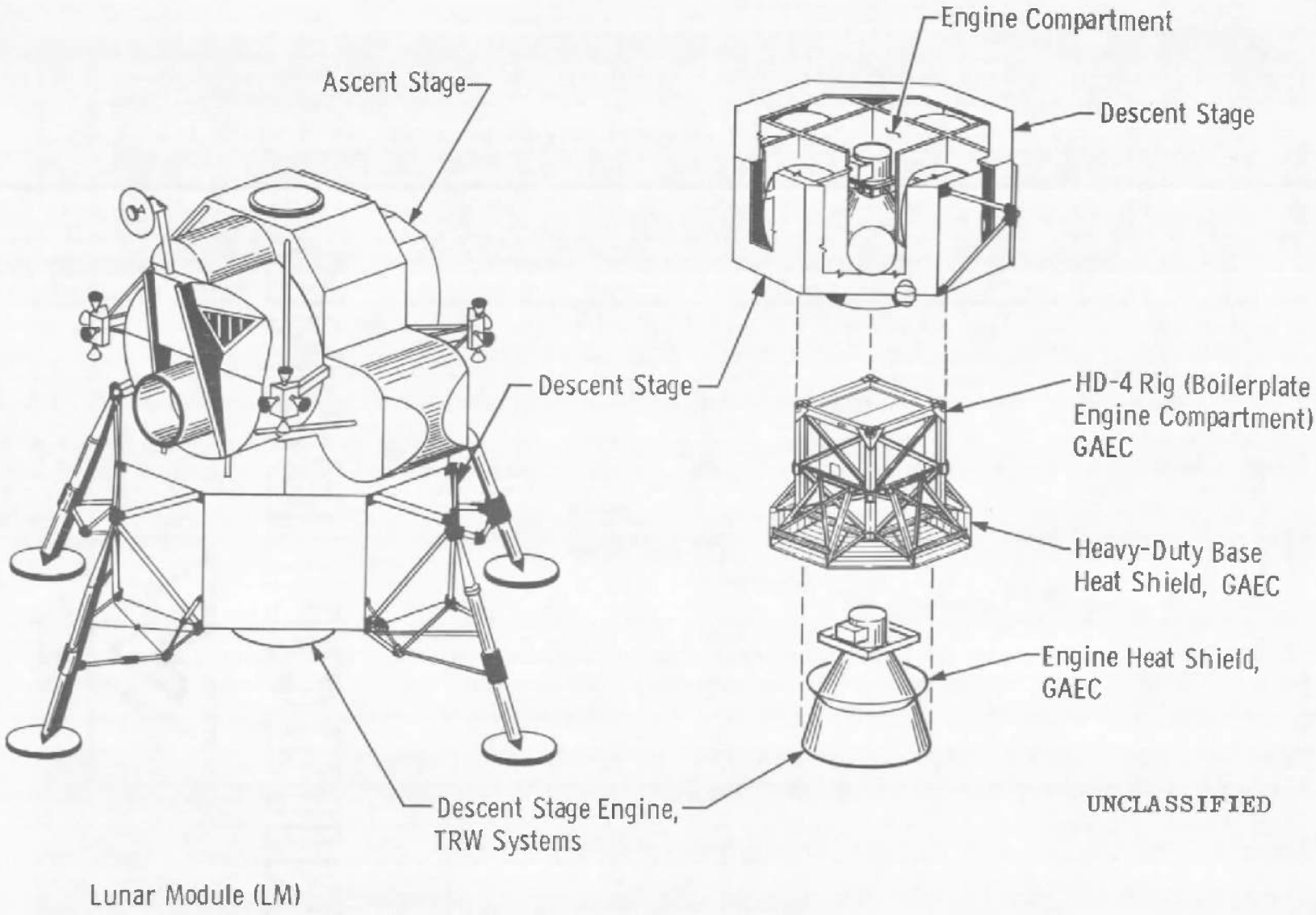

Fig. 1 Relationship of the Test Articles to the Lunar Module

UNCLASSIFIED

AEDC-TR-67-87

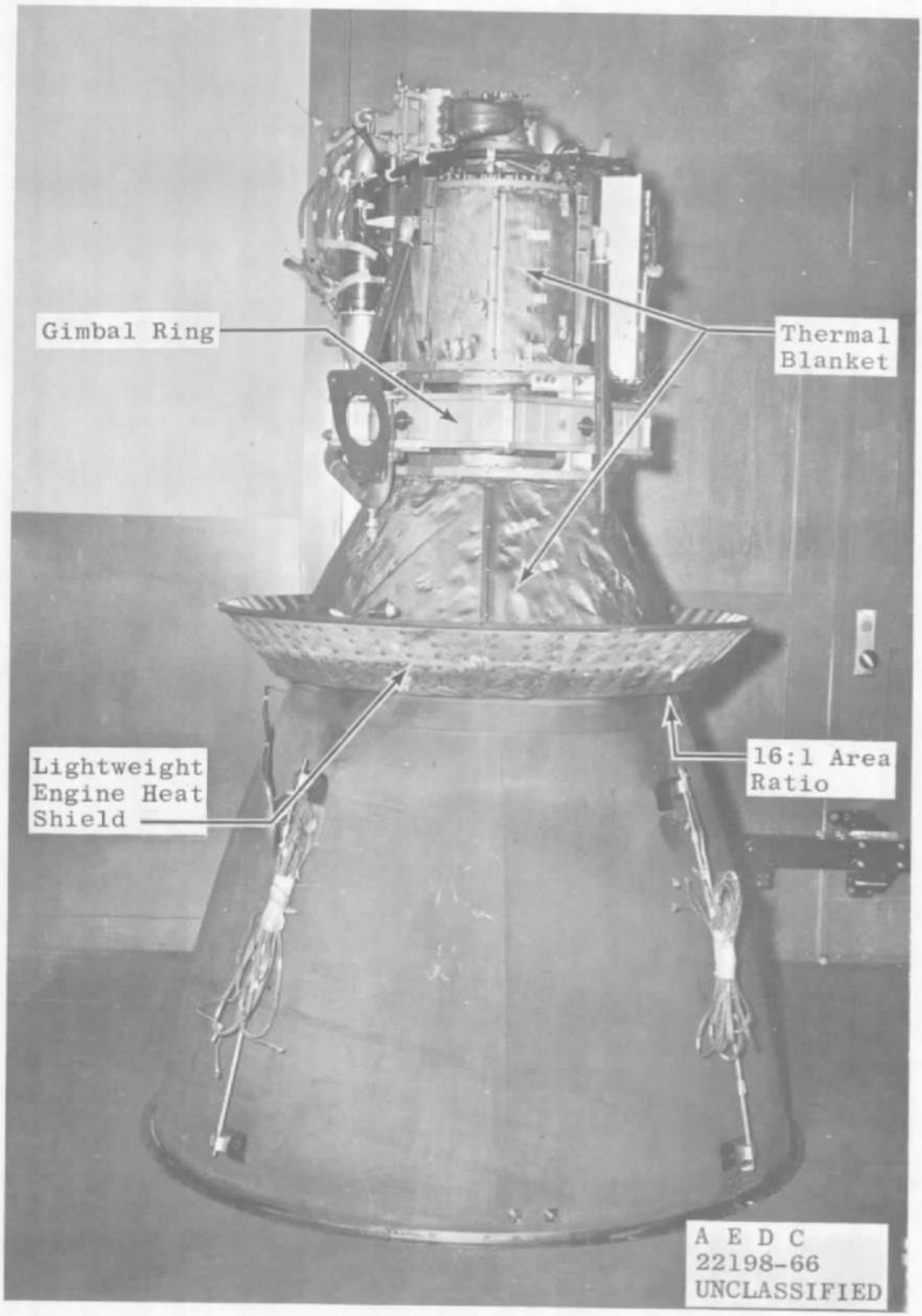

Fig. 2 LM Descent Engine

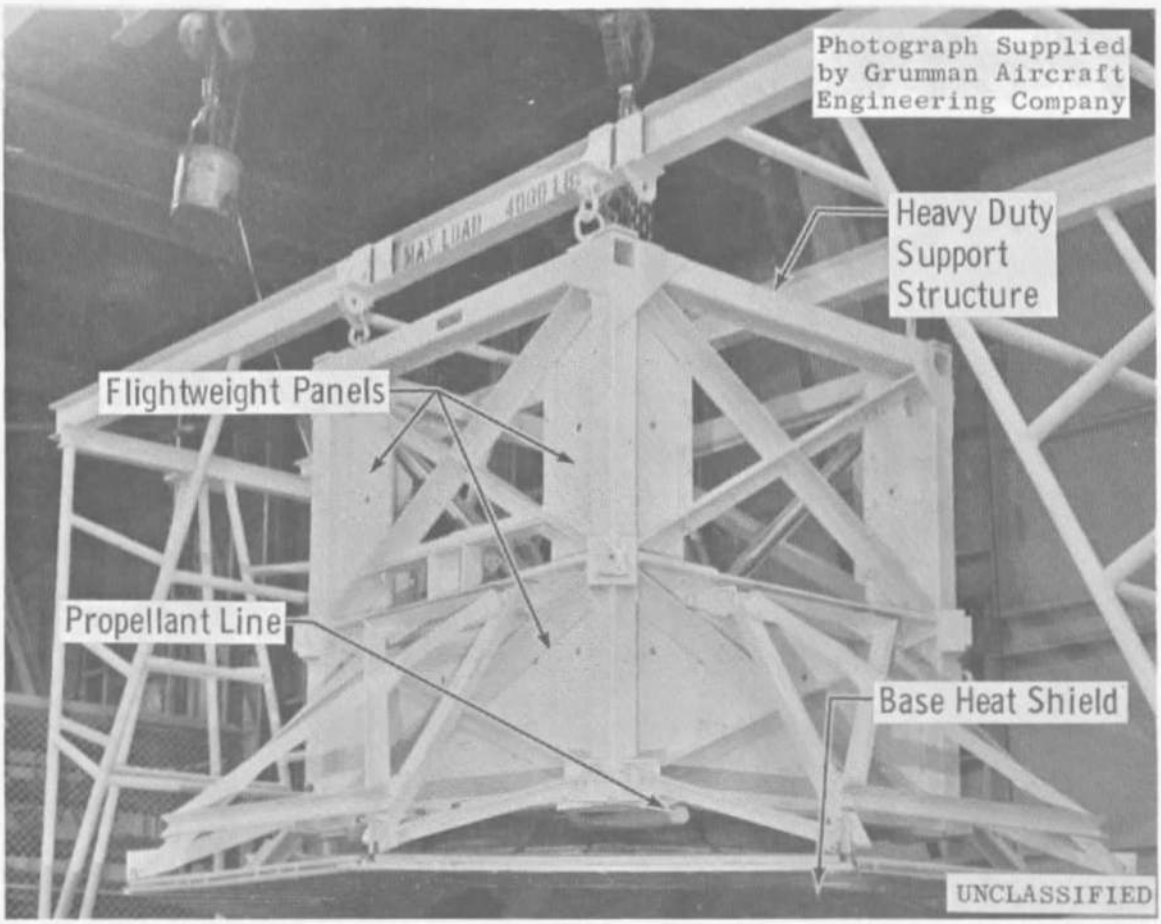

Fig. 3 Engine Compartment (HD–4 Rig)

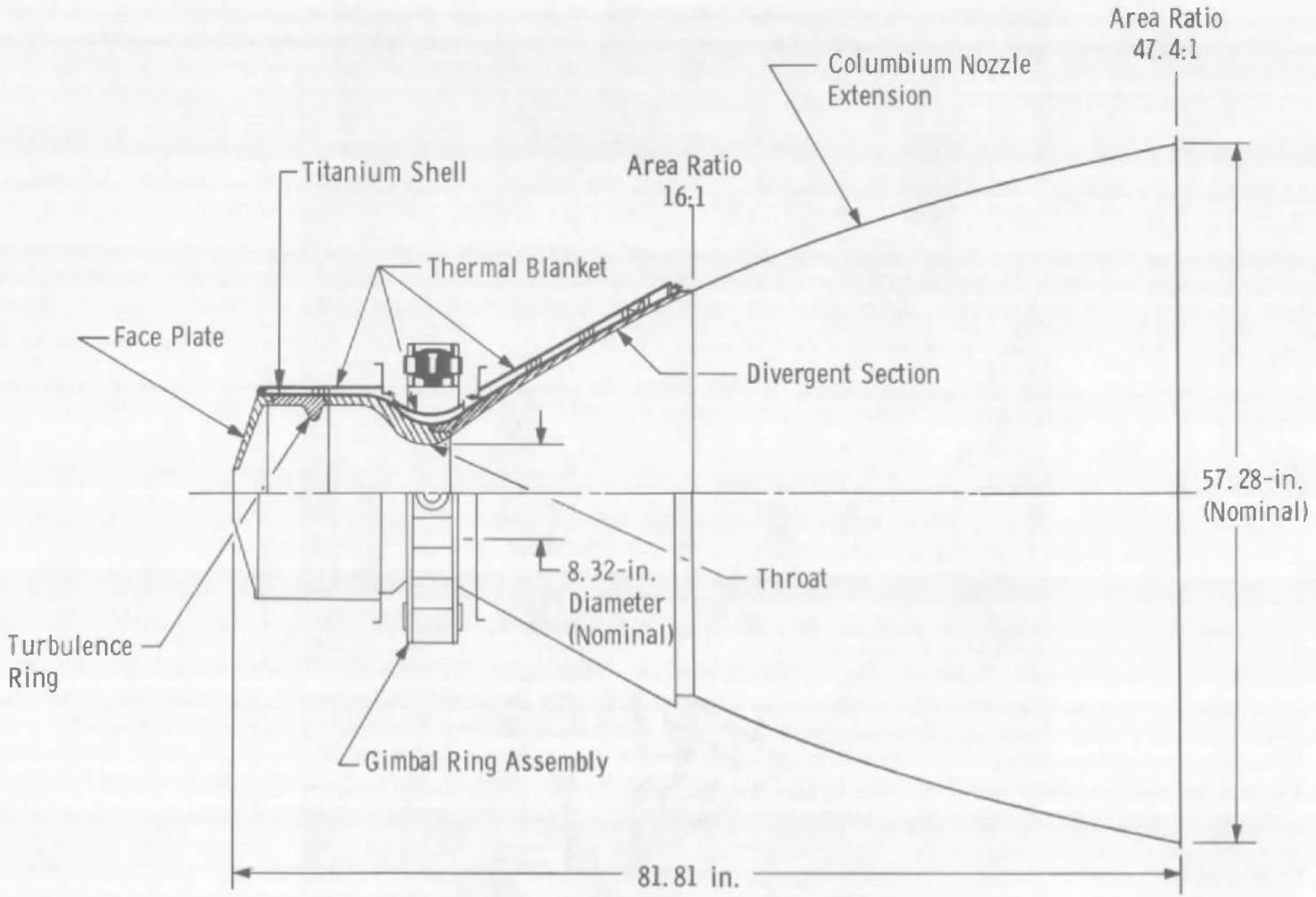

UNCLASSIFIED

Fig. 4 Cross Section of the LMDE Chamber and Nozzle Extension

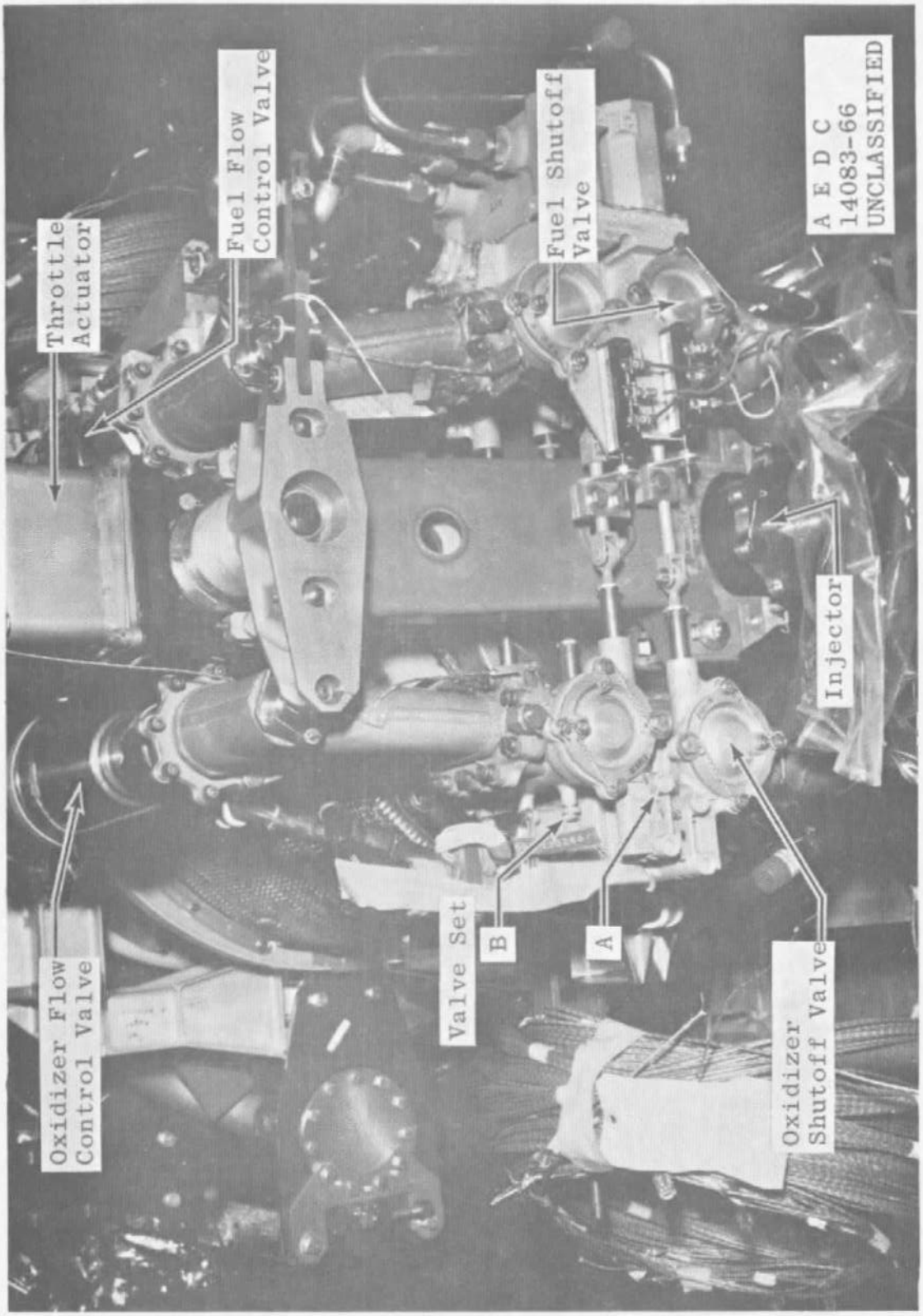

Fig. 5 Thrust Control Assembly

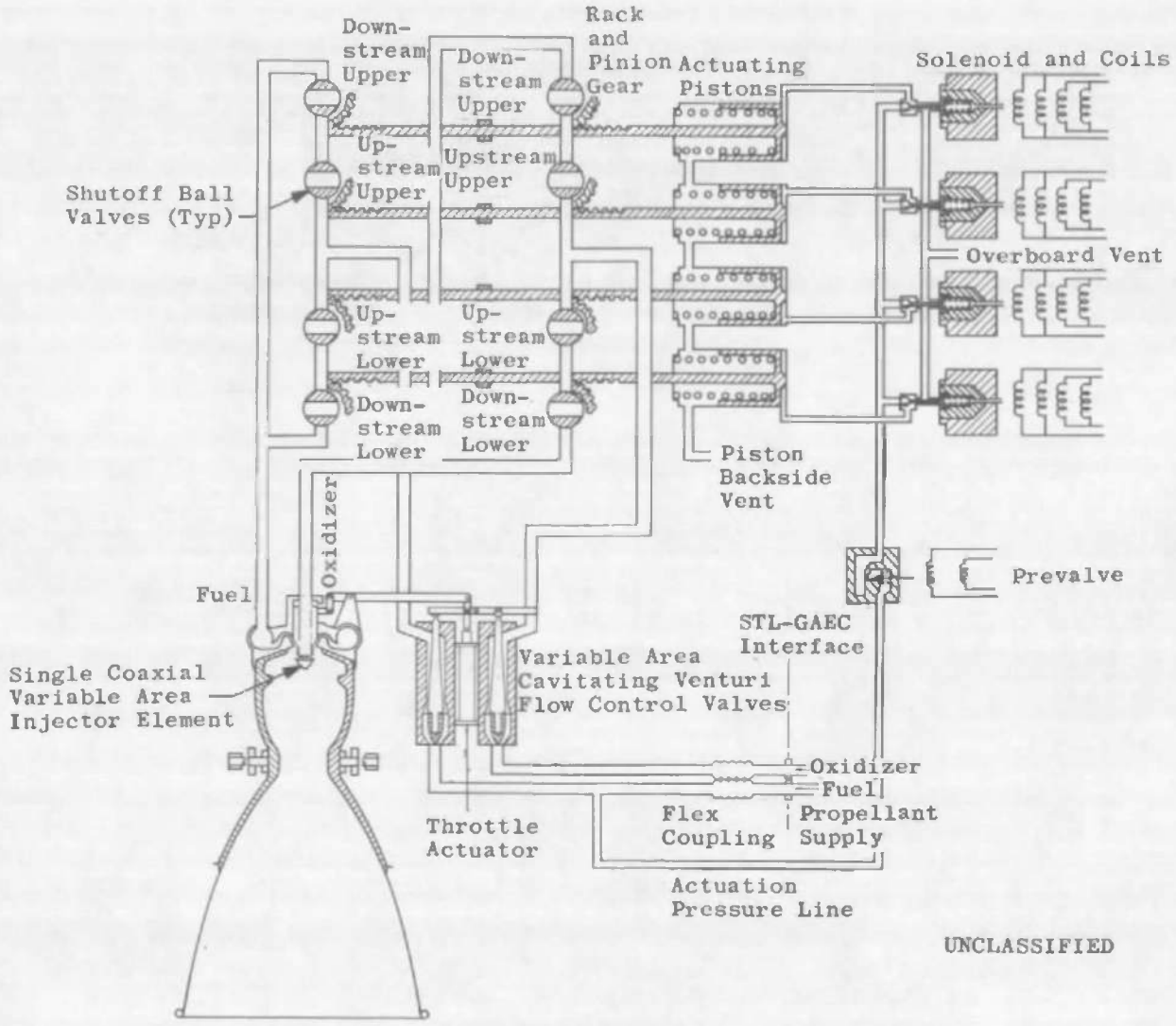

Fig. 6 Schematic of the Thrust Control System

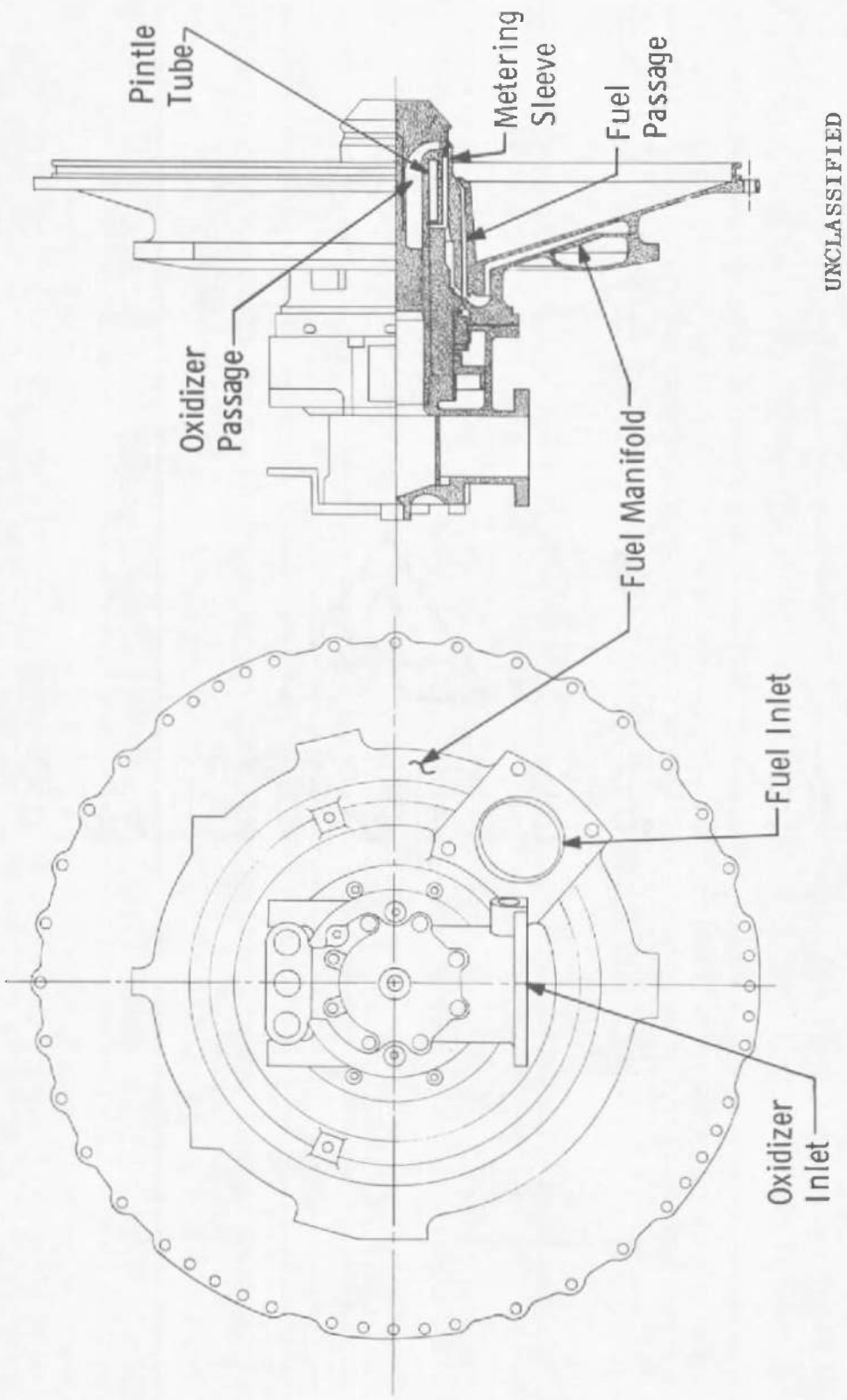

a. Assembly

Fig. 7 Propellant Injector

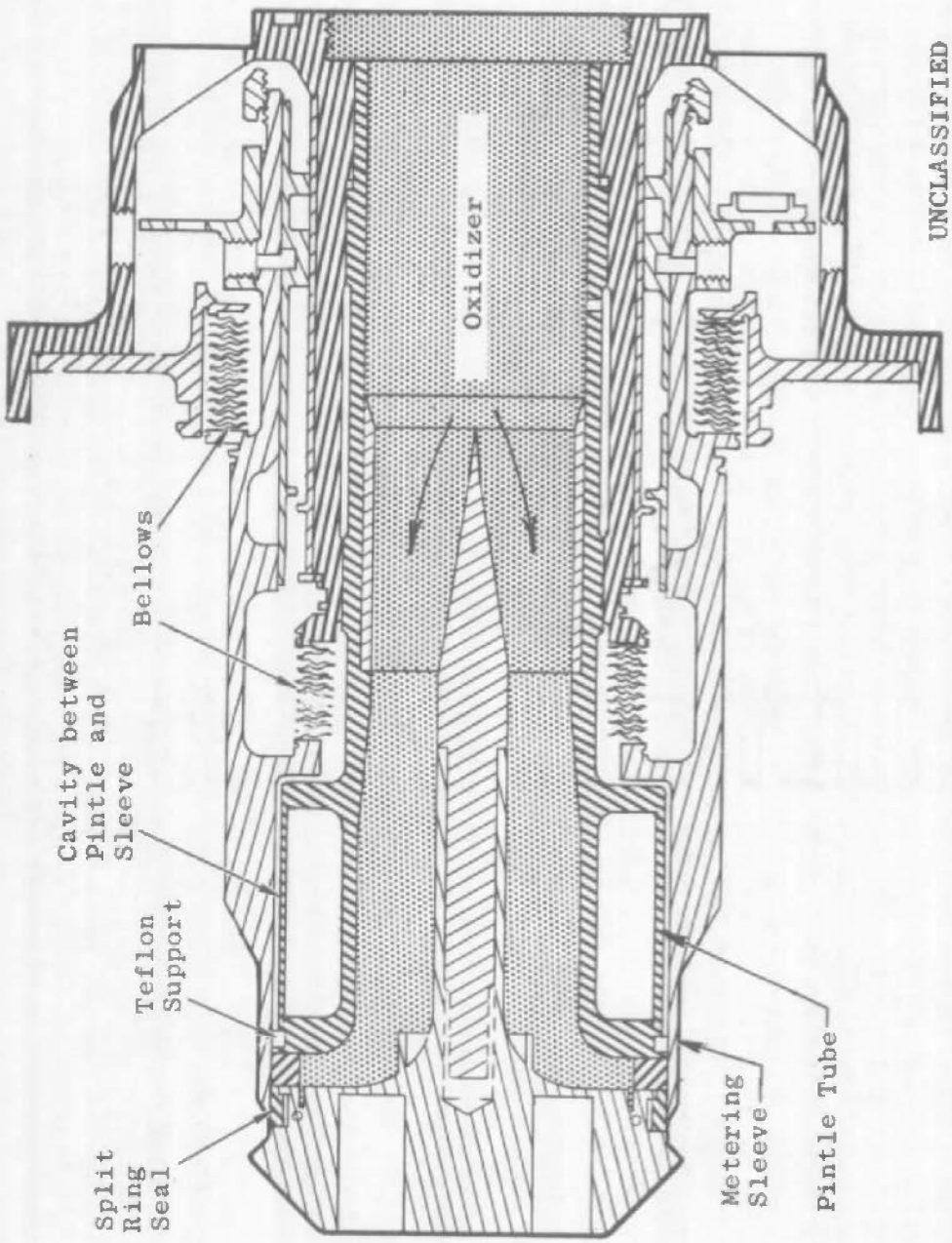

b. Pintle Schematic

Fig. 7 Concluded

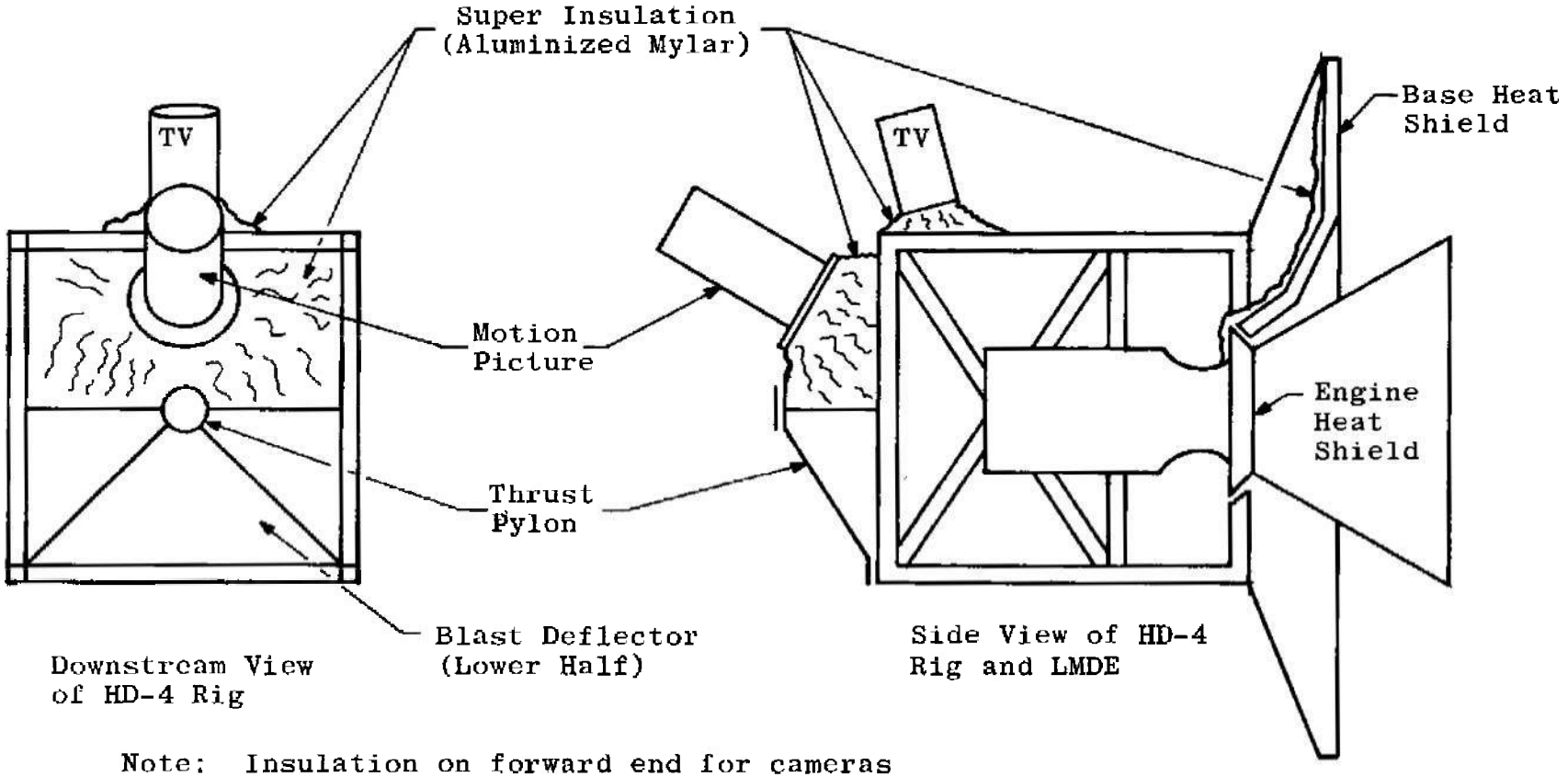

Note: Insulation on forward end for cameras used during test AC only.

Fifty layers of Aluminized Mylar taped to the outside surface of the blast deflectors during test AB.

UNCLASSIFIED

Fig. 8 Super Insulation Installation

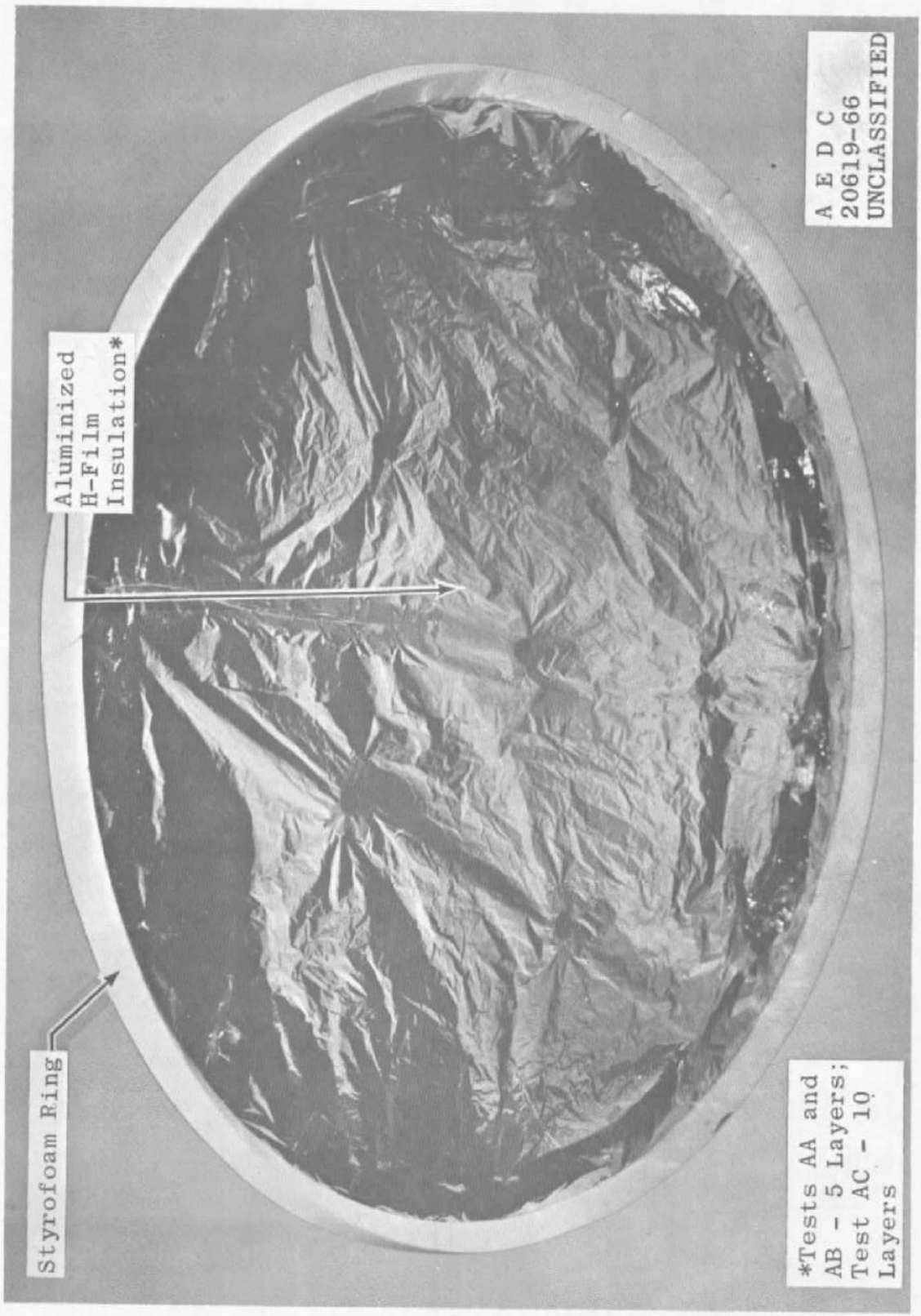

Fig. 9 Nozzle Radiation Plug

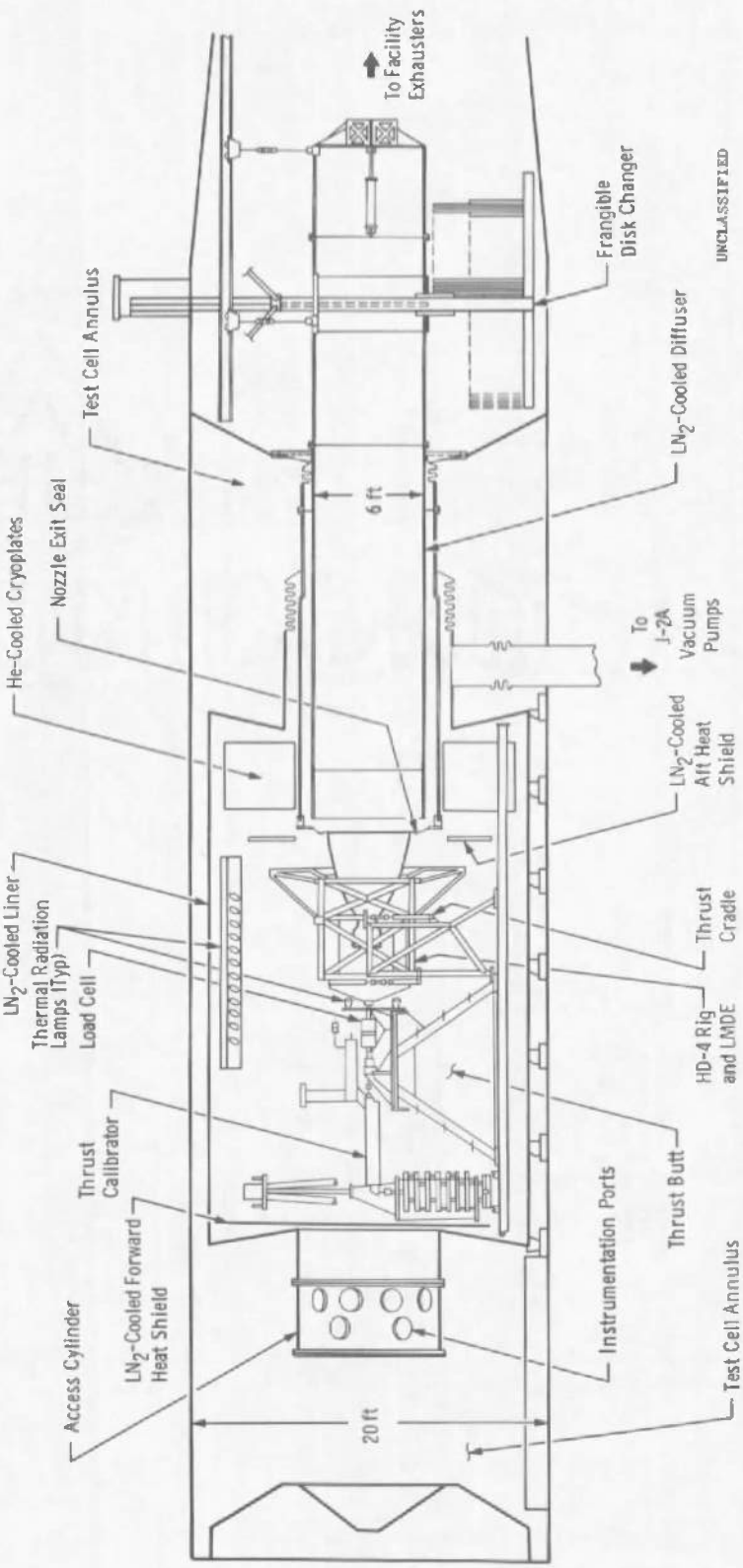

Fig. 10 Test Article Installation in the J-2A Test Cell

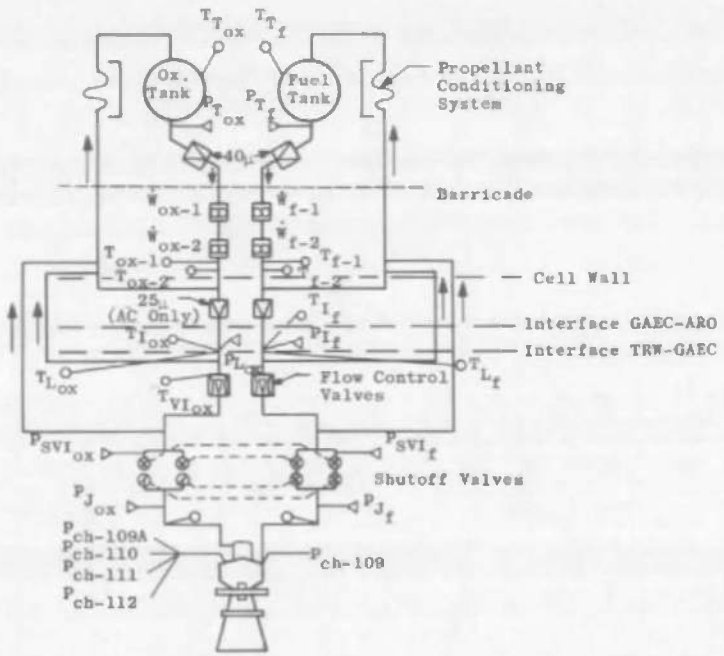

Nomenclature	Identification
	Pressures
$P_{T_{ox}}$	Oxidizer Tank
P_{T_f}	Fuel Tank
$P_{I_{ox}}$	Oxidizer Interface
P_{I_f}	Fuel Interface
$P_{SVI_{ox}}$	Oxidizer Shutoff Valve Inlet
P_{SVI_f}	Fuel Shutoff Valve Inlet
$P_{J_{ox}}$	Oxidizer Injector Inlet
P_{J_f}	Fuel Injector Inlet
P_{ch-109}	Chamber Pressure
$P_{ch-109A}$	
P_{ch-110}	
P_{ch-111}	
P_{ch-112}	
	Temperatures
$T_{T_{ox}}$	Oxidizer Tank
T_{T_f}	Fuel Tank
T_{ox-1}	Oxidizer (at Flowmeter)
T_{ox-2}	Oxidizer (at Flowmeter)
T_{f-1}	Fuel (at Flowmeter)
T_{f-2}	Fuel (at Flowmeter)
$T_{I_{ox}}$	Oxidizer Interface
T_{I_f}	Fuel Interface
$T_{VI_{ox}}$	Oxidizer Flow Control Valve Inlet
$T_{L_{ox}}$	Oxidizer Line
T_{L_f}	Fuel Line
	Flows
$\dot{W}_{ox-1}$	Oxidizer
$\dot{W}_{ox-2}$	Oxidizer
$\dot{W}_{f-1}$	Fuel
$\dot{W}_{f-2}$	Fuel

UNCLASSIFIED

a. Propellant System

Fig. 11 Instrumentation Locations

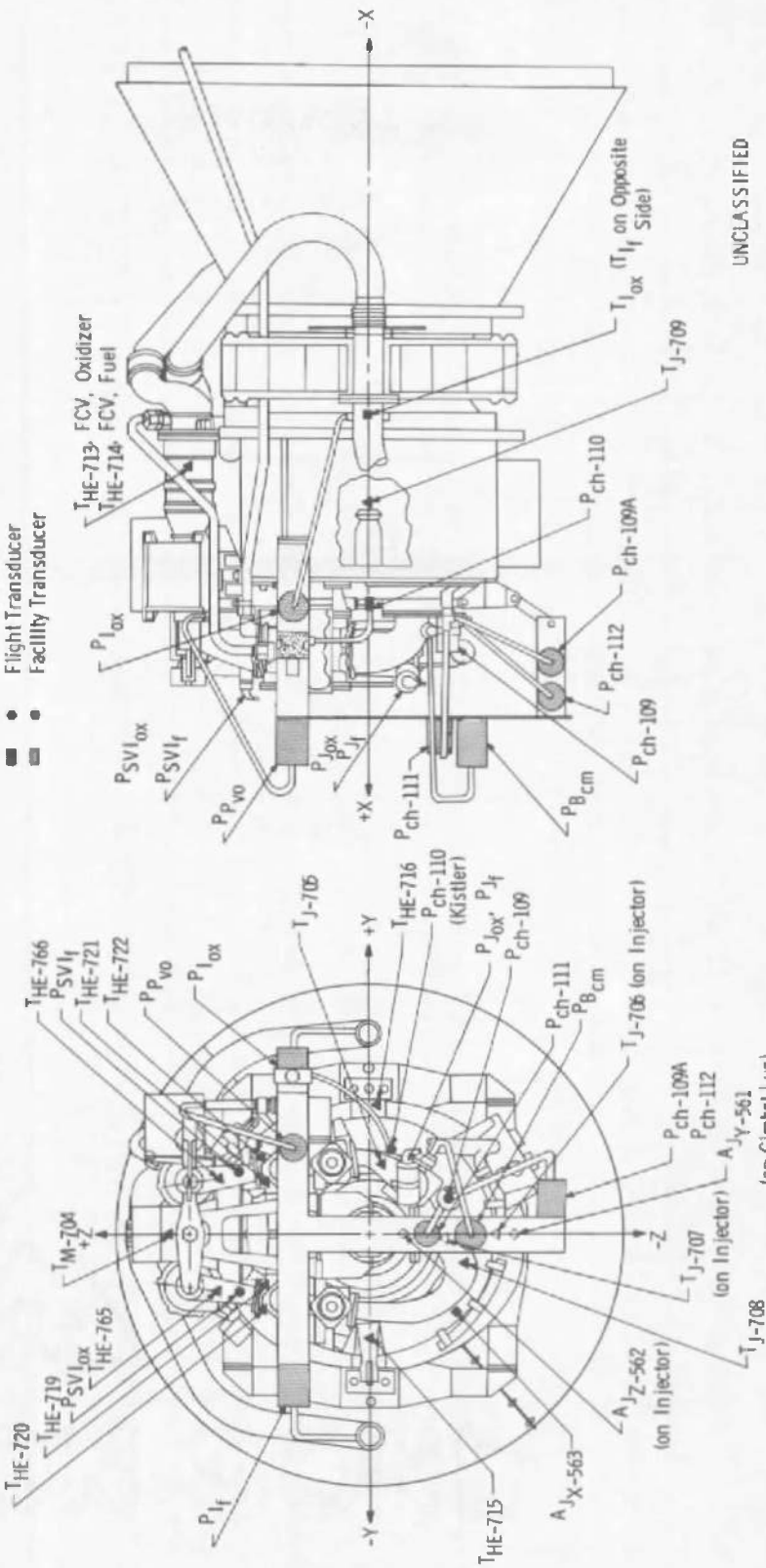

b. Engine Headend Assembly

Fig. 11 Continued

Nomenclature	Identification
	Pressures
$P_{I_{ox}}$	Oxidizer Interface
P_{I_f}	Fuel Interface
$P_{SVI_{ox}}$	Oxidizer Shutoff Valve Inlet
P_{SVI_f}	Fuel Shutoff Valve Inlet
$P_{J_{ox}}$	Oxidizer Injector Inlet
P_{J_f}	Fuel Injector Inlet
$P_{P_{vo}}$	Pre-Valve Outlet
$P_{B_{cm}}$	Barrier Coolant Manifold
$P_{ch-109A}$	Chamber Pressure
P_{ch-109}	↓
P_{ch-110}	
P_{ch-111}	
P_{ch-112}	
	Temperatures
$T_{I_{ox}}$	Oxidizer Interface
T_{I_f}	Fuel Interface
$T_{VI_{ox}}$	Oxidizer Flow Control Valve
T_{M-704}	Throttle Actuator Housing
T_{J-705}	Injector
T_{J-706}	↓
T_{J-707}	
T_{J-708}	
T_{J-709}	
T_{HE-713}	Headend Assembly
T_{HE-714}	↓
T_{HE-719}	
T_{HE-720}	
T_{HE-721}	
T_{HE-722}	
T_{HE-765}	
T_{HE-766}	
	Accelerometers
$A_{J_{X-563}}$	Headend Assembly X-X Axis
$A_{J_{Y-561}}$	Headend Assembly Y-Y Axis
$A_{J_{Z-562}}$	Headend Assembly Z-Z Axis

UNCLASSIFIED

b. Concluded

Fig. 11 Continued

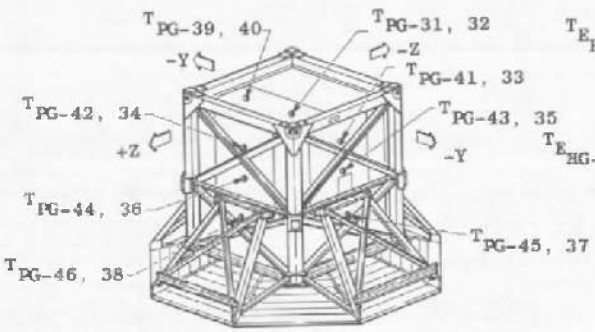

HD-4 Rig with Base Heat Shield Installed

$T_{E_{HA-1}}$ through 4 are on the upstream side of the heat shield.

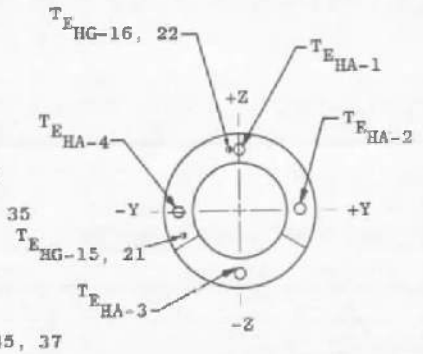

Thermocouples 21 and 22 are mounted on the nozzle extension side of the shield.

Engine Heat Shield (Looking Downstream)

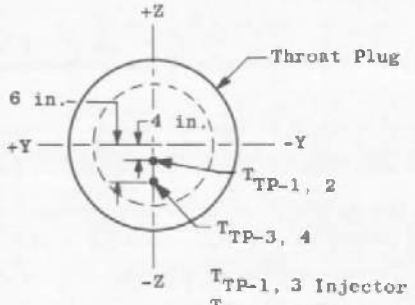

Nozzle Radiation Plug

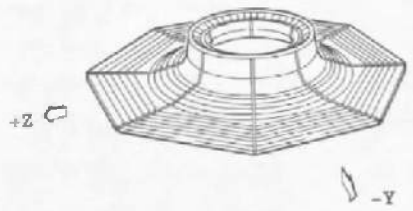

Base Heat Shield

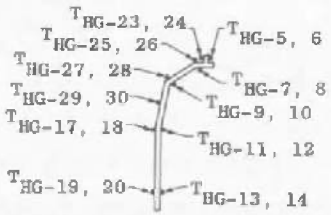

Even Numbers on +Z Axis Panel
Odd Numbers on -Y Axis Panel

Section of Base Heat Shield

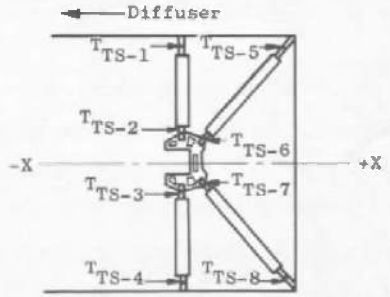

HD-4 Rig Truss Strut

UNCLASSIFIED

c. Engine Compartment (HD-4 Rig), Heat Shield, and Nozzle Plug

Fig. 11 Continued

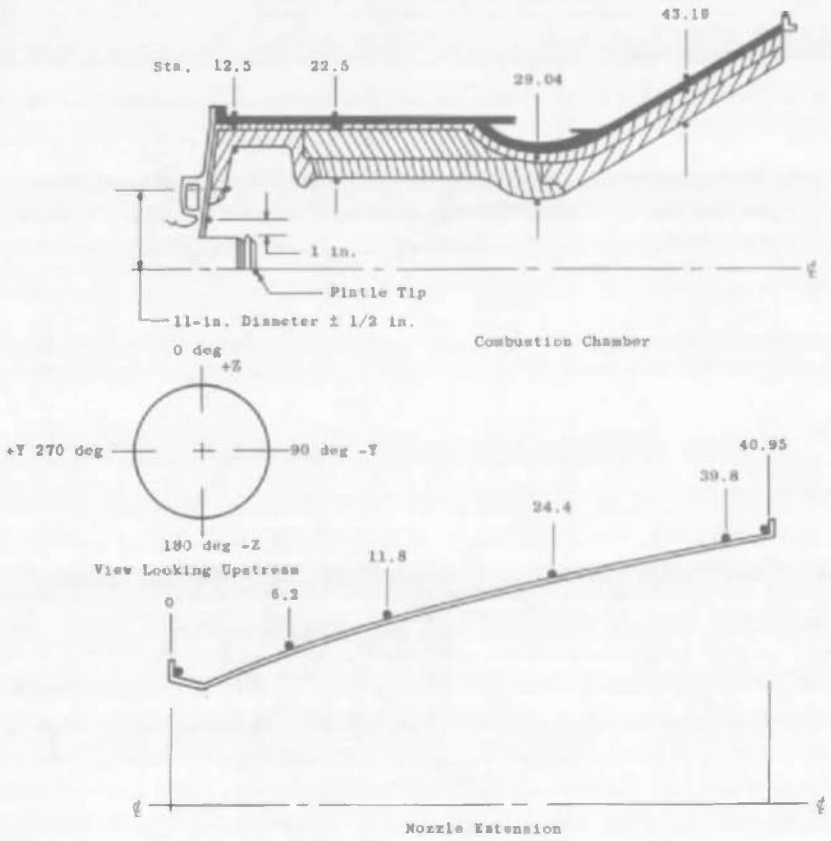

Thermocouples	Station, in.	Angular Location, deg	Remarks
T_{J-709}	-	-	Pintle Tip
T_{J-710}	-	180	Injector Manifold, Internal Adjacent to Snout (Approx. 1 in.)
T_{J-711}	-	0	Combustion Chamber Faceplate,
-712		180	Internal (11-in. Diameter ± 1/2 in.)
T_{C-723}	12.5	0	Combustion Chamber Wall, Int.
-724	12.5	180	Combustion Chamber Wall, Int.
-725	12.5	0	Titanium Case, Ext.
-726	12.5	180	Titanium Case, Ext.
-727	12.5	0	Eng. Insulation Blanket, Ext.
-728	12.5	180	Eng. Insulation Blanket, Ext.
T_{C-729}	22.5	0	Combustion Chamber Wall, Int.
-730	22.5	180	Combustion Chamber Wall, Int.
-731	22.5	0	Titanium Case, Ext.
-732	22.5	180	Titanium Case, Ext.
-733	22.5	0	Eng. Insulation Blanket, Ext.
-734	22.5	180	Eng. Insulation Blanket, Ext.
-768	22.5	0	Nanmac® Thermocouples (Combustion
-769	22.5	90	Nanmac Thermocouples (Chamber
-770	22.5	180	Nanmac Thermocouples (Wall,
-771	22.5	270	Nanmac Thermocouples) Int.
T_{C-735}	29.04	0	Combustion Chamber Wall, Int.
-736	29.04	180	Combustion Chamber Wall, Int.
-737	29.04	0	Titanium Case, Ext.
-738	29.04	180	Titanium Case, Ext.
T_{C-739}	43.19	0	Combustion Chamber Wall, Int.
-740	43.19	180	Combustion Chamber Wall, Int.
-741	43.19	0	Titanium Case, Ext.
-742	43.19	180	Titanium Case, Ext.
-743	43.19	0	Eng. Insulation Blanket, Ext.
-744	43.19	180	Eng. Insulation Blanket, Ext.
-745	-	180	Nozzle Extension Flange
-746	-	0	Nozzle Extension Flange
T_{NX-753}	0	0	Nozzle Extension
-754	0	180	
-755	6.2	0	
-756	6.2	180	
-757	11.8	180	
-758	11.8	0	
-759	24.4	0	
-760	24.4	180	
-761	39.8	0	
-762	39.8	180	
-763	40.95	0	
-764	40.95	180	

UNCLASSIFIED

d. Engine Combustion Chamber and Nozzle Extension

Fig. 11 Continued

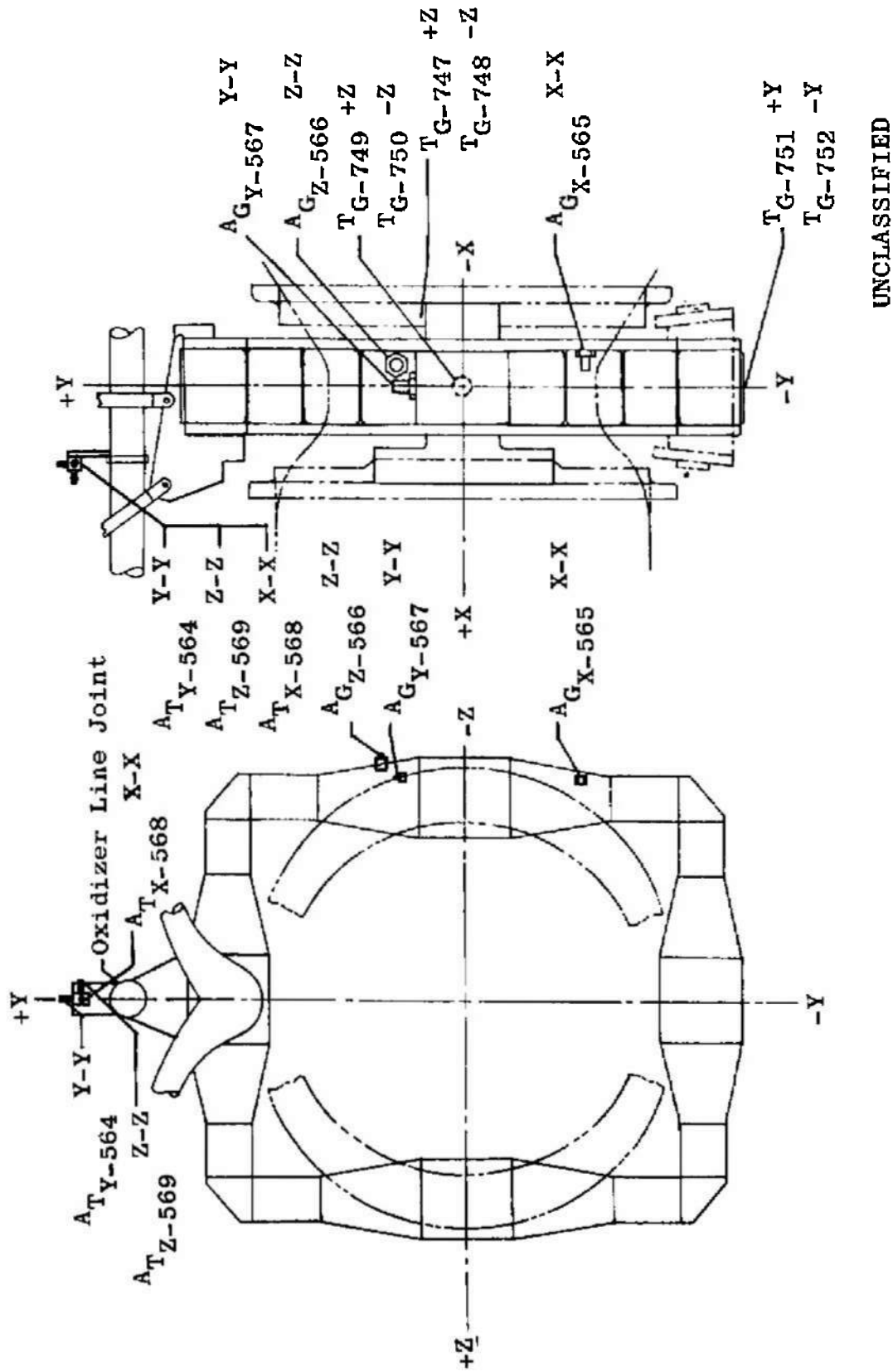

UNCLASSIFIED

e. Gimbal Assembly

Fig. 11 Concluded

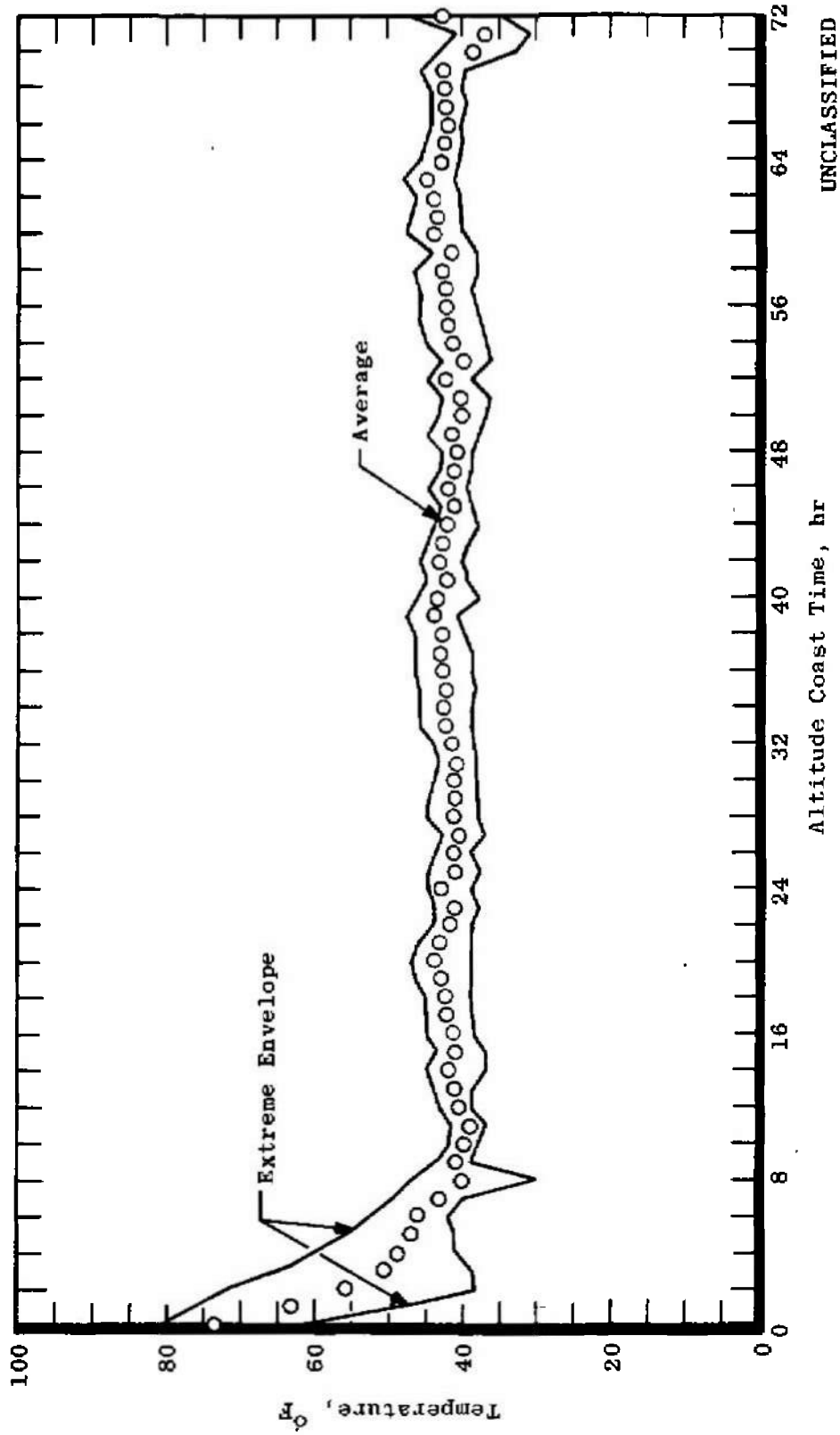

Fig. 12 Typical HD-4 Rig Panel Temperatures (Coast AB)

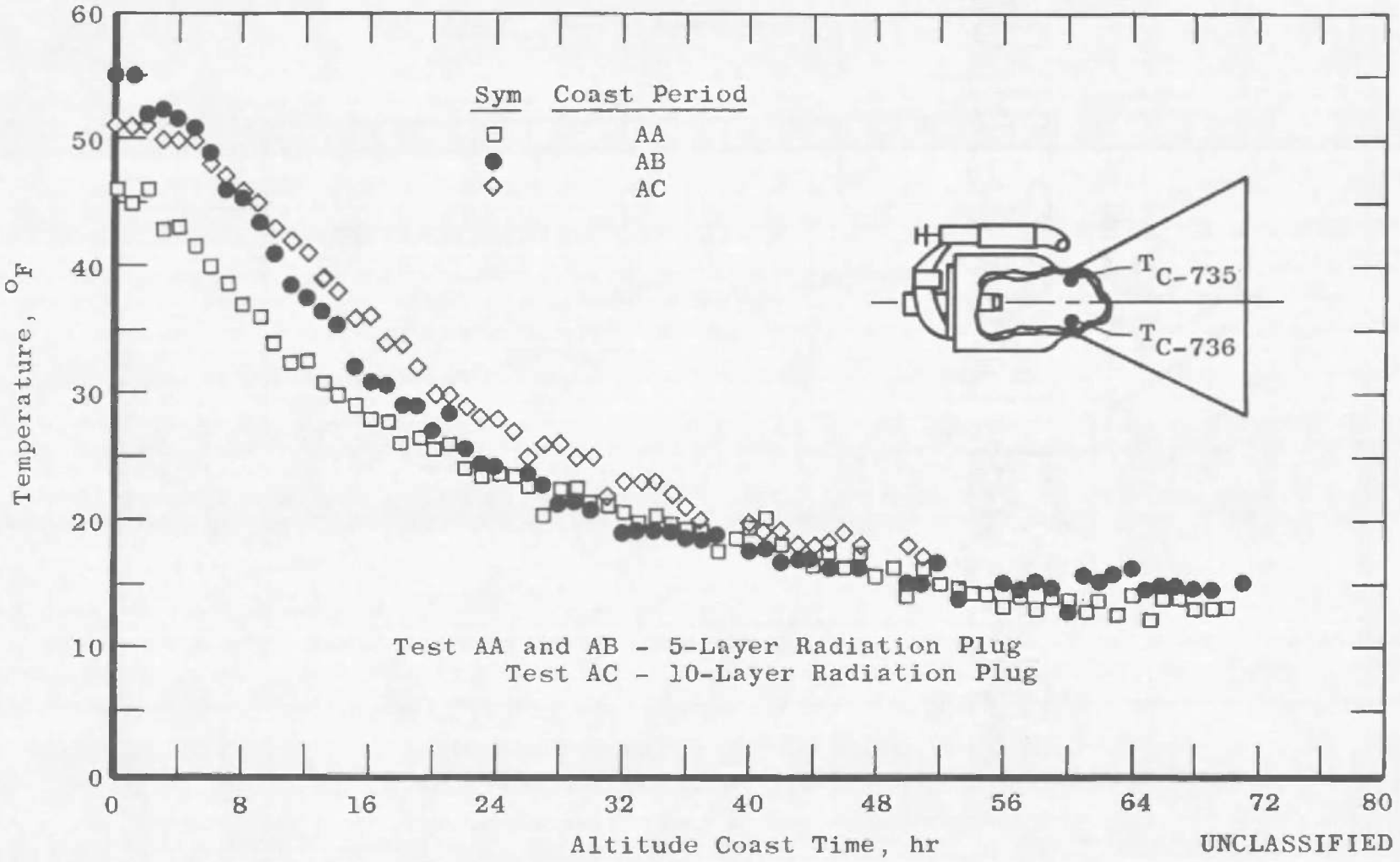

Fig. 13 Internal Chamber Throat Temperature History

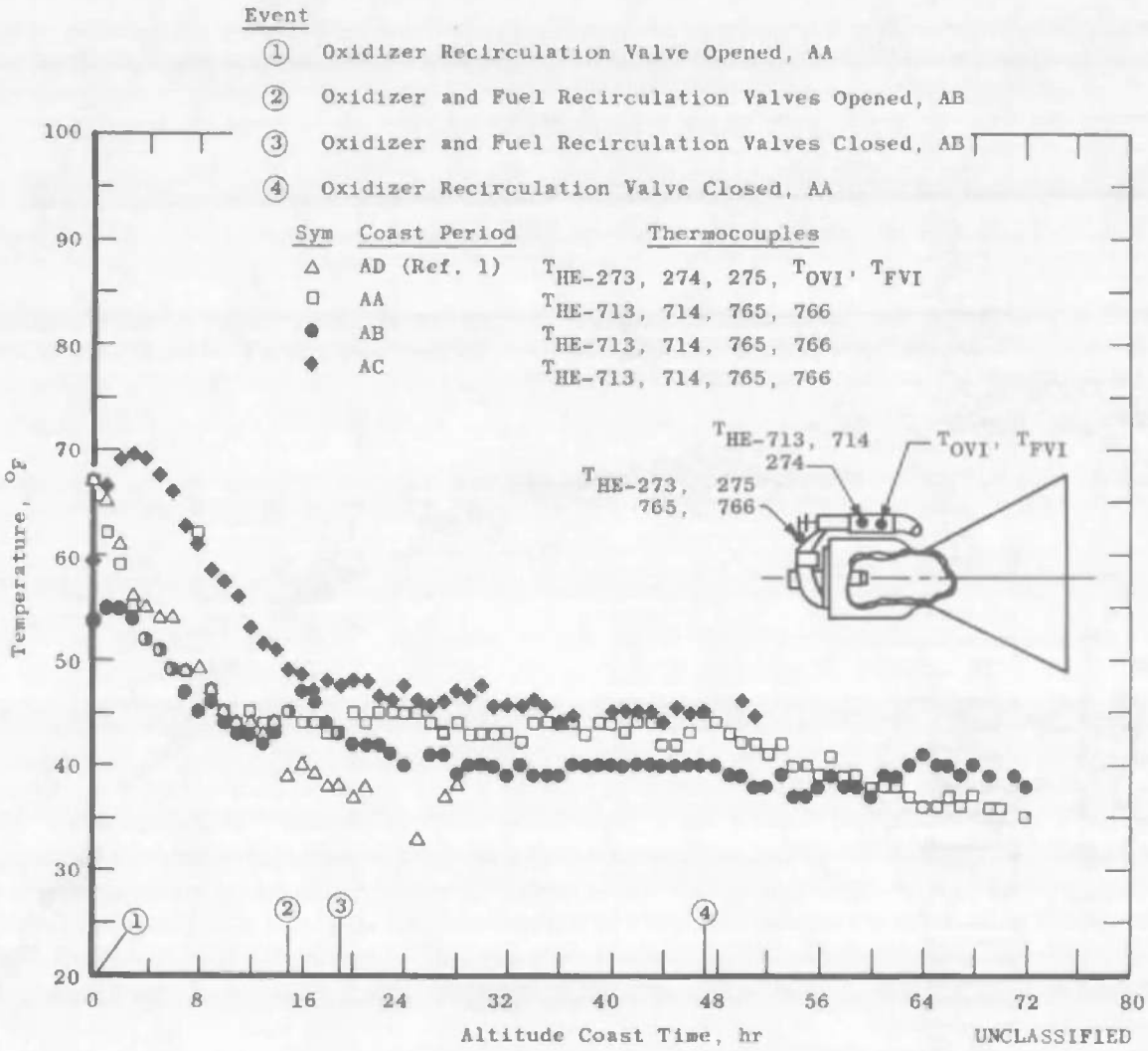

a. Flow Control Valves

Fig. 14 Engine Valves Temperature Histories

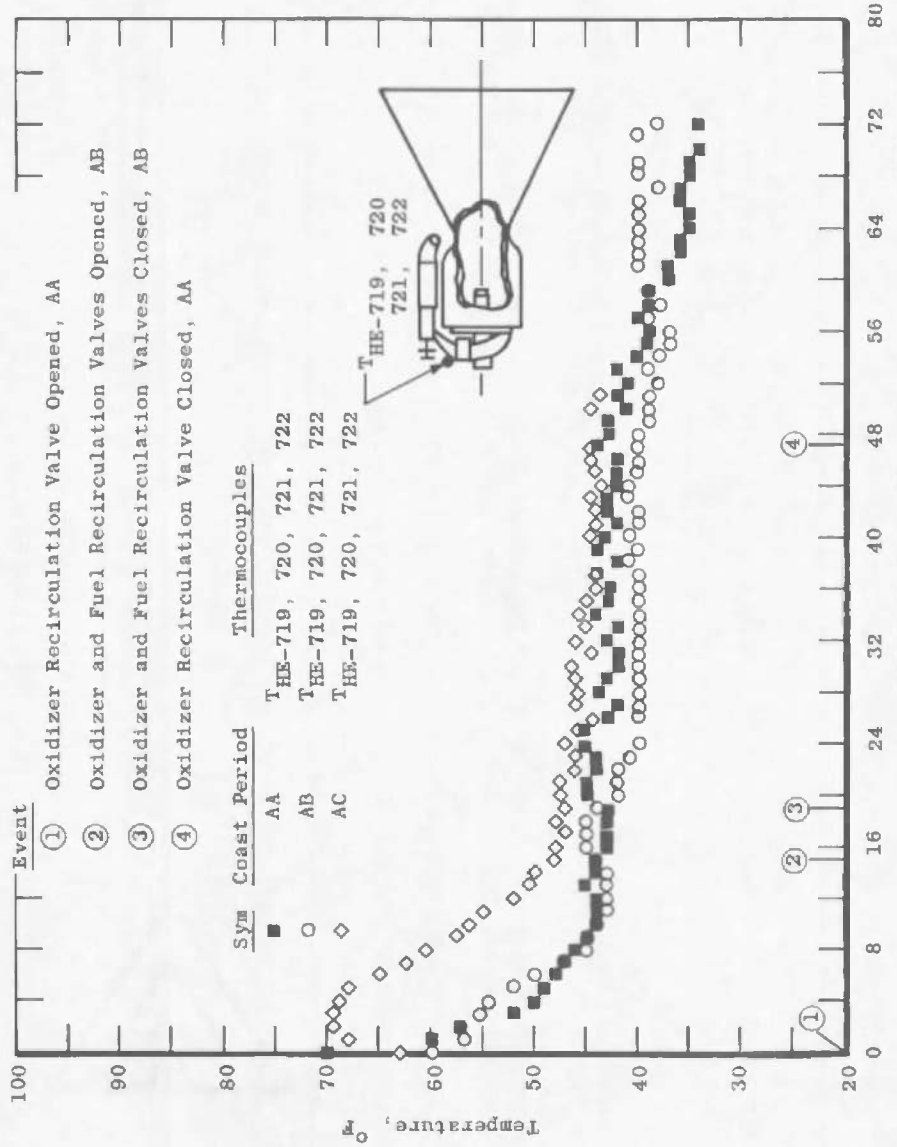

b. Shutoff Valves

Fig. 14 Concluded

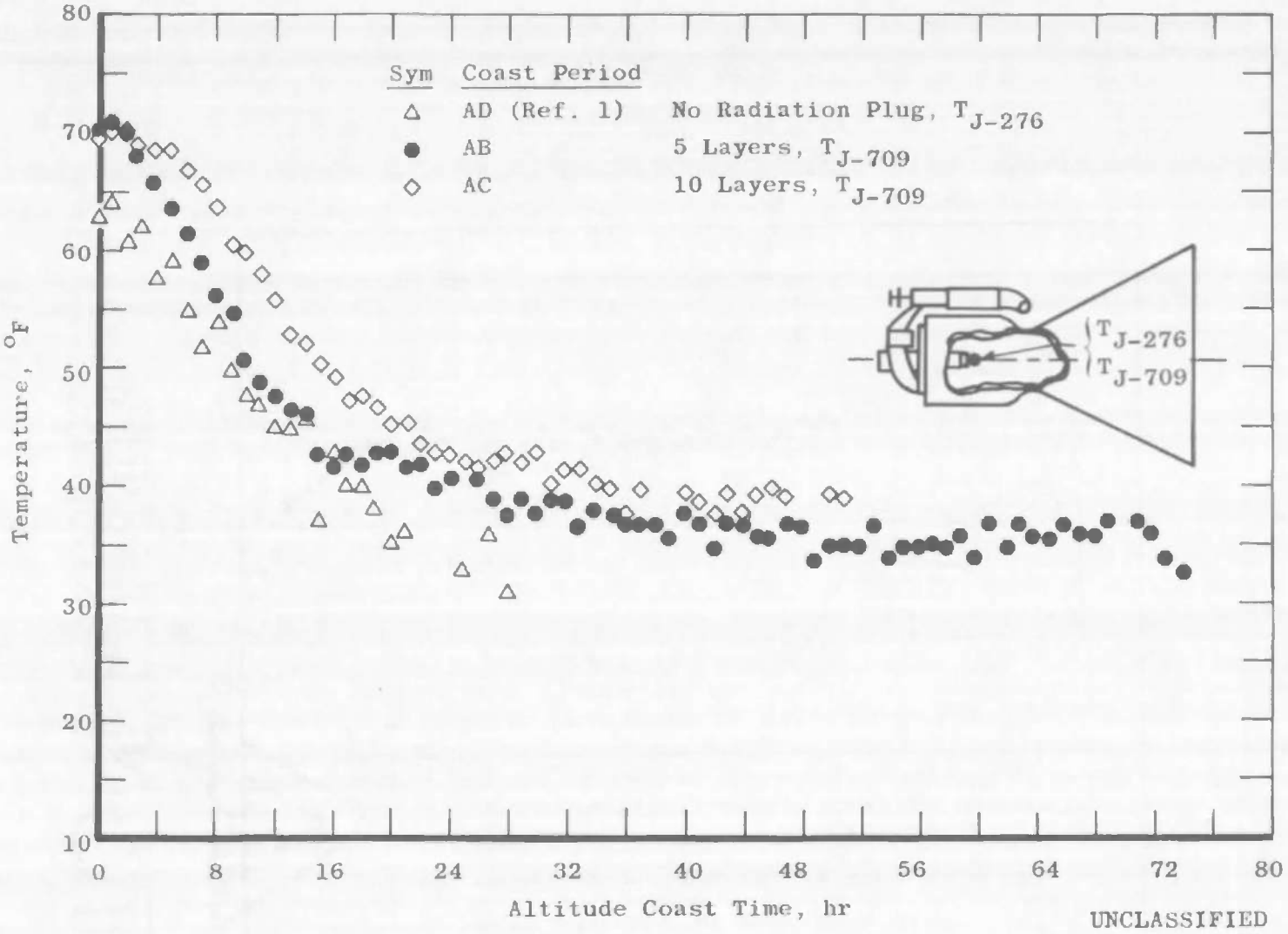

Fig. 15 Injector Pintle Tip Temperature History

UNCLASSIFIED

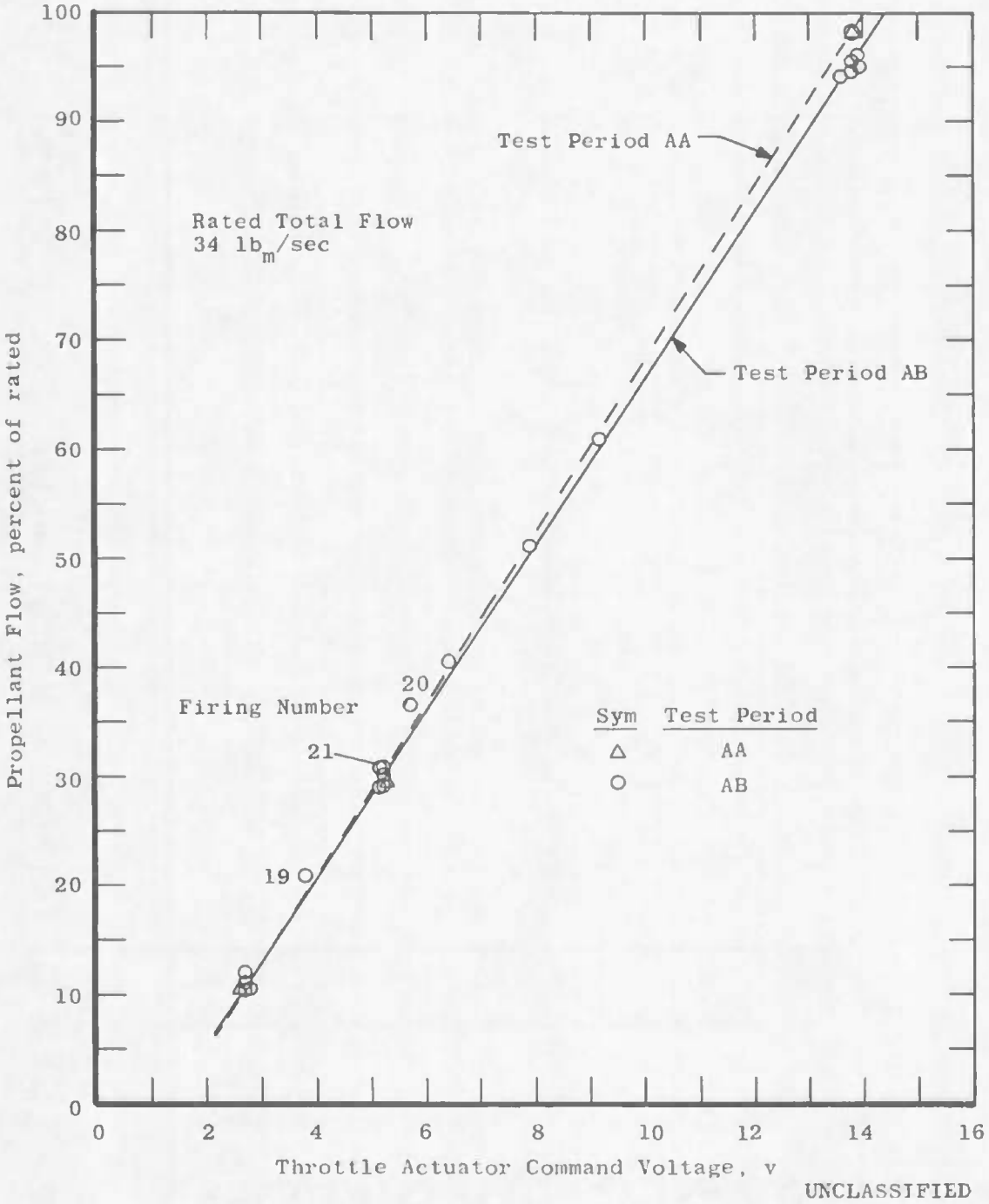

Fig. 16 Total Flow as a Function of Command Voltage

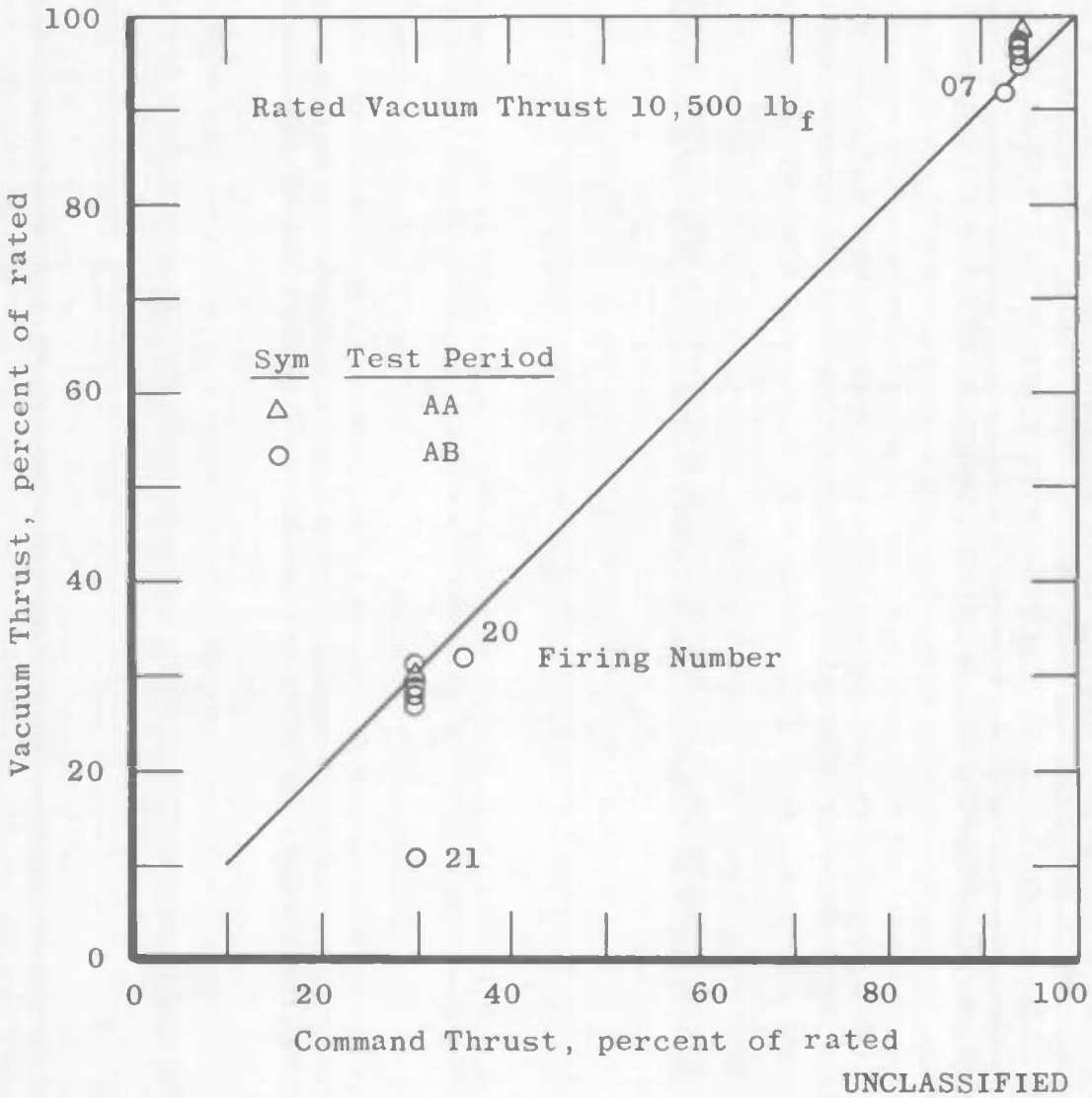

Fig. 17 Vacuum Thrust as a Function of Commond Thrust

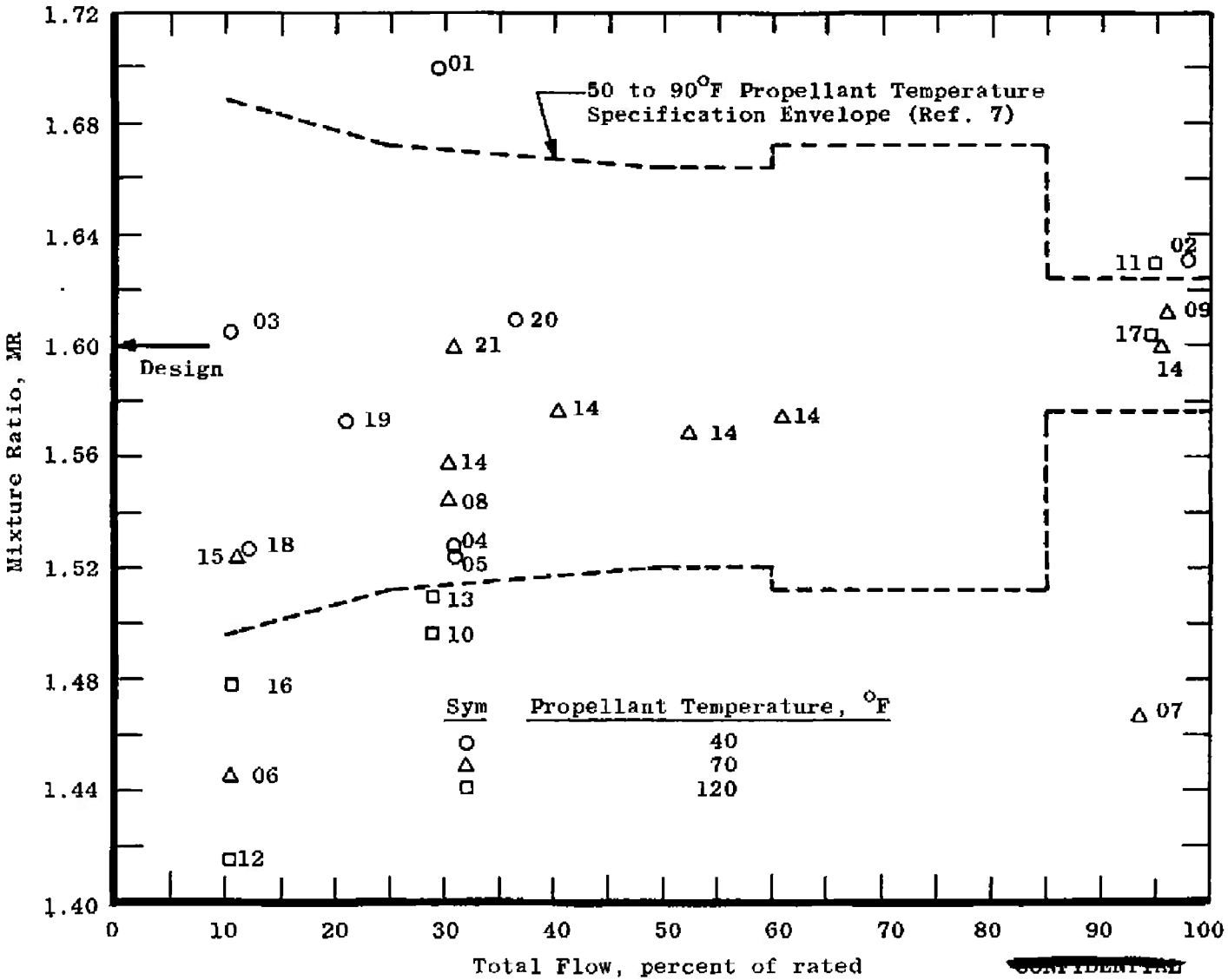

Fig. 18 Mixture Ratio as a Function of Flow

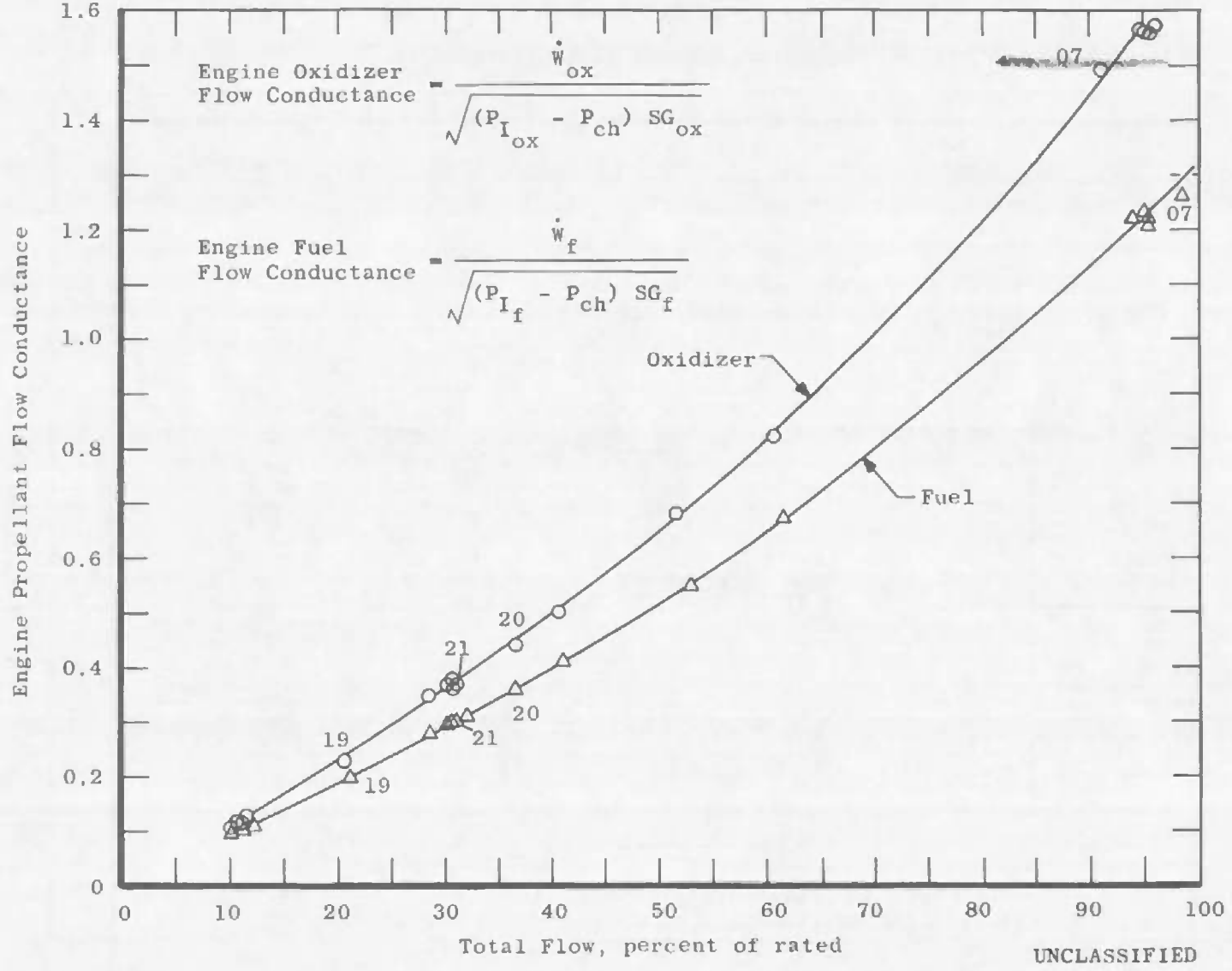

Fig. 19 Conductance as a Function of Flow

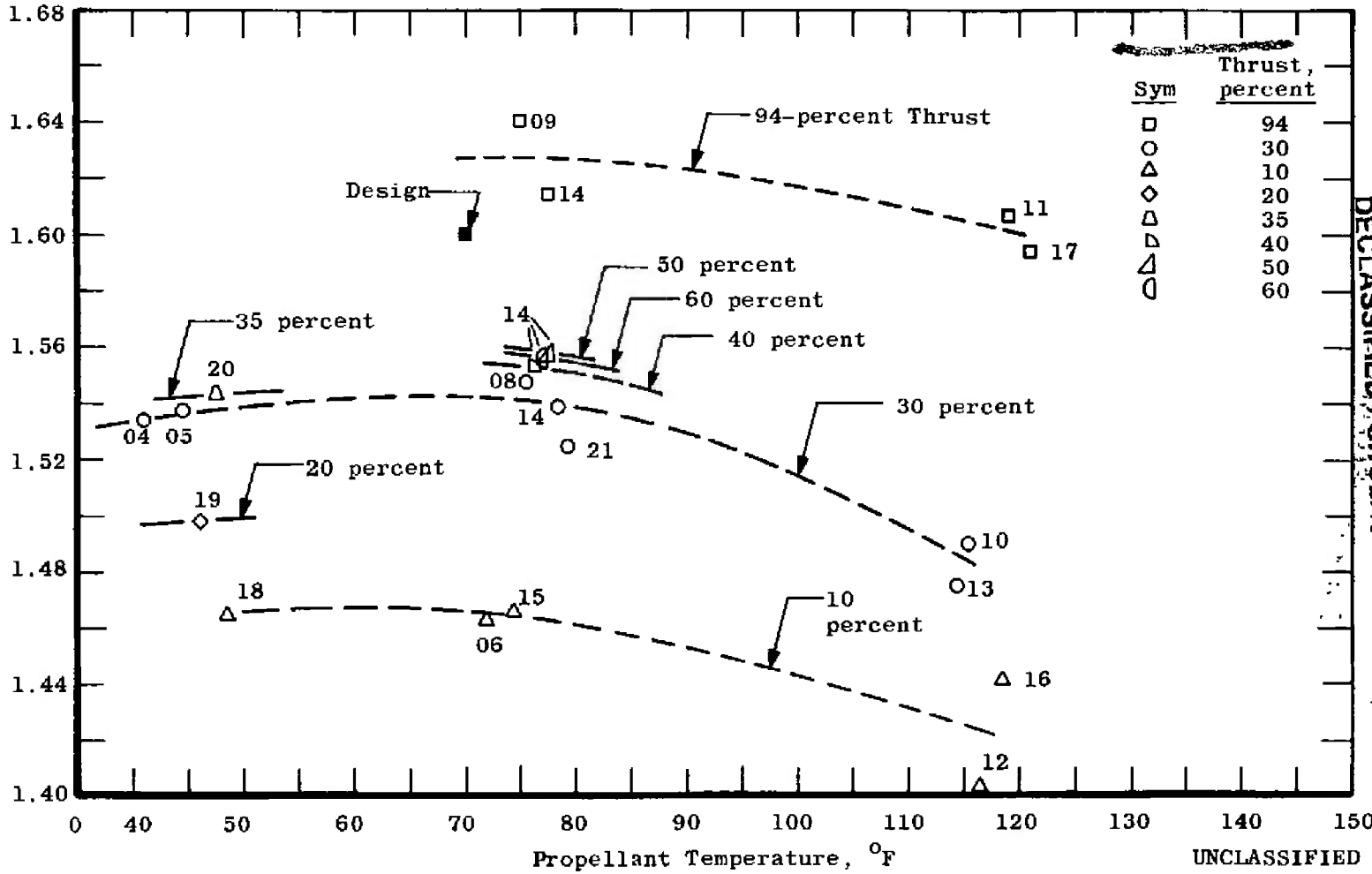

Fig. 20 Adjusted Mixture Ratio as a Function of Propellant Temperature

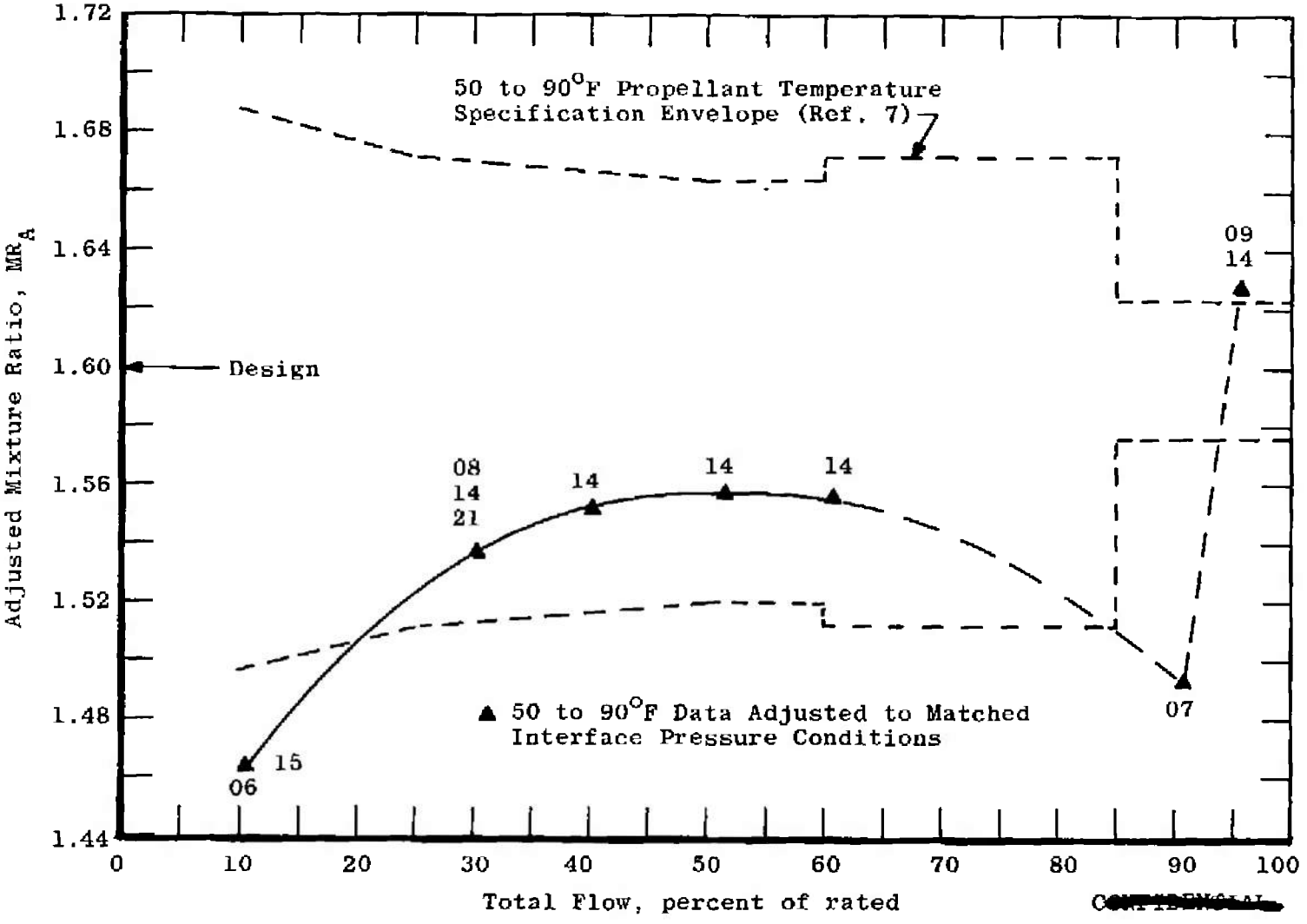

Fig. 21 Mixture Ratio Control Capability (Engine P1009)

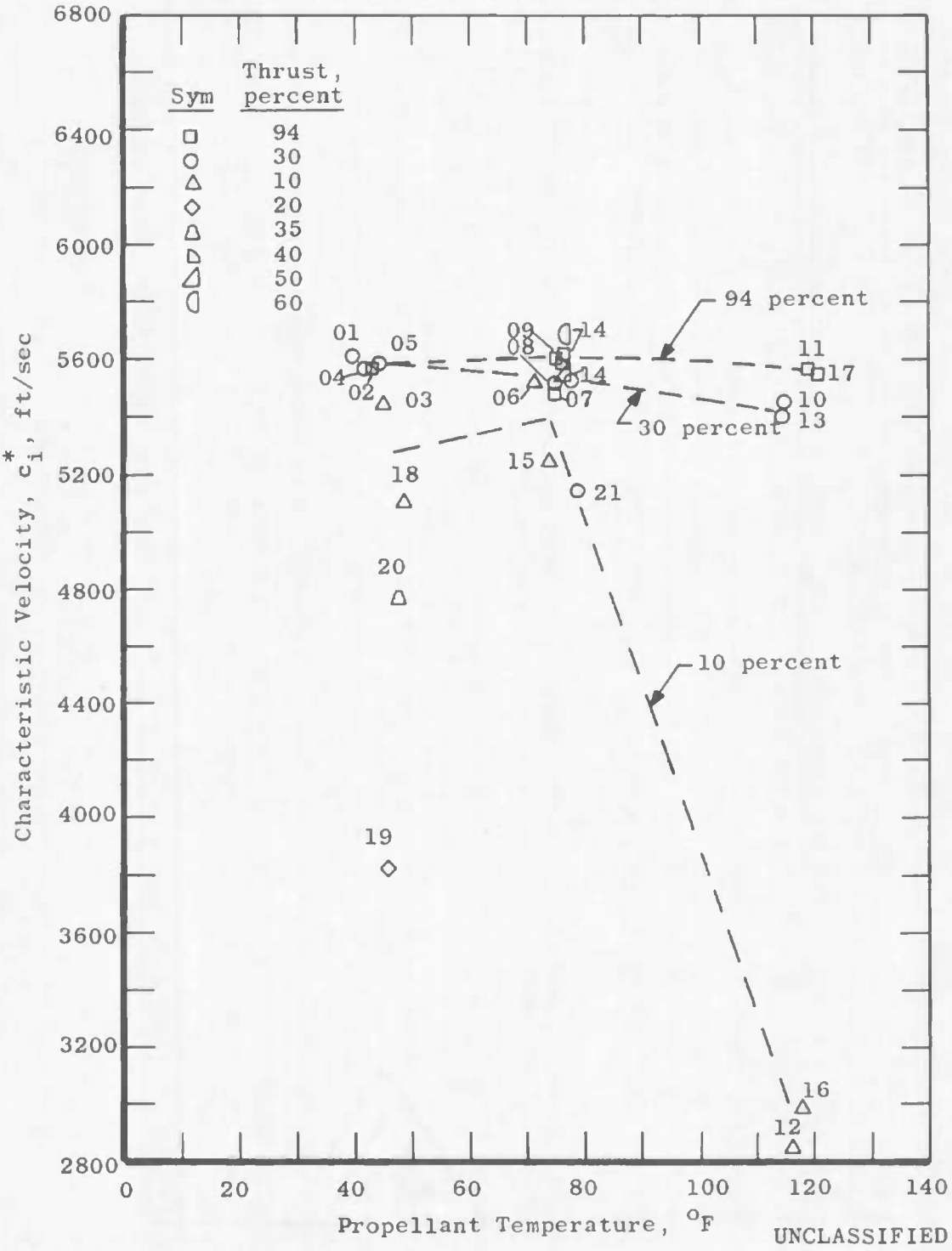

Fig. 22 Characteristic Velocity as a Function of Propellant Temperature

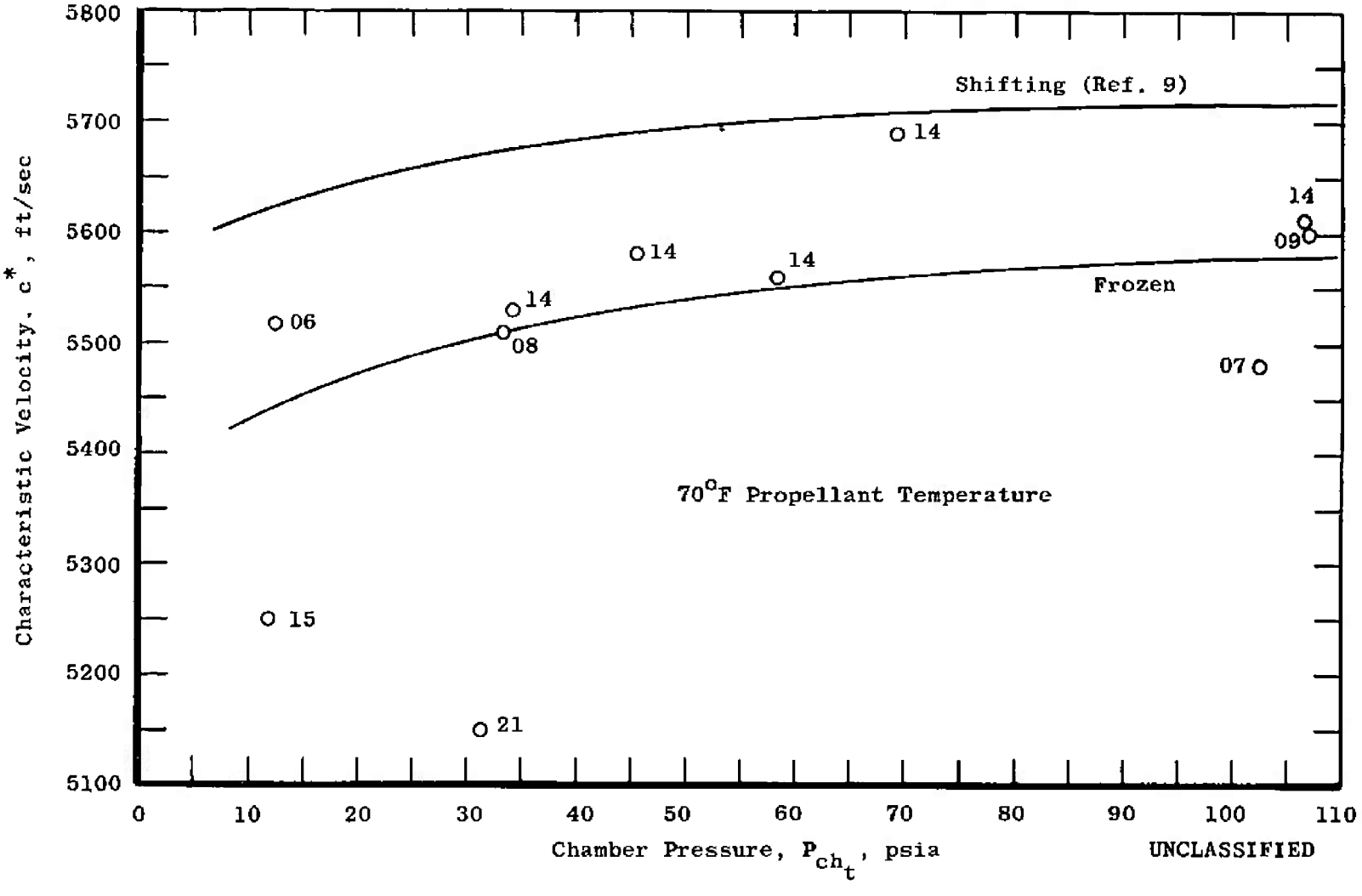

Fig. 23 Characteristic Velocity as a Function of Chamber Pressure

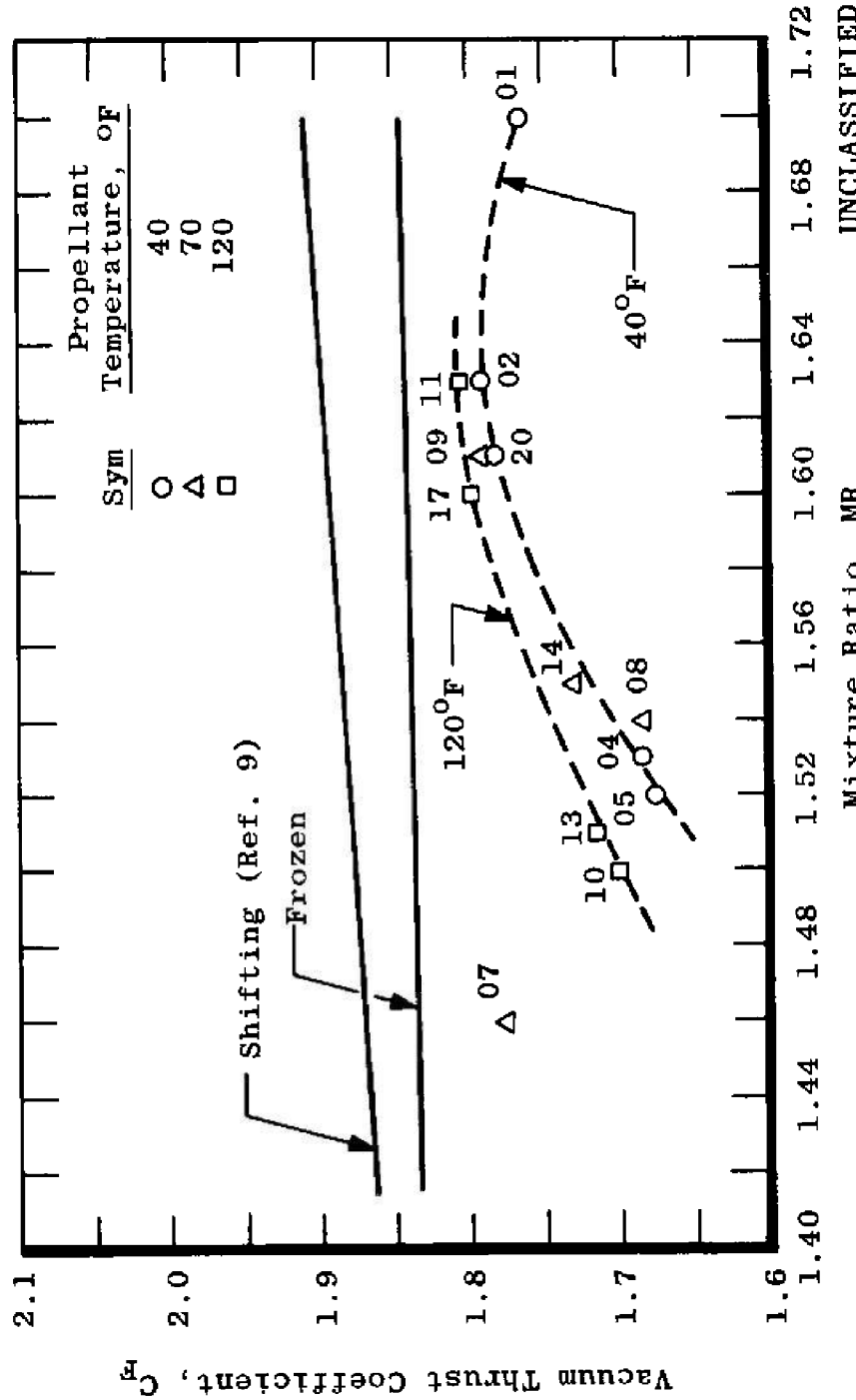

Fig. 24 Thrust Coefficient as a Function of Mixture Ratio

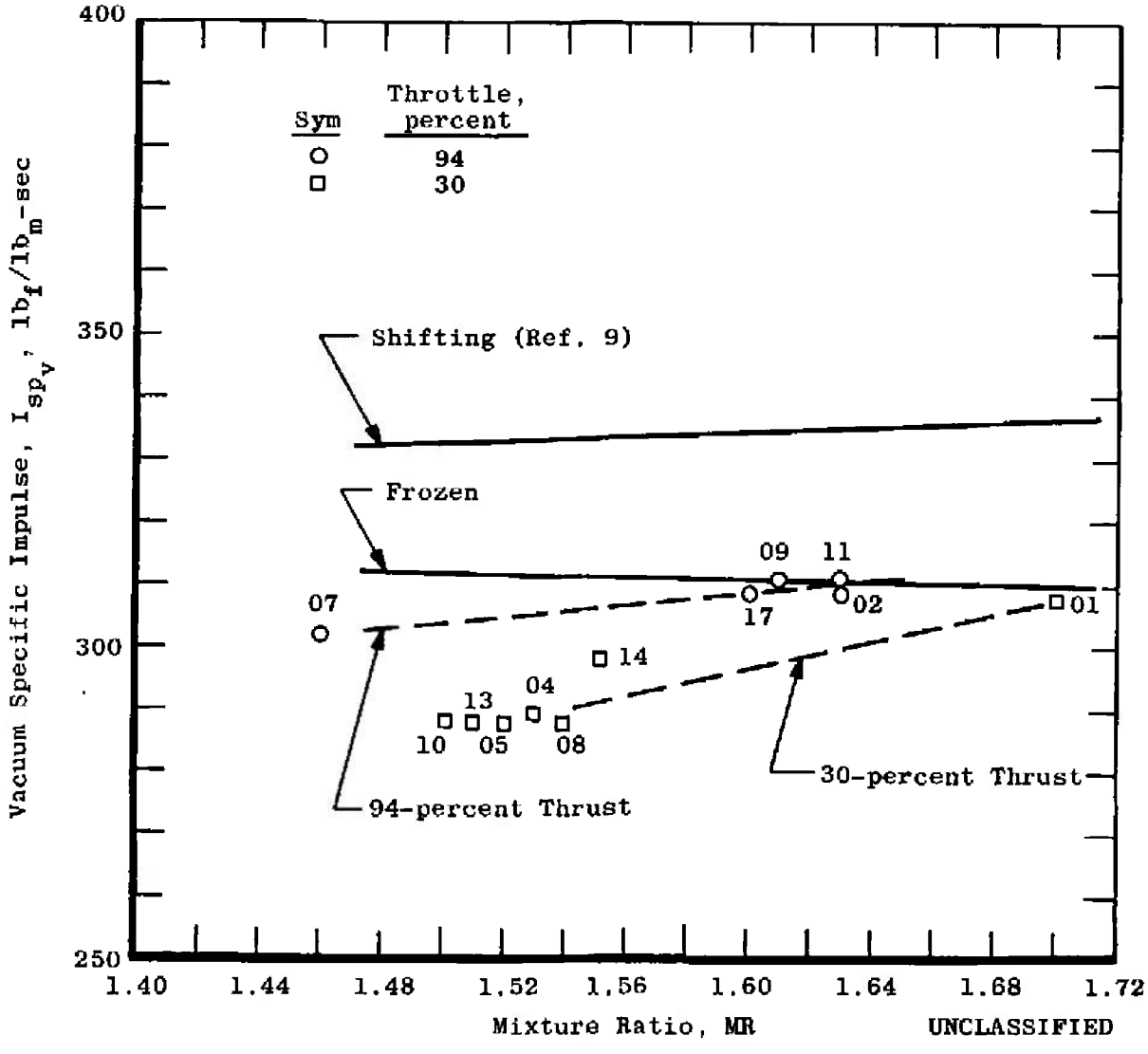

Fig. 25 Vacuum Specific Impulse as a Function of Mixture Ratio

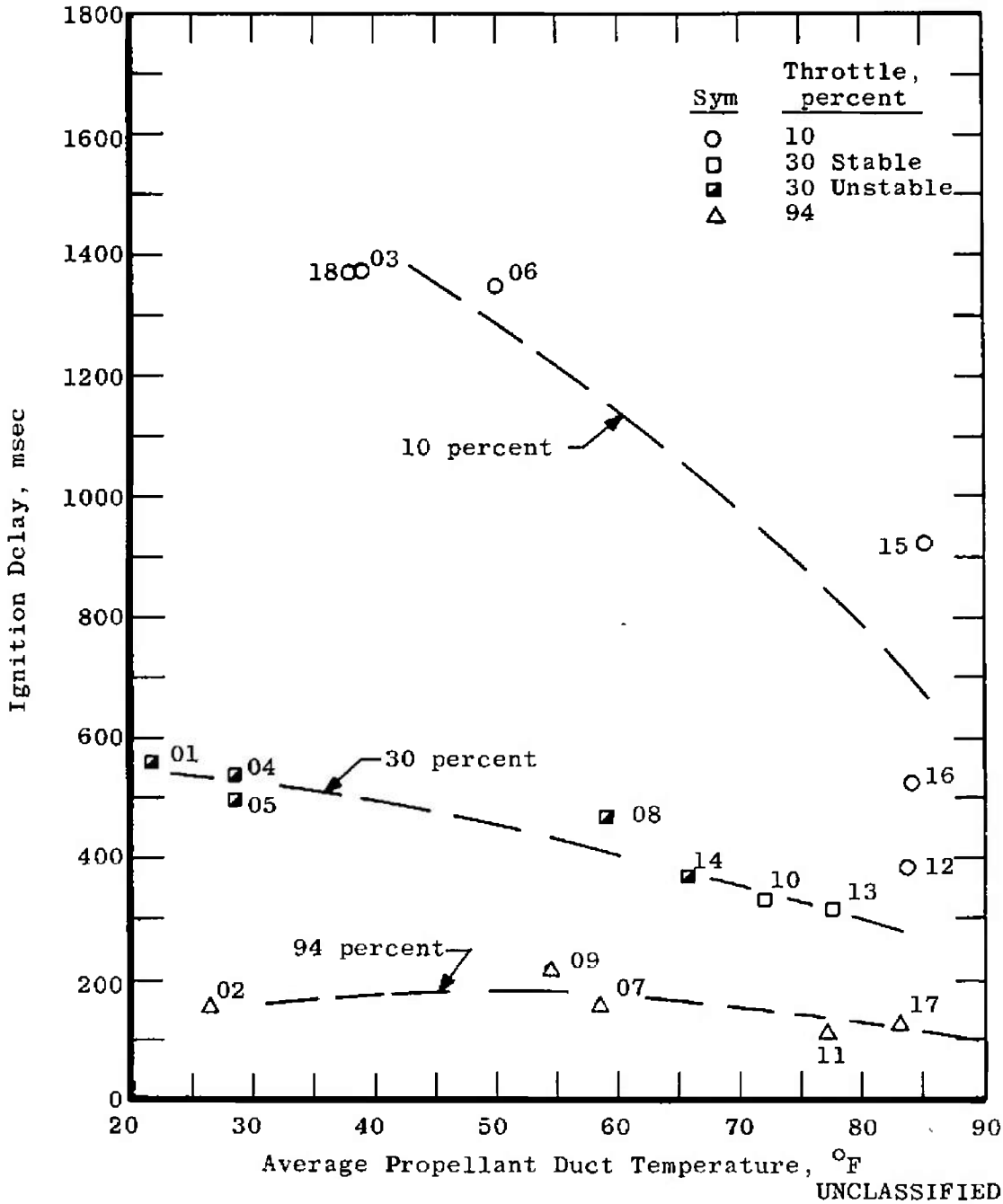

Fig. 26 Ignition Delay as a Function of Propellant Temperature

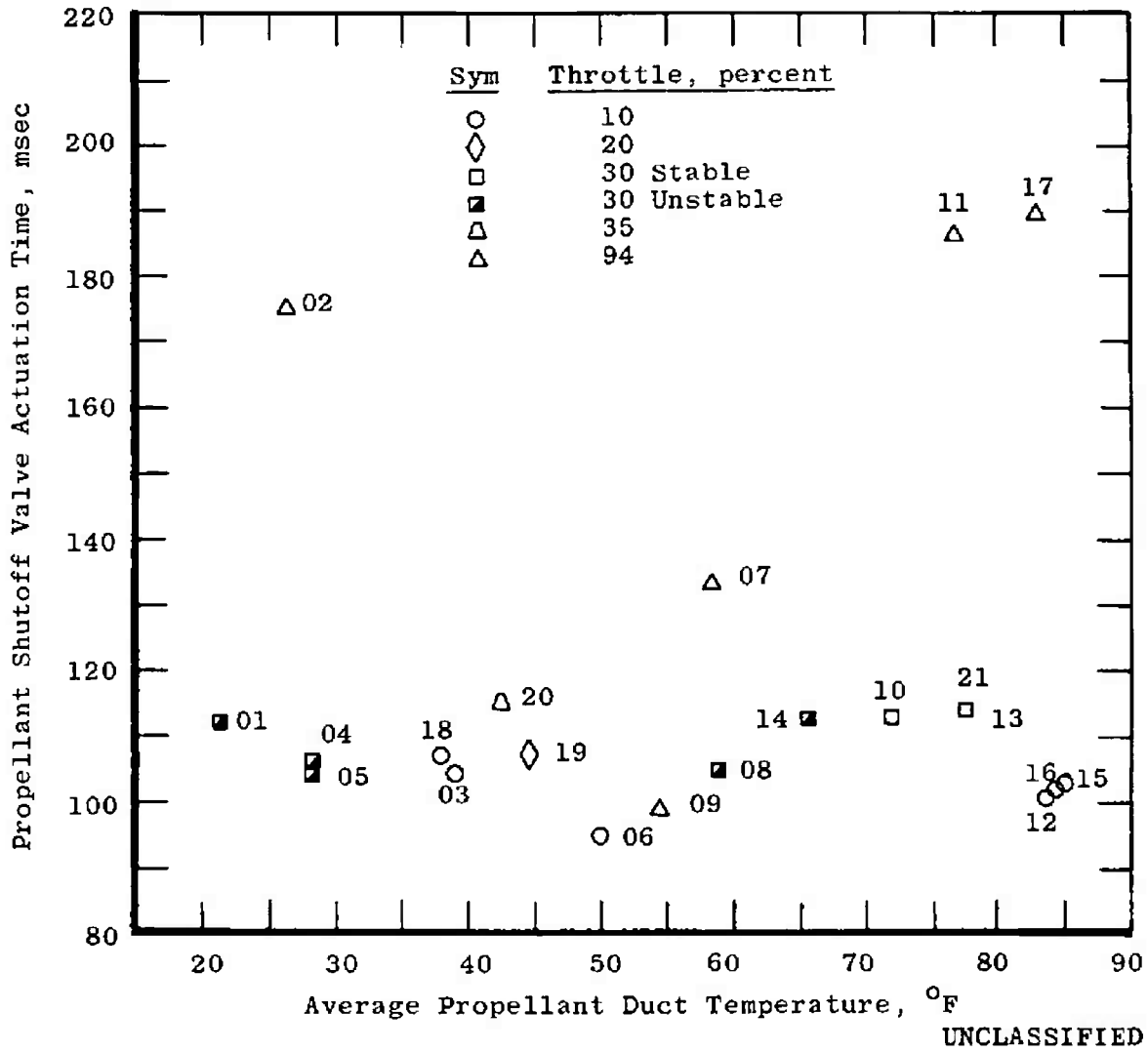

Fig. 27 Shutoff Valve Actuation Time as a Function of Propellant Temperature

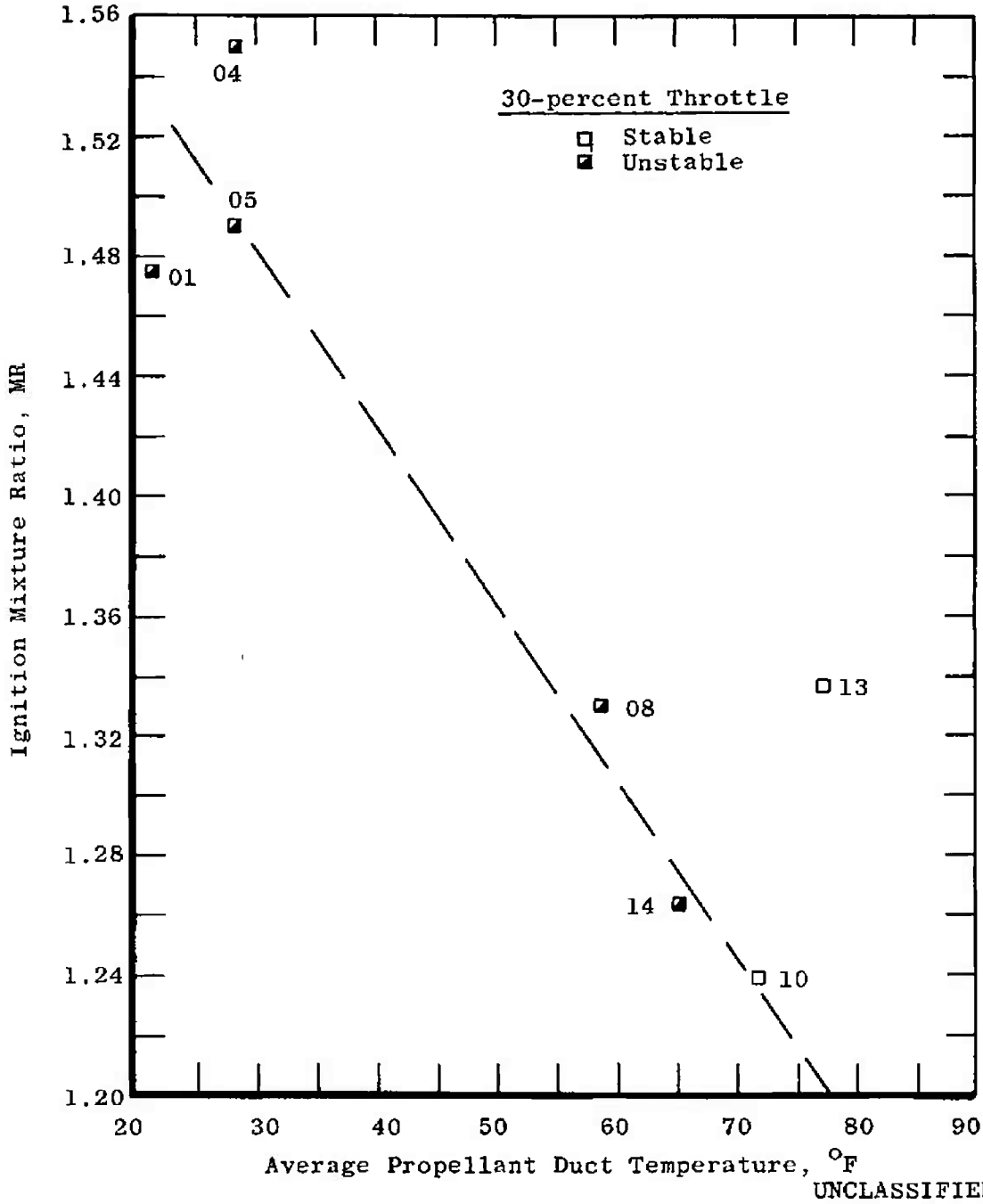

Fig. 28 Ignition Mixture Ratio as a Function of Propellant Temperature

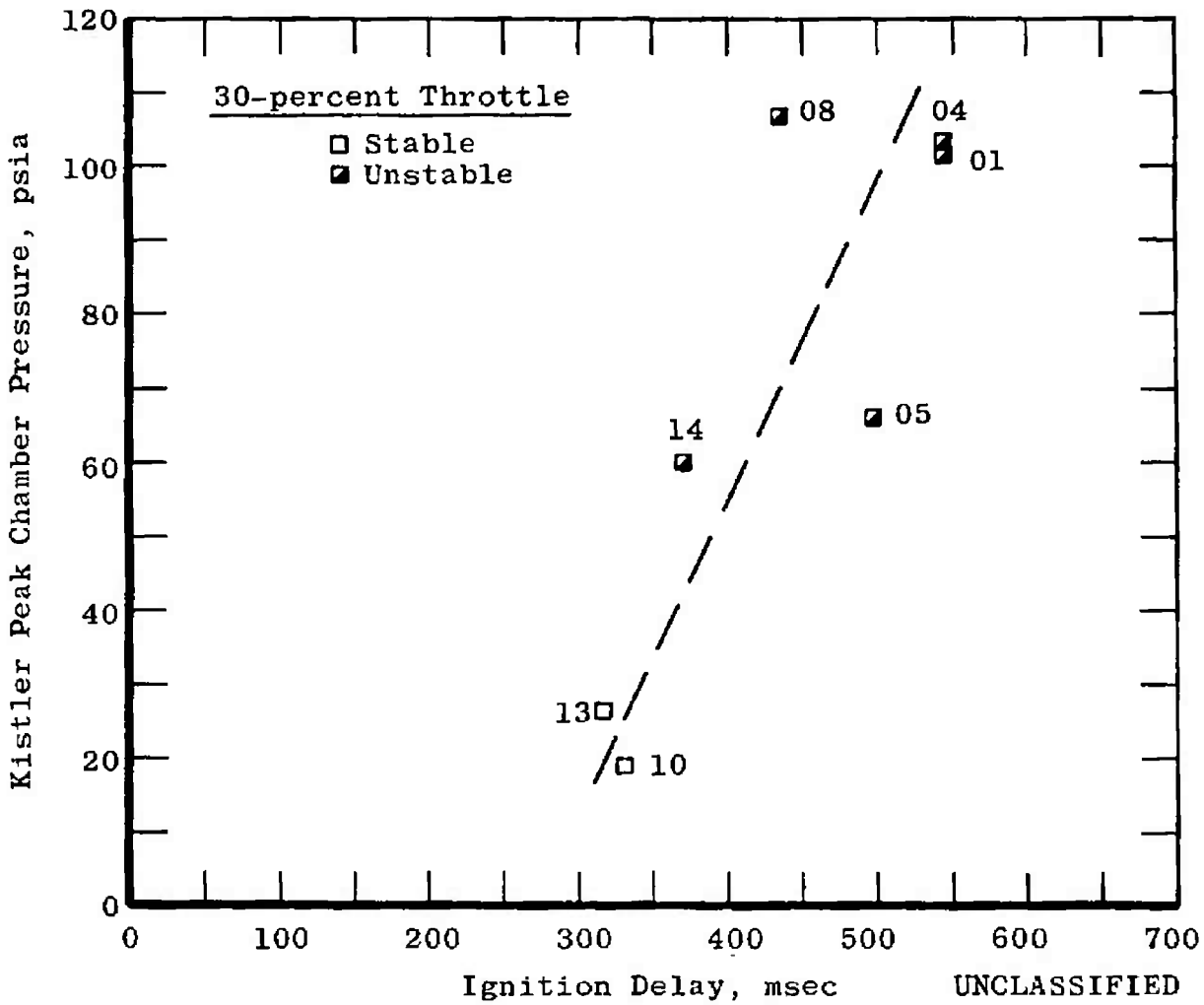

Fig. 29 Ignition Chamber Pressure Peaks Related to Ignition Delay

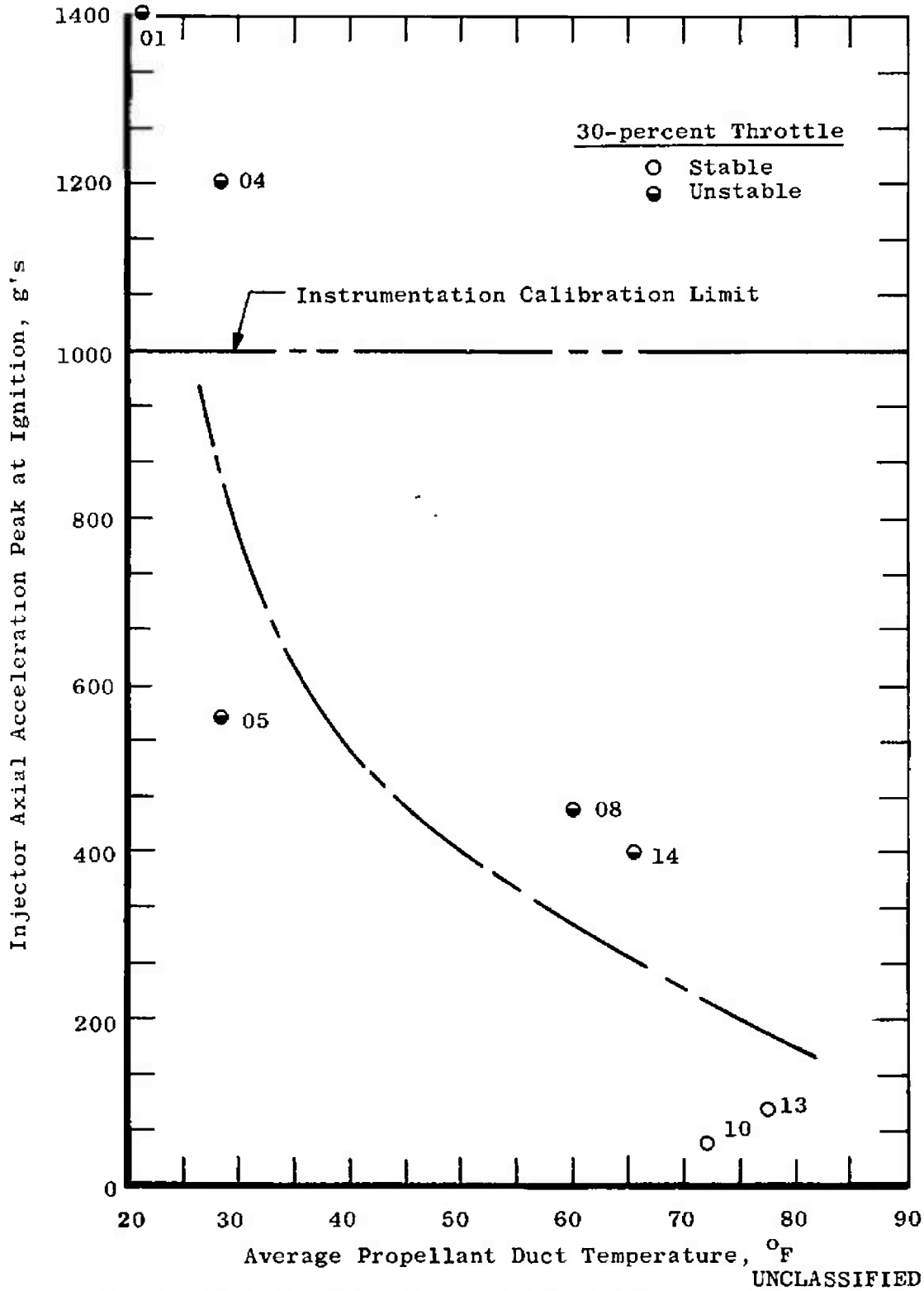

Fig. 30 Initial Acceleration Ignition Shock as a Function of Propellant Temperature

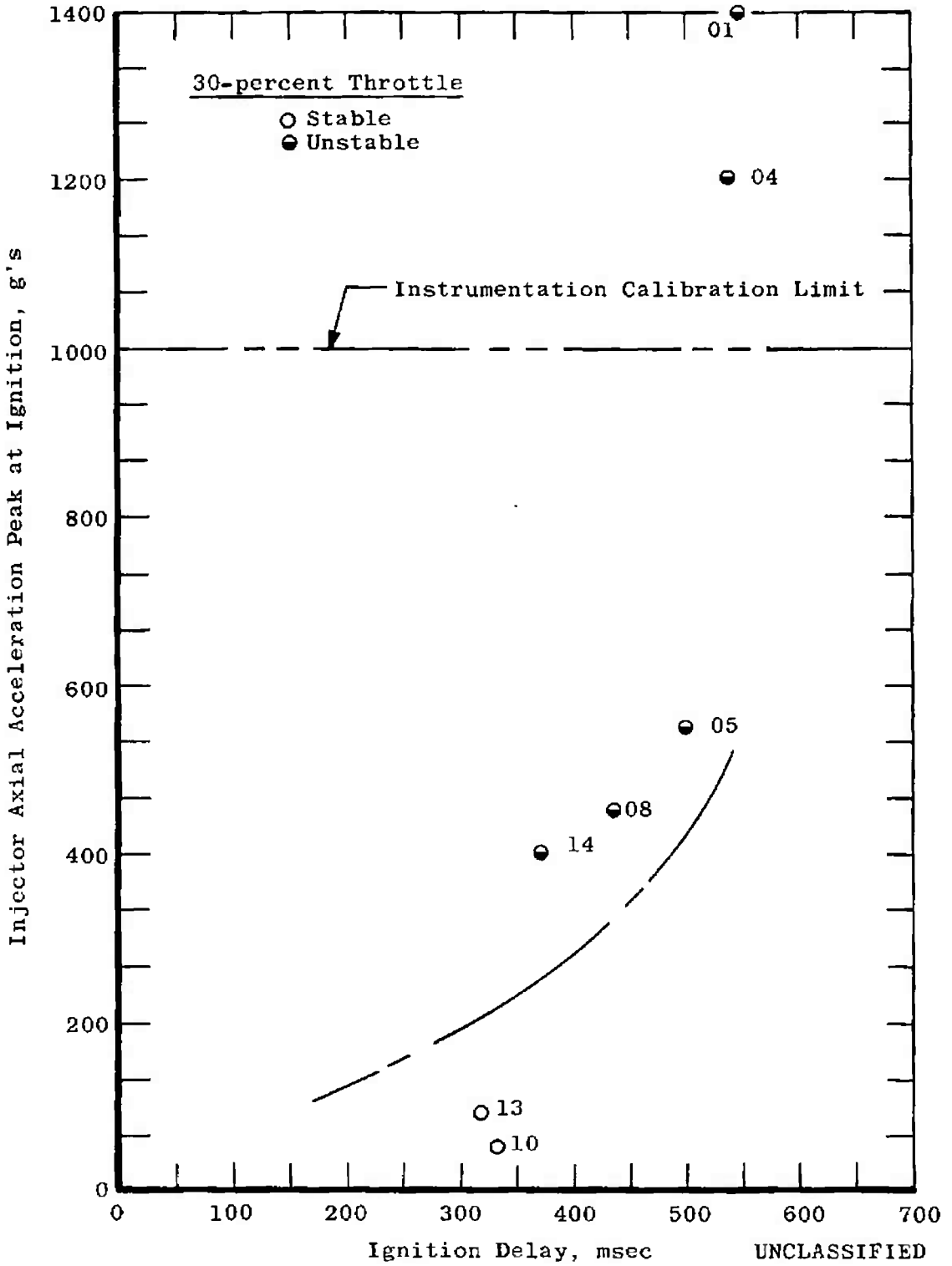

Fig. 31 Initial Acceleration Ignition Shock as a Function of Ignition Delay

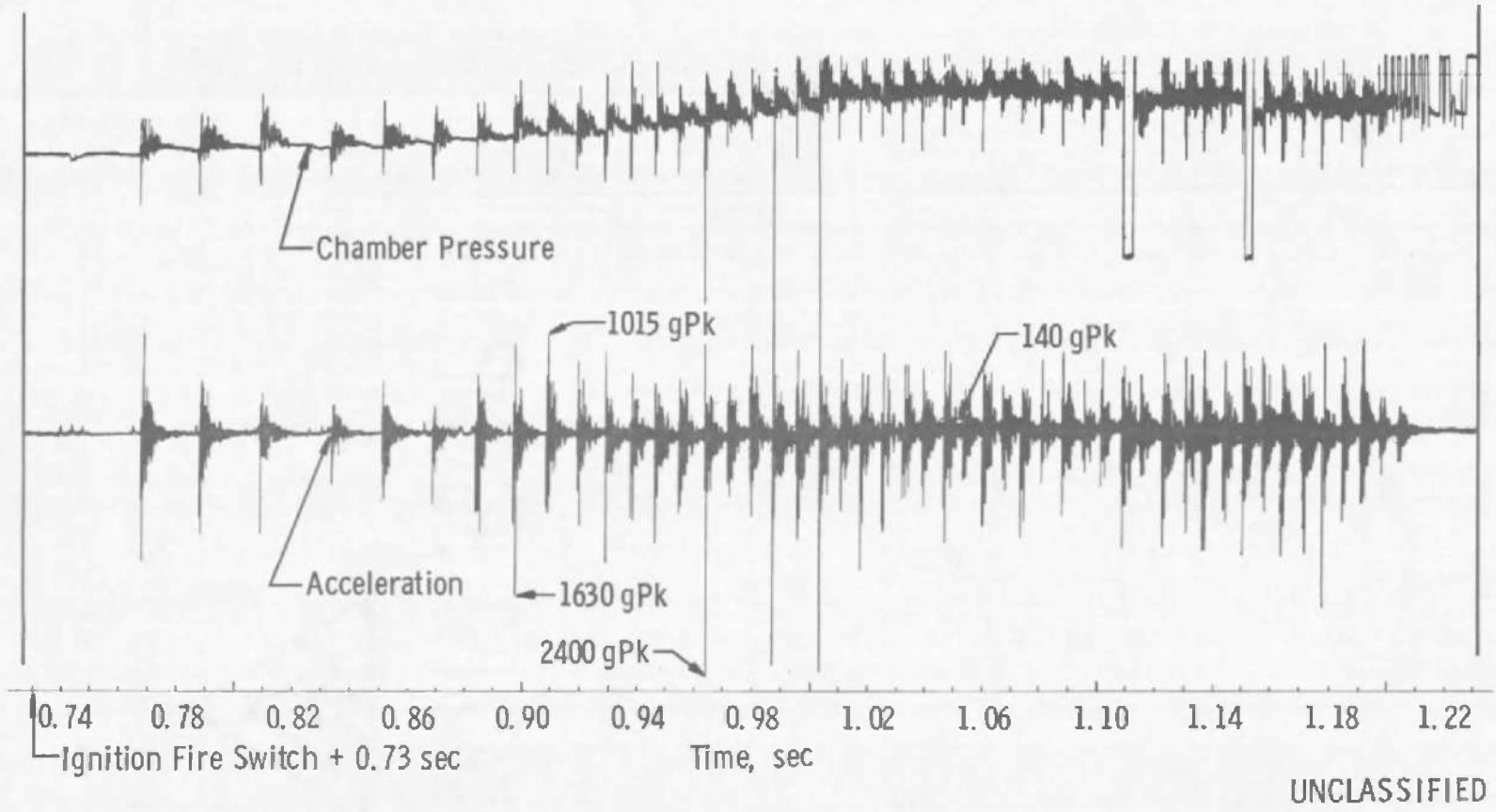

Fig. 32 Chamber Pressure and Injector Thrust Axis Acceleration for a Typical Combustion Instability Firing (AA-01)

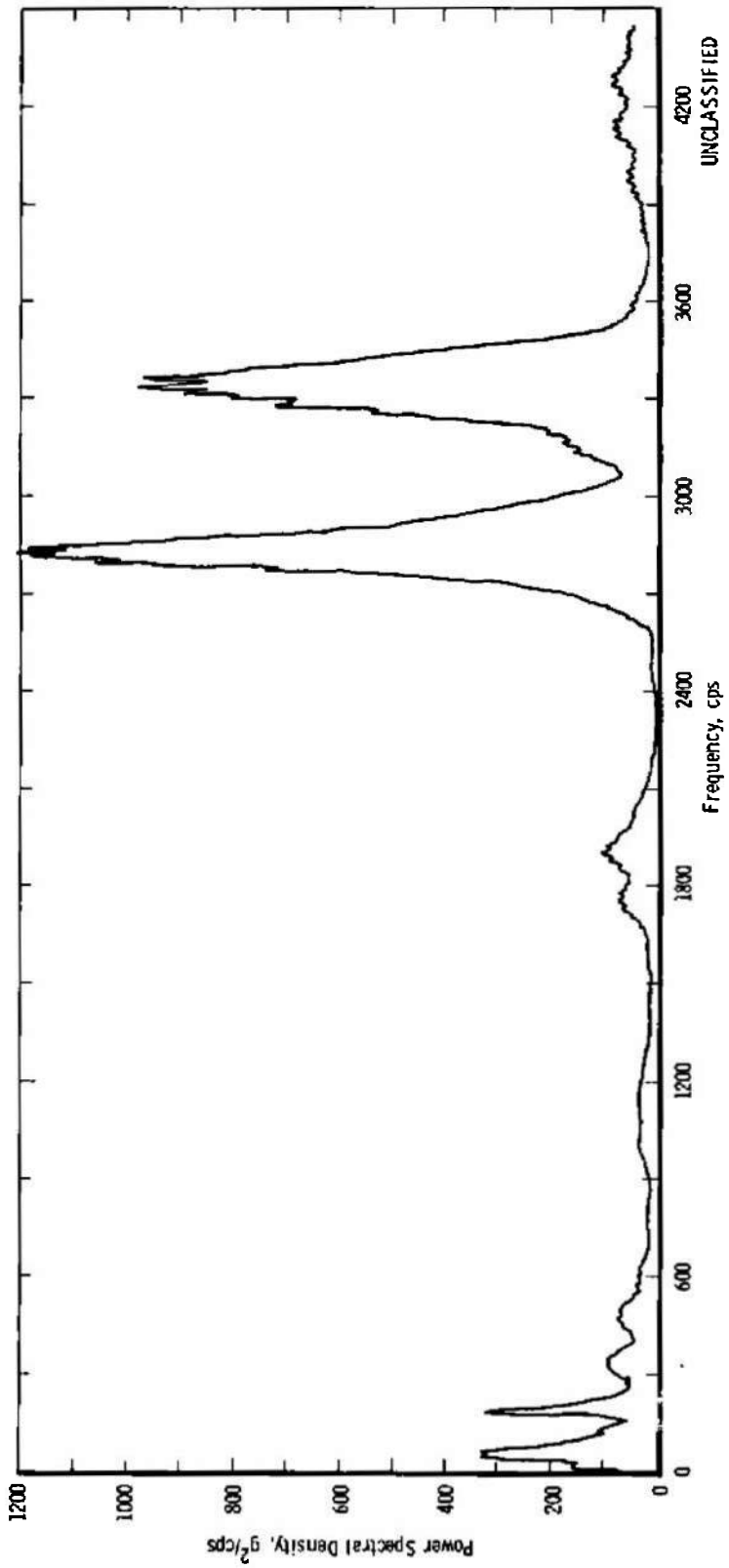

Fig. 33 Power Spectral Density for Thrust Axis Acceleration (Firing AA-01)

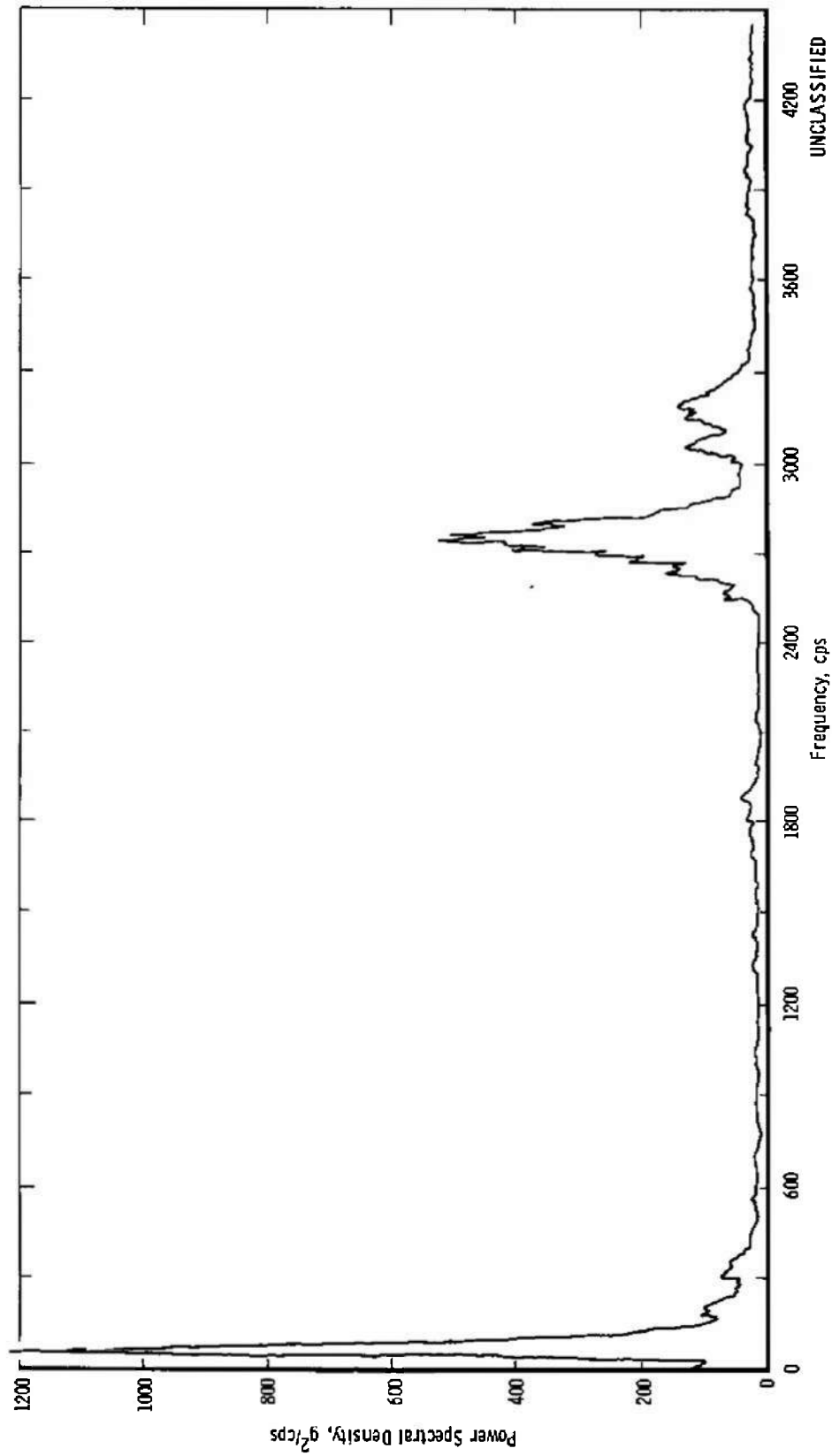

Fig. 34 Power Spectral Density for Thrust Axis Acceleration (Firing AB-05)

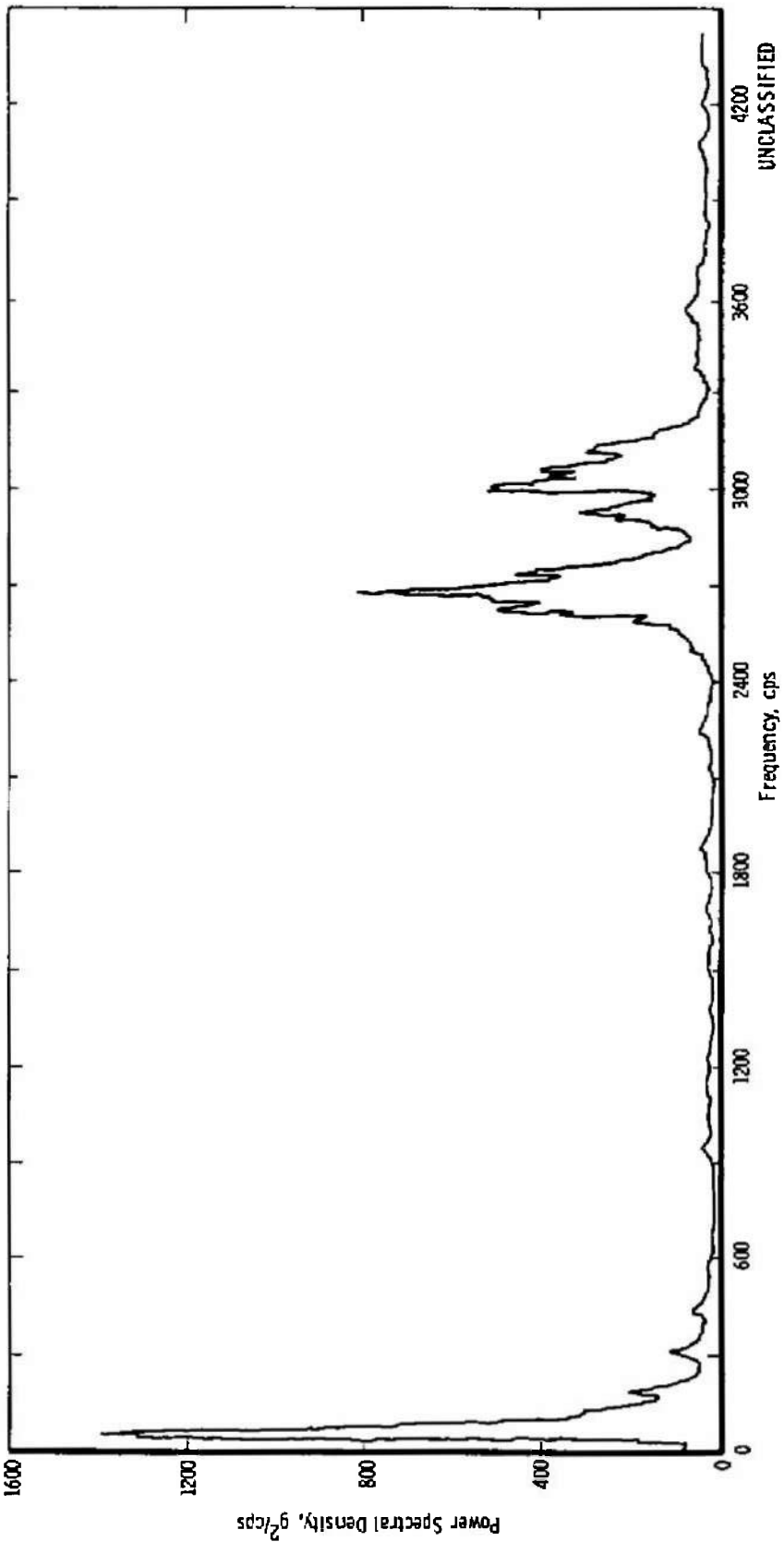

Fig. 35 Power Spectral Density for Thrust Axis Acceleration (Firing AB-14)

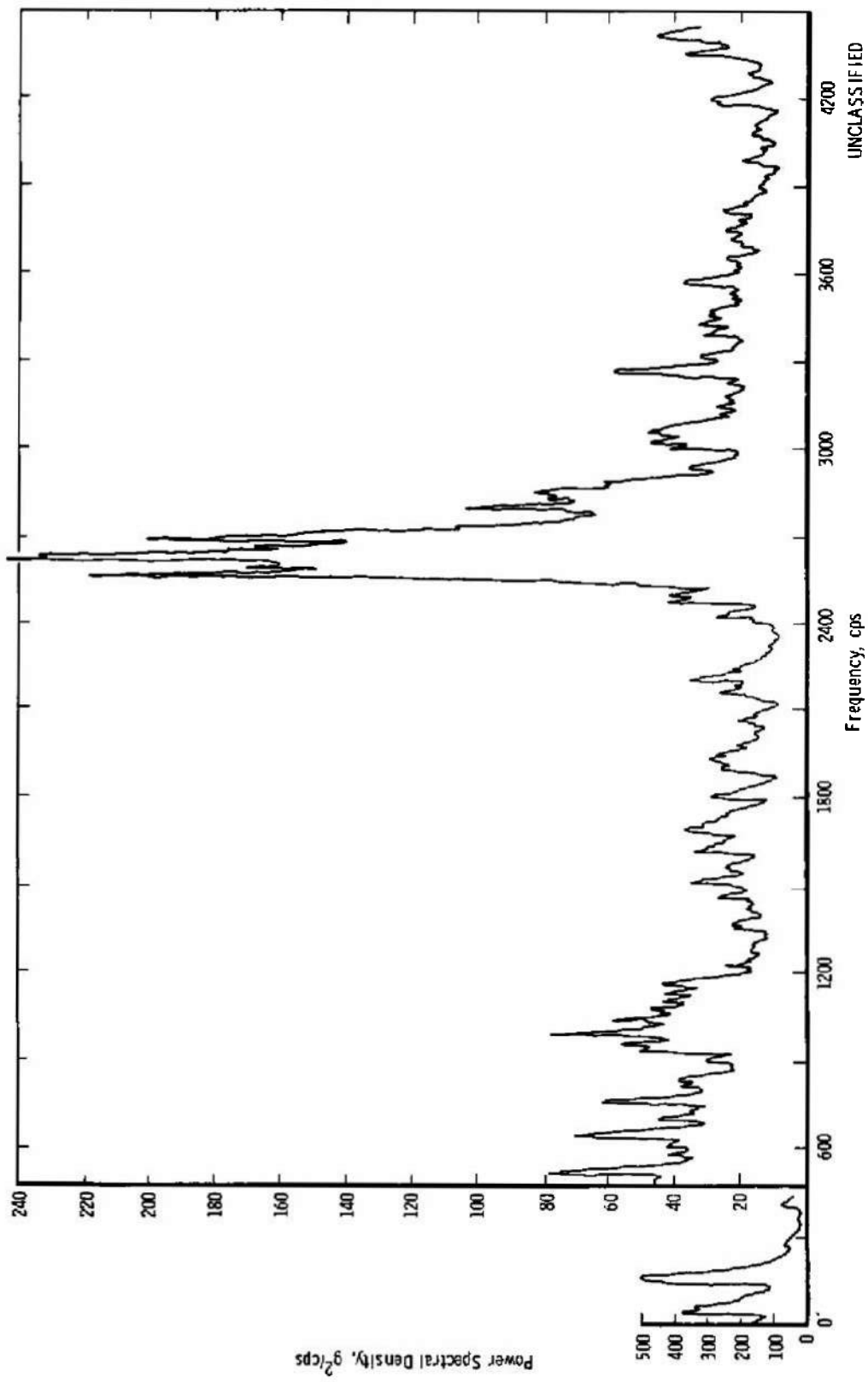

Fig. 36 Power Spectral Density for Thrust Axis Acceleration (Firing AB-19)

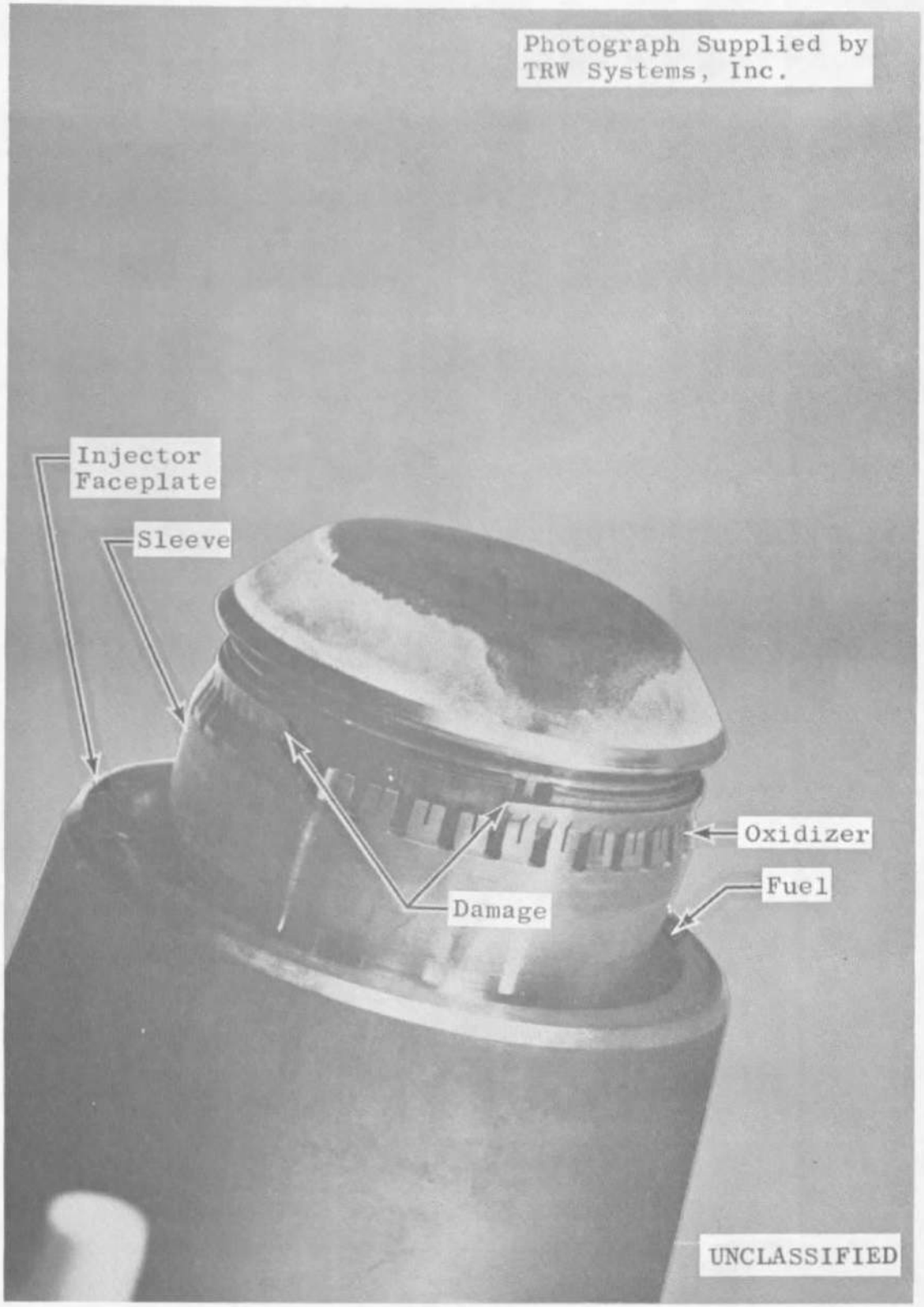

a. Pintle Assembly

Fig. 37 Injector Damage (1009)

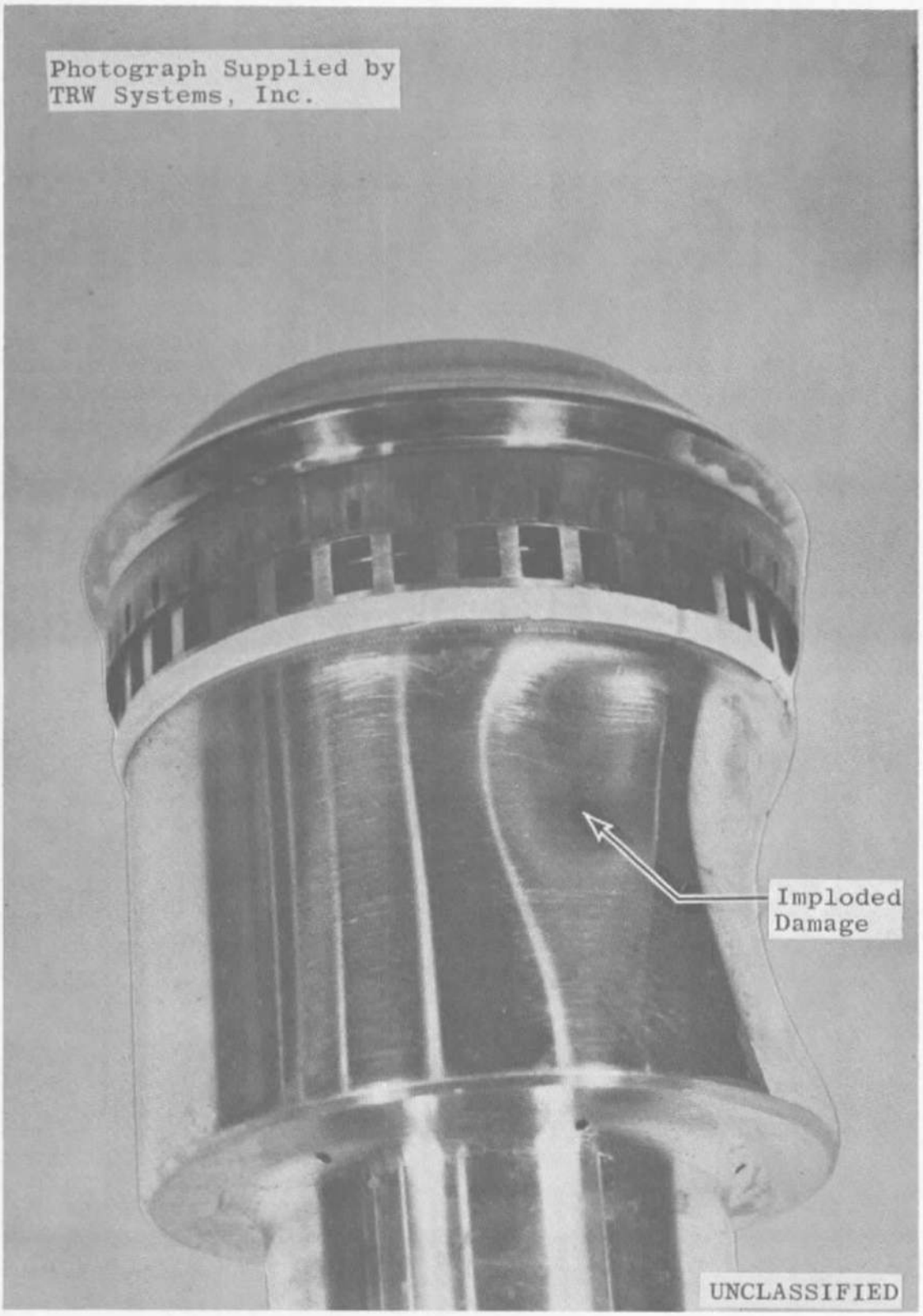

b. Pintle Tube and Tip
Fig. 37 Concluded

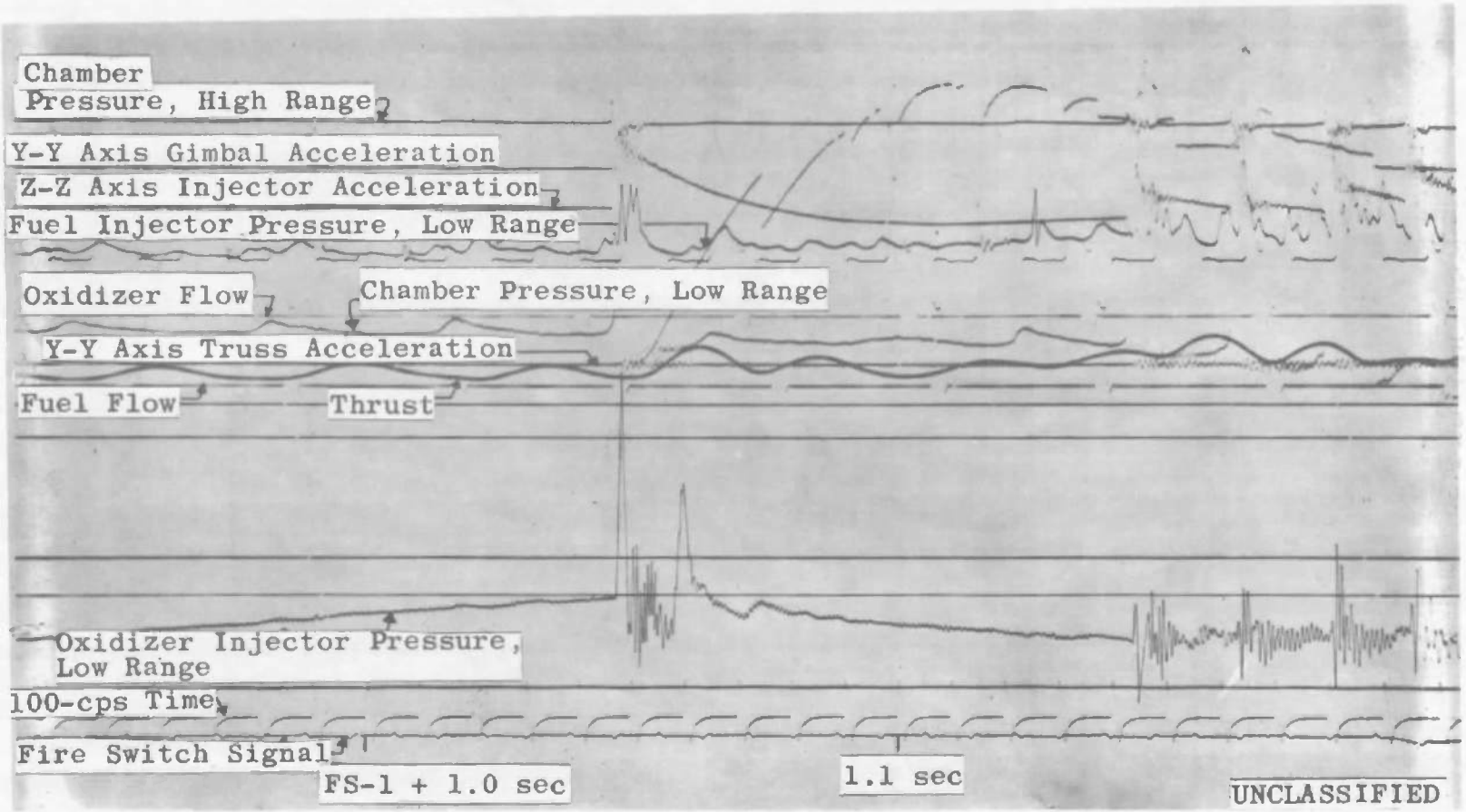

Fig. 38 Ignition Characteristics, Firing AB-19

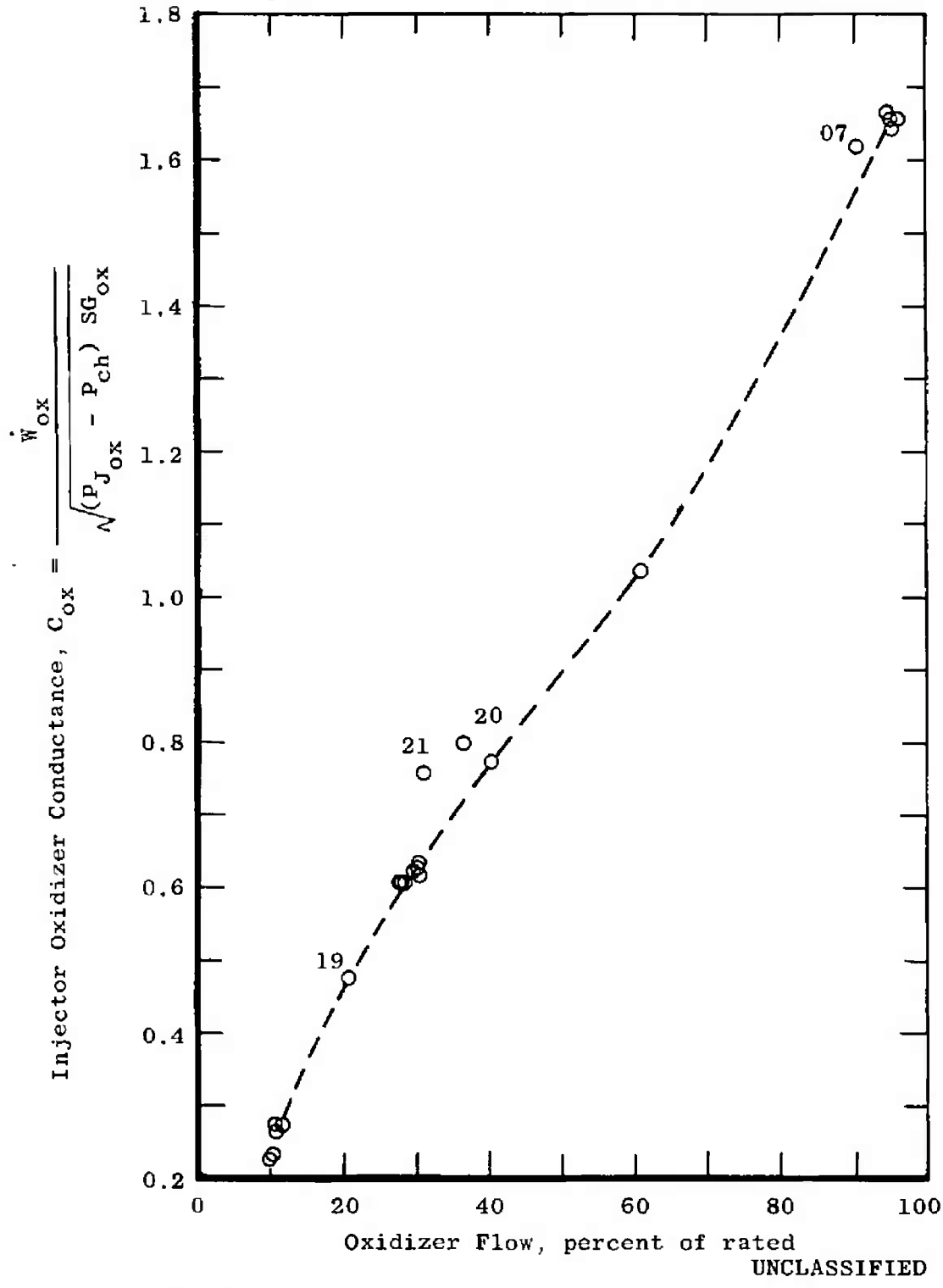

Fig. 39 Injector Oxidizer Conductance as a Function of Flow Rate

TABLE I
LMDE PERFORMANCE SPECIFICATIONS AND NOMINAL DESIGN CHARACTERISTICS (REF. 7)

Performance Specifications:	
Thrust (vacuum), lb_f	
After 50 sec of steady-state operation	9710^{+3}_{-0}
At maximum thrust portion of duty cycle	Thrust at 5 sec ±35 lb_f
After 410 sec of braking phase	Thrust at start of duty cycle +5 percent
Tolerance during 410-sec braking phase	Linear variation ±35 lb_f at beginning of phase to ±100 lb_f at end of phase
Chamber pressure	To be specified
Mixture ratio	See Fig. 18
Specific Impulse (vacuum), $lb_f/lb_m/sec$	
Average during fixed point thrust	302 (3σ min)
Average during 115 sec of 50-percent thrust	302.7 (3σ min)
Average during 215 sec of 25-percent thrust	300.2 (3σ min)
Average during 10-percent start phase	285 (3σ min)
Thrust coefficient (vacuum) at t_o maximum thrust	1.80
Characteristic velocity at t_o maximum thrust, ft/sec	5510
Interface pressure, psia	
10-percent thrust	235 ± 2
25-percent thrust	234 ± 2
50-percent thrust	231 ± 2
94-percent thrust	220 ± 2

NOTE: (1) Thrust specification is for 70°F propellants.

(2) Specific impulse specification is for 50 to 90°F propellants.

TABLE I (Concluded)

Nominal Design Characteristics:

Expansion area ratio	47.4:1
Contraction area ratio	2.9:1
Throat area, $in.^2$	54.37
Throat diameter, in.	8.32
Exit area, $in.^2$	2577
Exit diameter, in.	57.28
Chamber inside diameter, max., in.	14.2
Chamber length, injector face to throat, in.	19.7
Nozzle length, throat to exit plane, in.	62.11
Overall length, in.	90
Nozzle contour, percent bell	72.3
Total engine dry weight, lb_m	350
Throttling range, percent of rated	10 to 60

TABLE II
LMDE COMPONENT IDENTIFICATION

Component	Engine 1009		Engine 1014	
	Serial Number	Part Number	Serial Number	Part Number
Engine Assembly	1009	SK112928a	1014	SK114050a
Headend Assembly	009	E108602-2	014	SK114049b
Thrust Control Assembly		X108580-2		X108580-2
Injector Assembly (Manifold)	121	X112202-5		X113673-3
Shutoff Valve Assembly	124	C104619-2	124	XC104619-24
Prevalve Assembly	002	X113159	Same as Engine 1009	
Oxidizer Propellant Line Assembly		X108611		
Fuel Propellant Line Assembly		X108604		
Fuel Flow Control Valve Assembly	119	SK108734-1		
Oxidizer Flow Control Valve Assembly	119	E108733-2		
Throttle Actuator Assembly	206	C104622-5		
Thrust Chamber Assembly	16MB8	SK113160c		
Nozzle Extension Assembly	002	110029		
Gimbal Assembly	119	105947-4		
Electrical Package Installation (Modified B-2)	128	X112924		

TABLE III
ENGINE COMPARTMENT COMPONENT IDENTIFICATION

Component	Part or Drawing Number
HD-4 Rig Assembly	LDW430-6290
Main Frame Assembly	LDW430-6335-1
Heat Shield Support Assembly	
Cross Member	LDW430-1066-1
Support Brace	LDW430-6531-11
	LDW430-6531-13
Suspension Brace	LDW430-1064-1
	LDW430-1064-3
Blast Deflector	LDW430-1278-1
Heat Shield, Aft	LTM280-20753-3
	LTM280-20752-1
Heat Shield, Engine Skirt (Lightweight)	LTN280-20931
Engine Mount Truss Assembly	
Upper Struts	LTM280-20726-13
Lower Struts	LTM280-20815-11
Yoke (-Y Axis)	LTM280M20165-3
Yoke (+Y Axis)	LTM280M20165-1
Gimbal Actuator Stiff Links	LDW300-11700-3

TABLE IV
SUMMARY OF ESTIMATED DATA ACCURACY

	3σ Error, percent	
Parameter	94% Thrust	30% Thrust
Vacuum Corrected Thrust	0.354	0.342
Oxidizer Flow	0.687	1.425
Fuel Flow	0.756	3.075
Chamber Pressure	---	1.03

TABLE V
FIRING SUMMARY*

Firing Number	1966 Date	Clock Time of Firing	Soak Time, hr	Thrust, percent	Nominal Propellant Temp., °F	Pre-Fire Altitude, ft (Ref. 6)	Firing Duration, sec
AA-01	7/24	0134	73.6	30	40±5	323,000	5.975
-02	7/24	1905	17.5	94	40±5	323,000	6.044
-03	7/25	2030	25.4	10	40±5	299,000	9.990
AB-04	8/24	1250	74.8	30	40±5	299,000	5.908
-05	8/25	0840	19.1	30	40±5	346,000	6.149
-06	8/25	1950	11.1	10	70±5	315,000	9.986
-07	8/26	0325	7.6	94	↓	313,000	6.260
-08	8/26	1242	9.4	30	↓	306,000	6.085
-09	8/27	0810	31.5	94	↓	316,000	6.091
-10	↓	1429	6.3	30	120±5	326,000	6.086
-11	↓	1839	4.2	94	↓	324,000	6.067
-12	↓	2202	3.7	10	↓	316,000	10.267
-13	8/28	0215	4.2	30	↓	325,000	6.181
-14	↓	0829	6.3	30, 60, 94, 50, 40	70±5	345,000	50.256
-15	↓	1156	3.4	10	70±5	326,000	10.003
-16	↓	1517	3.3	10	120±5	339,000	10.093
-17	↓	1926	4.2	94	120±5	325,000	6.172
-18	8/30	0938	38.2	10	40±5	308,000	10.115
-19	8/30	1940	10.0	20	↓	311,000	6.073
-20	8/31	0327	7.8	35	↓	313,000	3.218
-21	8/31	1452	11.4	30	70±5	76,000	3.046
AC-22	12/8	0259	51.5	10, 30	40±5	334,000	13.095
-23	12/8	2015	17.3	10, 30, 16 10	40±5	311,000	27.146
-24	12/9	0934	13.4	10, 94, 60 30, 10	40±5	319,000	38.169
-25	12/10	0345	18.2	10, 30	40±5	322,000	16.104

*LMDE Serial No. P1009 used for AA and AB Series
LMDE Serial No. P1014 used for AC Series

TABLE VI
STEADY-STATE PERFORMANCE SUMMARY

Nominal Thrust, percent	Firing No.	Propellant Temp., °F	Mixture Ratio	Chamber Pressure, psia	Total Propellant Flow, lb/sec	Vacuum Thrust, lbf	I_{sp_V}, lb_f-sec / lb_m/sec	c*, ft/sec	C_F
10	AA-03	45.7	1.61	10.9	3.5	---	---	5450	---
	AB-06	72.1	1.45	11.9	3.8	---	---	5516	---
	AB-12	116.4	1.42	5.7	3.6	---	---	2840	---
	AB-15	74.7	1.52	11.4	3.8	---	---	5250	---
	AB-16	118.4	1.47	6.2	3.6	---	---	2980	---
	AB-18	48.4	1.53	11.6	4.0	---	---	5100	---
20	AB-19	45.8	1.57	15.5	7.1	---	---	3820	---
30	AA-01	39.8	1.70	32.5	10.1	3115	308.0	5610	1.766
	AB-04	41.2	1.53	33.6	10.5	3070	289.5	5570	1.683
	AB-05	44.4	1.52	33.4	10.5	3030	288.0	5580	1.675
	AB-08	75.3	1.54	32.3	10.3	2957	287.8	5510	1.684
	AB-10	115.4	1.50	30.9	9.9	2854	287.7	5450	1.699
	AB-13	114.5	1.51	30.7	9.9	2866	288.0	5400	1.716
	AB-14	78.3	1.55	33.0	10.4	3110	297.8	5533	1.732
	AB-21	79.0	1.60	31.0	10.5	---	---	5150	---
35	AB-20	47.6	1.61	34.6	12.4	3177	270.4	4770	1.787
40	AB-14	76.2	1.57	44.1	13.8	---	---	5580	---
50	AB-14	77.5	1.57	56.5	17.8	---	---	5560	---
60	AB-14	77.0	1.57	67.4	20.8	---	---	5690	---
94	AA-02	43.0	1.63	106.4	33.4	10340	309.1	5570	1.791
	AB-07	74.9	1.46	99.9	31.9	9634	301.8	5480	1.775
	AB-09	75.0	1.61	104.4	32.7	10166	311.2	5600	1.792
	AB-11	119.1	1.63	102.7	32.3	10070	311.4	5560	1.806
	AB-14	77.7	1.59	103.8	32.4	---	---	5610	---
	AB-17	120.8	1.60	102.0	32.2	9952	308.8	5550	1.795

NOTE: Data are an average from the last 1 sec of operation or thrust level.

TABLE VII
SHUTOFF VALVE ACTUATION TIME

Firing	FS-1 to Shutoff Valve Full Open, sec		Shutoff Valve Actuation Time, sec		FS-1 to Initial P_c Rise, sec
	"A"	"B"	"A"	"B"	
AA-01	0.163	0.158	0.116	0.112	0.590
-02	0.221	0.218	0.179	0.175	0.201
-03	0.160	0.150	0.112	0.104	1.420
AB-04	0.158	0.158	0.106	0.106	0.594
-05	---	0.146	---	0.104	0.540
-06	---	0.127	---	0.095	1.381
-07	---	0.177	---	0.133	0.200
-08	---	0.147	---	0.105	0.476
-09	0.347	0.141	0.129	0.099	0.249
-10	0.162	0.158	0.112	0.113	0.376
-11	0.224	0.234	0.177	0.186	0.154
-12	0.156	0.150	0.107	0.101	0.435
-13	0.167	0.158	0.114	0.114	0.360
-14	0.164	0.155	0.112	0.113	0.411
-15	0.144	0.149	0.103	0.103	0.966
-16	0.144	0.155	0.106	0.102	0.566
-17	0.230	0.219	0.177	0.189	0.168
-18	0.150	0.153	0.107	0.107	1.415
-19	0.149	0.149	0.107	0.107	0.841
-20	0.158	0.156	0.117	0.115	0.417
-21	0.159	0.155	0.117	0.117	0.441

TABLE VIII
ACCELERATION DATA SUMMARY

Firing	$A_{J_{Y-561}}$	$A_{J_{Z-562}}$	$A_{J_{X-563}}$		$A_{G_{X-565}}$	$A_{G_{Z-566}}$	$A_{G_{Y-567}}$	$A_{T_{X-568}}$	$A_{T_{Z-569}}$
			Ignition Level	Maximum Level					
AA-01	120	>1000	1400	>1000	>1000	490	200	---	---
-02	---	---	---	180	---	66	52	---	---
-03	---	---	---	---	---	---	---	---	---
AB-04	>1000	>1000	1200	>1000	760	880[1]	295	---[1]	523
-05	>1000	>1000	540	>1000	840	>1000[1]	272	---[1]	567
**-06	---	---	---	---	---	---	---	---[1]	---
-07	>1000[1]	>1000[1]	30	382	708	---	172	---[1]	340
-08	>1000[1]	>1000	450	>1000	932	---	424	---[1]	624
-09	---[1]	150	37	37	115	---	41	---[1]	141
-10	---[1]	---	53	53	121	---	48	---[1]	79
**-11	>1000[1]	>1000[1]	20	510	358	---	208	---[1]	300
-12	---[1]	113	49	49	56	---	---	---[1]	68
-13	---[1]	53	95	97	118	44[1]	---	---[1]	75
*-14	>1000[1]	>1000[1]	400	>1000	>1000	>1000[1]	>1000	51[1]	565
-15	---[1]	---	---	---	---	---	---	---[1]	---
-16	---[1]	>1000[1]	900[1]	900[1]	311	49	125	---[1]	210
-17	---[1]	23	40	40	97	---[1]	---	29[1]	280
**-18	>1000[1]	>1000[1]	---	848	391	48	175	---[1]	276
-19	>1000[1]	>1000[1]	2000[1]	>1000	>1000[1]	---[1]	450	---[1]	860
-20	open	>1000[1]	open	open	---[1]	---[1]	170[1]	---[1]	360
-21	open	>1000[1]	open	open	487[1]	165[1]	275	---[1]	1000

*Data recorded during 30-percent ignition

**Not ignition; recorded during instability

[1]Data questionable because of dc shifts and erratic behavior

DECLASSIFIED / UNCLASSIFIED

DOCUMENT CONTROL DATA - R&D

(Security classification of title, body of abstract and indexing annotation must be entered when the overall report is classified)

1 ORIGINATING ACTIVITY (Corporate author)
Arnold Engineering Development Center
ARO, Inc., Operating Contractor
Arnold Air Force Station, Tennessee

2a REPORT SECURITY CLASSIFICATION
[redacted]

2b GROUP
[redacted]

3 REPORT TITLE
SIMULATED SPACE START INVESTIGATION OF THE INTEGRATED LUNAR MODULE DESCENT STAGE THROTTLABLE ENGINE AND ENGINE COMPARTMENT (U)

4 DESCRIPTIVE NOTES (Type of report and inclusive dates)
N/A

This document has been approved for public release and its distribution is unlimited. Per A.F. Letter dated 27 July 1973

5 AUTHOR(S) (Last name, first name, initial)
Farrow, K. L., German, J. A., Gernstein, T. M., and Matkins, E. H., ARO, Inc.

6 REPORT DATE	7a TOTAL NO. OF PAGES	7b NO. OF REFS
June 1967	100	12

8a CONTRACT OR GRANT NO.	9a ORIGINATOR'S REPORT NUMBER(S)
AF 40(600)-1200	
b. PROJECT NO. 9158	AEDC-TR-67-87
c. Program Area 921E	9b. OTHER REPORT NO(S) (Any other numbers that may be assigned this report)
d	N/A

10 AVAILABILITY/LIMITATION NOTICES ~~In addition to security requirements which~~ must be met, this document is subject to special export controls and each transmittal to foreign governments or foreign nationals may be made only with prior approval of NASA (MSC), Houston, Texas. (EP-2)

11 SUPPLEMENTARY NOTES	12 SPONSORING MILITARY ACTIVITY
Available in DDC	National Aeronautics and Space Administration Manned Space Flight Center Houston, Texas

13 ABSTRACT Two Lunar Module Descent Engines (LMDE) were tested under simulated altitude conditions in Propulsion Engine Test Cell (J-2A) to (1) evaluate the thermal characteristics of the engine and engine compartment, and (2) evaluate starting characteristics of the engine after temperature conditioning in the simulated space environment. The first engine was subjected to an initial simulated space coast of 73.6 hr followed by three short firings alternated with two shorter coast periods. Combustion instability occurred during the first firing conducted at the 30-percent thrust level. Testing was discontinued because of an oxidizer leak and apparent loss of the primary instrumentation. After repairs, testing was resumed, and coast periods ranging from 3.3 to 74.8 hr followed by firings ranging from 3 to 50 sec were made at thrust levels ranging from 10 to 94 percent of rated thrust. Combustion instability occurred during seven of these 18 firings at thrust levels of 20, 30, and 35 percent, and acceleration levels above 1000 g's were experienced during 111 firings. Post-test inspection revealed a damaged injector pintle. The injector and engine were rebuilt and returned as the second test engine which was subjected to a 51.5-hr coast. The subsequent four short firings resulted in off-mixture-ratio operation of the engine because of propellant system contamination. Analysis of the test article thermal data and engine starting and operating characteristics are presented over the pre-fire pressure altitude range from 299,000 to 346,000 ft.

DD FORM 1 JAN 64 1473 (AFR 310-2, Statement 2)

DECLASSIFIED / UNCLASSIFIED

14 KEY WORDS	LINK A		LINK B		LINK C	
	ROLE	WT	ROLE	WT	ROLE	WT
1 Lunar module descent ~~engine~~ motor						
space starts						
2 throttlable ~~engines~~ motors						
temperature						
performance						
3. Rocket motors			Starting			
4 " "			Space Starting			
5 " "			Performance			
6 " "			Restart capability			

INSTRUCTIONS

1. ORIGINATING ACTIVITY: Enter the name and address of the contractor, subcontractor, grantee, Department of Defense activity or other organization *(corporate author)* issuing the report.

2a. REPORT SECURITY CLASSIFICATION: Enter the overall security classification of the report. Indicate whether "Restricted Data" is included. Marking is to be in accordance with appropriate security regulations.

2b. GROUP: Automatic downgrading is specified in DoD Directive 5200.10 and Armed Forces Industrial Manual. Enter the group number. Also, when applicable, show that optional markings have been used for Group 3 and Group 4 as authorized.

3. REPORT TITLE: Enter the complete report title in all capital letters. Titles in all cases should be unclassified. If a meaningful title cannot be selected without classification, show title classification in all capitals in parenthesis immediately following the title.

4. DESCRIPTIVE NOTES: If appropriate, enter the type of report, e.g., interim, progress, summary, annual, or final. Give the inclusive dates when a specific reporting period is covered.

5. AUTHOR(S): Enter the name(s) of author(s) as shown on or in the report. Enter last name, first name, middle initial. If military, show rank and branch of service. The name of the principal author is an absolute minimum requirement.

6. REPORT DATE: Enter the date of the report as day, month, year, or month, year. If more than one date appears on the report, use date of publication.

7a. TOTAL NUMBER OF PAGES: The total page count should follow normal pagination procedures, i.e., enter the number of pages containing information.

7b. NUMBER OF REFERENCES: Enter the total number of references cited in the report.

8a. CONTRACT OR GRANT NUMBER: If appropriate, enter the applicable number of the contract or grant under which the report was written.

8b, 8c, & 8d. PROJECT NUMBER: Enter the appropriate military department identification, such as project number, subproject number, system numbers, task number, etc.

9a. ORIGINATOR'S REPORT NUMBER(S): Enter the official report number by which the document will be identified and controlled by the originating activity. This number must be unique to this report.

9b. OTHER REPORT NUMBER(S): If the report has been assigned any other report numbers *(either by the originator or by the sponsor)*, also enter this number(s).

10. AVAILABILITY/LIMITATION NOTICES: Enter any limitations on further dissemination of the report, other than those imposed by security classification, using standard statements such as:

(1) "Qualified requesters may obtain copies of this report from DDC."

(2) "Foreign announcement and dissemination of this report by DDC is not authorized."

(3) "U. S. Government agencies may obtain copies of this report directly from DDC. Other qualified DDC users shall request through _____."

(4) "U. S. military agencies may obtain copies of this report directly from DDC. Other qualified users shall request through _____."

(5) "All distribution of this report is controlled. Qualified DDC users shall request through _____."

If the report has been furnished to the Office of Technical Services, Department of Commerce, for sale to the public, indicate this fact and enter the price, if known.

11. SUPPLEMENTARY NOTES: Use for additional explanatory notes.

12. SPONSORING MILITARY ACTIVITY: Enter the name of the departmental project office or laboratory sponsoring *(paying for)* the research and development. Include address.

13. ABSTRACT: Enter an abstract giving a brief and factual summary of the document indicative of the report, even though it may also appear elsewhere in the body of the technical report. If additional space is required, a continuation sheet shall be attached.

It is highly desirable that the abstract of classified reports be unclassified. Each paragraph of the abstract shall end with an indication of the military security classification of the information in the paragraph, represented as *(TS)*, *(S)*, *(C)*, or *(U)*.

There is no limitation on the length of the abstract. However, the suggested length is from 150 to 225 words.

14. KEY WORDS: Key words are technically meaningful terms or short phrases that characterize a report and may be used as index entries for cataloging the report. Key words must be selected so that no security classification is required. Identifiers, such as equipment model designation, trade name, military project code name, geographic location, may be used as key words but will be followed by an indication of technical context. The assignment of links, rules, and weights is optional.